SINGLE SPAN WEB BUCKLING DUE TO ROLLER IMPERFECTIONS IN WEB PROCESS MACHINERY

By

JOSEPH A. BEISEL

Bachelor of Science Physics Engineering
Southwestern Oklahoma State University
Weatherford, OK
1997

Master of Science Mechanical Engineering
Oklahoma State University
Stillwater, OK
2000

Submitted to the Faculty of the
Graduate College of the
Oklahoma State University
in partial fulfillment of
the requirements for
the Degree of
DOCTOR OF PHILOSOPHY
December, 2006

SINGLE SPAN WEB BUCKLING DUE TO

ROLLER IMPERFECTIONS IN WEB

PROCESS MACHINERY

Dissertation Approved:

Dr. J.K. Good

Dissertation Adviser

Dr. C.E. Price

Dr H. Lu

Dr. G.S. Gipson

Dr. A. Gordon Emslie

Dean of the Graduate College

Acknowledgements

I would first like to thank my advisor Dr. J.K. Good. His seemingly unlimited patience with me has been greatly appreciated. His guidance and assistance have always inspired me and led me to the accomplishments presented here. I have never for a minute doubted my good fortune at having him for my advisor.

Secondly, I would like to thank my committee members. I have had the good fortune to have been a student of each one of theirs for numerous classes. Dr. Price has imparted to me most of what I know about materials, both science and application. Dr Lu and Dr Gipson have been my primary sources for knowledge in mechanics and stress analysis, although Dr. Good has also contributed greatly through many research projects. I would like to thank each committee member for their time, effort, and patience required to conduct each of the three exams required for this degree.

The funding of the sponsors of the WHRC was invaluable. Their contributions make research possible. A special thanks goes out to Ron Markum, his help in the lab being invaluable. Also, thanks to fellow students, Balaji, Dustin, and Brian who were always ready to lend a hand as well as being good friends. I am also grateful to my

family, friends, and to my girlfriend Jamie, all of whom have been a great encouragement to me. Finally, I want to acknowledge God for giving me the strength and patience to persevere.

Table of Contents

Chapter **Page**

1 Introduction 1
1.0 Wrinkling in Web Handling 1

2 Literature Review 5
2.0 Journal and Conference Articles 5
2.1 Relevant texts 18
2.2 Summary of Current State of Wrinkling Analysis 19
2.3 Research Objectives 21

3 Prediction of Troughs Due to Shear 22
3.0 Modeling Webs as Beams (Deflection Due to Taper) 22
3.1 Experimental Verification of Deflection due to Taper 29
3.2 Trough Formation in Web Spans; Instability Criteria 38
3.3 Troughs Due to Misaligned Rollers 44
3.4 Troughs Due to Tapered Rollers 51
3.5 Measurement of Troughs Due to Tapered Rollers 53
3.6 Misaligned – Tapered Rollers 59
3.7 Introduction to the Use of Finite Elements in Webs 64
3.8 Conclusions of Troughs Due to Shear 69

4 Prediction of Wrinkles Due to Shear 70
4.0 Wrinkle Formation on Rollers, Instability Criteria 70
4.1 Stabilized Shell Buckling, Experimentation 75
4.2 Wrinkling and Finite Elements; Previous Efforts 85
4.3 Wrinkles Due to Misaligned Rollers; Finite Elements 89
4.4 Wrinkles Due to Tapered Rollers; Finite Elements 97
4.5 Conclusions of Wrinkles Due to Shear 105

5 Prediction of Machine Direction Wrinkles 107
5.0 Introduction to Crowned Rollers 107
5.1 Creation of an Adjustable Low Crown Roller 110
5.2 Strain Measurement with LDVs 116
5.3 Strain Measurement with Speckle Interferometry 122
5.4 Strain Measurement with Strain Gauges 128

5.5 Trough Formation Due to Crowned Rollers 133
5.6 Wrinkles Due to Crowned Rollers; Finite Elements 138
5.7 Wrinkle Due to an Enlarged Sector; Finite Elements 143
5.8 Conclusions of Machine Direction Wrinkles 149

6 Summary and Conclusions 152
6.0 Summary of Troughs Due to Shear 154
6.1 Summary of Wrinkling Due to Shear 155
6.2 Summary of Machine Direction Wrinkles 157
6.3 Recommendations for Future Study 159

Bibliography 160

Appendix A 164

Table of Figures

Figure **Page**

1 – Tapered Roller Profile 23

2 – Positive Sign Conventions for a Beam 24

3 – Roller Profiler 30

4 – Sample Output for Taper Qualification 30

5 – Low Taper Roller Profiles 31

6 – High Taper Roller Profiles 32

7 – Data From Stretch Test, 92 ga Polyester, E_x = 712000 psi 33

8 – Apparatus for Deflection Experiment 34

9 – Deflection Due to Taper, T = 10lbs 35

10 – Deflection Due to Taper, T = 15lbs 35

11 – Deflection Due to Taper, T = 20lbs 36

12 – Deflection Due to Taper, T = 25lbs 36

13 – Deflection Due to Taper, T = 30lbs 36

14 – Positive Sign Conventions for Loaded Plate 38

15 – Troughs Due to Misalignment, Polyester, T = 6.3 lbs 47

16 – Troughs Due to Misalignment, Polyester, T = 12.3 lbs 47

17 – Troughs Due to Misalignment, Polyester, T = 19.2 lbs 48

18 – Properties of Orthotropic Materials 49

19 – Troughs Due to Misalignment, Newsprint, T = 15 lbs 49

20 – Troughs Due to Misalignment, Non-woven, T = 1.5 lbs 50

21 – Trough Visualization 54

22 – Troughs Due to Taper, 92 ga Polyester, L = 10” 55

23 – Troughs Due to Taper, 92 ga Polyester, L = 20” 55

24 – Troughs Due to Taper, 92 ga Polyester, L = 30” 55

25 = Troughs Due to Taper, 92 ga Polyester, L = 40” 56

26 – Troughs Due to Taper, 56 ga Polyester, L = 20” 57

27 – Troughs Due to Taper, 56 ga Polyester, L = 30” 57

28 – Troughs Due to Taper, 56 ga Polyester, L = 40” 57

29 – Orientations of a Misaligned-Tapered Roller 60

30 – Misaligned-Tapered Roller, m = 0.0010 radial in/in, L = 30” 62

31 – Misaligned-Tapered Roller, m = 0.00144 radial in/in, L = 30” 62

32 – Misaligned-Tapered Roller, m = 0.0010 radial in/in, L = 10” 63

33 – FE Trough Model, Tapered Roller 65

34 – FE Trough Model, σ_x Stress Output 65

35 – FE Trough Model, Compressive Principle Stress 66

36 – Troughs Due to Taper, 92 ga Polyester, L = 10” 67

37 – Troughs Due to Taper, 92 ga Polyester, L = 30” 67

38 – 56 ga Polyester, L = 30” 68

39 – Shell Instability Conventions 71

40 – Mandrel Supports for Internally Pressurized shell 78

41 – Pressurized shell, $P_{internal}$ = 0 psi 79

42 – Buckling at Outer Edge of Shell 80

43 – Clamps to Prevent Shell Buckling Near End of Can 81

44 – Rigidly Supported Shell Buckling 83

45 – Correlation Between Troughs and Wrinkles..... 85

46 – Deflection Due to a Misaligned Roller; 92 ga Polyester, L = 18” 86

47 –Boundary Conditions and Applied Loads as Used by Webb..... 87

48 – Webb’s FE Model and Experiment, 92 ga Polyester, R_o = 1.45” 88

49 – States of Wrinkling Membrane Elements 90

50 – FE Wrinkle Model, Misaligned Roller 90

51 – Deformed Model (10x) Depicting σ_y Stress 91

52 – Deformed Nodal Coordinates 92

53 – Critical σ_2 Stress Developed in FE Analysis of Misaligned Rollers 93

54 – Wrinkles Due to Misalignment, 92 ga Polyester, L = 6” 93

55 – Wrinkles Due to Misalignment, 92 ga Polyester, L = 18” 94

56 – Wrinkles Due to Misalignment, 92 ga Polyester, L = 30” 94

57 – Comparison of Webb’s Model to Current FE Model 95

58 – FE Wrinkle Model, Tapered Roller 97

59 – Deformed Model (25X) Depicting σ_x Stress 98

60 – Critical σ_y Stress Developed in FE Analysis of Tapered Roller..... 99

61 – Wrinkles Due to Taper, 92 ga Polyester, L = 10” 100

62 – Wrinkles Due to Taper, 92 ga Polyester, L = 20” 101

63 – Wrinkles Due to Taper, 92 ga Polyester, L = 30” 101

64 – Wrinkles Due to Taper, 92 ga Polyester, L = 40” 101

65 – Wrinkles Due to Taper, 56 ga Polyester, L = 10” 102
66 – Wrinkles Due to Taper, 56 ga Polyester, L = 20” 103
67 – Wrinkles Due to Taper, 56 ga Polyester, L = 30” 103
68 – Wrinkles Due to Taper, 56 ga Polyester, L = 40” 103
69 – Fife Crown Roller Profiles 108
70 – Proposed Crown Roller Shell Profile 111
71 – FE Deformations Compared to Desired Profiles 111
72 – Machined Shell for Pressurized Roller 112
73 – Pressurized Roller 112
74 – Pressurized Crown Roller Profiles 113
75 – Machined Parts for the Dynamically Variable Crown Roller 114
76 – Thrust Bearing Isolation of Piston 114
77 – Dynamically Variable Crown Roller 115
78 – Concave Roller Profiles 117
79 – First Test of MD strain Due to 0.037” Concave Roller 118
80 – Determining Cause of Steering Forces 119
81 – MD Strain Profile, 0.037” Concave Roller 120
82 – MD Strain Profile, 0.014” Concave Roller 120
83 – Tension Effects on Strain Due to 0.037” Concave Roller, d = 1” 121
84 – Speckle Interferometry Experiment 123
85 – Sample Speckle Pattern 124
86 – 380 ga Coated Paper, 10 lb Increments 124
87 – 380 ga Coated Paper, 5 lb Increments 125
88 – 380 ga Coated Paper, 1 lb Increments 125

89 – 380 ga Coated Paper, 1 lb Increments 125

90 –Software Comparison, 200 ga Polyester, W = 6” 126

91 – Strain Mapping with Strain Gauges 129

92 – Sample Strain Gauge Output 130

93 – Measured Strain due to a Crowned Roller, L = 19.5” 130

94 – Strain at Crowned Roller, P_{int} = 1000 psi 131

95 – Strain at Crowned Roller, P_{int} = 500 psi 132

96 – Troughs Generated By Crowned Roller 133

97 – Boundary Conditions for FE Trough Model 134

98 – MD Stress Profiles, L = 30”, T = 20 lbs 135

99 – CMD Stress Along Web Centerline, L = 30”, T = 20 lbs 136

100 – Wrinkle Generated By Crowned Roller 138

101 – Wrinkles Generated by a Crowned Roller, R_o = 1.5” 139

102 – Boundary Conditions for Wrinkling Due to Crown 139

103 – Critical Compressive Stress, FE Crowned Roller Model 140

104 – FE Wrinkle Model; L = 20”, T = 18.6 lbs 141

105 – FE Wrinkle Model; L = 30”, T = 17.6 lbs 141

106 – FE Wrinkle Model; L = 40”, T = 17.4 lbs 141

107 – Diagram of Roller with Enlarged Sector 143

108 – Wrinkle Data Due to a Roller with an Enlarged Sector 144

109 – Boundary Conditions for Wrinkling Due to an Enlarged Sector 145

110 – Roller Profile, P_{int} = 5 psi 145

111 – FE Wrinkle Model; L – 31.5”, T = 20 lbs 146

112 – FE Wrinkle Model; L = 31.5”, T = 20 lbs 146

113 – FE Wrinkle Model; L = 19.25”, T = 10 lbs 147

114 – FE Wrinkle Model; L = 31.5, T = 30 lbs 148

115 – Load Curves for FE models 166

Nomenclature

a	Half Wave Number
A	Cross Sectional Area
A_s	Area reacting shear force
A_{kn}	Deflection Amplitude
b	Web Width
CMD, MD	Cross Machine Direction, Machine Direction
D	Rigidity
D_1, D_2, D_3, D_k	Principal Directional Rigidities
E	Young's Modulus
E_x, E_y	Directional Young's Modulus
f, f_{yi}, f_{yj}	Lateral Forces on Beam Element
FE	Finite Elements
G	Shear Modulus
I, I_z	Area Moment of Inertia
L	Web Span Length
m	Roller Taper
m_{cr}	Critical Roller Taper
M_i, M_j	Moments Acting on Beam Element

M_{tot}	Net or Total Moment
k, n	Half Wave Numbers
N_x, N_y	Compressive Forces Per Unit Length
P_{int}	Internal Pressure
R_o, r	Nominal Roller Radius, Local Roller Radius
t	Web Caliper
T	Web Tension
T_{slack}	Tension Where Slack Edge Occurs
v_i, v_j	Lateral Deflections
V, V_{avg}	Velocity, Average Velocity
w	Out of Plane Deformation
W	Web Width
x, y, z	Coordinate Directions
α	Angle of Principal Direction
γ_{xy}	Shear Strains
ε_x, ε_y	Normal Strains
θ_i, θ_j	Beam Element End Rotation
π	3.1416
ν	Poisson's Ratio (isotropic)
ν_{xy}, ν_{yx}	Directional Poisson's Ratio
ω	Angular Velocity
σ_e	Normalized Normal Stress
σ_x, σ_y	Directional Normal Stresses

σ_{ycr}	Critical Lateral Normal Stress
σ_{cmd}	Cross Machine Direction Normal Stress
σ_{md}	Machine Direction Normal Stress
σ_1, σ_2	Principal Normal Stresses
τ	Shear Stress
τ_{cr}	Critical Shear Stress
τ_{xy}, σ_{xy}	Directional Shear Stress
ϕ	Shear Parameter

CHAPTER I

Introduction

1.0 Wrinkling in Web Handling

A web is defined as any media that is handled as a continuous entity. A more precise definition might require a web to have a rectangular cross section where the thickness is *much* less than the width. Similarly, web handling may be defined as the processing of continuous media. Typical webs may include plastic films, papers, sheet metals, foils, and non-wovens. Webs are processed in order to add value to or increase the usefulness of the web. Some typical examples of web handling include; coating, printing, slitting, laminating, or adding a surface finish.

Processing of webs requires the web to be unwound from a roll, where the web will then travel through a processing machine. The machine will transport the web over rollers or air bars which support and define the path of the web through the machine. After the web is processed, it is again wound onto a roll for storage or cut into other useful geometries for its final application. During the course of transport through a web

-line the web may experience forces that result in compressive stresses. These compressive stresses may induce instability in the web as it is being processed. Instability may be manifested in one of two forms, toughs and wrinkles. Troughs are defined as out of plane deformations of webs as they travel through free spans. A free span is a tensioned section of web between two rollers (or possibly air bars which are not discussed here). A wrinkle is defined as an out of plane deformation of the web as it transverses a roller. The plane previously mentioned is tangent to the roller while the web is in contact with the roller. In other words, a wrinkle occurs whenever the web lifts off the roller surface as the web travels around the roller.

The formation of wrinkles or troughs has long been a source of concern for the web handling industry. Wrinkling typically causes permanent damage to the web, breakage in the case of paper webs, and harmful effects to downstream winding rolls as well as interference with intermittent processes. The formation of troughs in web spans may adversely affect processes like printing, coating, etc, due to the non-planar geometry of the web in the span. Whether the web is permanently damaged, a value adding process is compromised, or something as catastrophic as web breakage occurs, the end result is often wasted web and costly downtime of web lines that may potentially be miles long.

A common cause of trough and wrinkle formation in webs is the presence of a lateral force acting across the web. For future reference, the direction of web travel through a web process machine will hereafter be termed the machine direction (MD) and the cross-machine direction (CMD) will refer to a coordinate direction which lies normal

to the machine direction and coincides with the plane of the web. These lateral (also termed "shear") forces combined with web line tension (MD stress), result in the compressive CMD stresses in the free span that lead to trough and wrinkle formation. Wrinkles that are the result of these lateral shear forces are termed shear wrinkles. Shear wrinkles are commonly encountered in the web handling industry as a result of misaligned rollers, imperfect rollers, and (potentially) web guidance systems.

Shear wrinkles are categorized as either regime 1 or regime 2, based on previous research in this area. Regime 1 wrinkles are independent of web velocity and assume that there is not a loss of traction due to air entrainment. Air entrainment is the process where air, being dragged along by a moving web, becomes trapped between the web and the roller as the web passes over the roller, thereby reducing web to roller traction. Regime 2 wrinkles are dependent on the web to roller traction. It has been shown by Good, et al. [16] that regime 2 wrinkles may be avoided altogether by using rollers with sufficient traction and appropriate web line conditions. Thus, only regime 1 wrinkles will be studied in this dissertation.

Wrinkles and troughs can also form where there is an absence of a net lateral or shear force applied at the downstream roller. Examples of this are wrinkles due to crowned rollers and machine direction wrinkles in "thin" webs. In these cases, compressive CMD stresses develop in the web without a lateral steering of the web caused by a net shear force.

The study of the trough and wrinkle phenomena in webs is necessary for establishing guidelines for design and modification of web process machinery. Accurate tolerances for roller shape are crucial for efficiently and economically specifying dimensions for new rollers and essential for setting up preventative maintenance schedules for roller replacement. With such guidelines available, the effort of setting up a new web line may be reduced. Furthermore, problems with wearing rollers may be measured, compared to meaningful tolerances, and replaced as necessary. Without these guidelines, the web process companies have to afford damaged materials, time consuming hit and miss installation processes, as well as the reality that any change of rollers or web line setup may result in a wrinkled web.

CHAPTER II

Literature Review

2.0 Journal and Conference Articles

The first studies of interactions between webs and rollers were not concerned with wrinkling but with the steering of drive belts. One of the earliest technical presentations on this subject was by Swift [39] in 1932. He mainly focuses on cambered pulleys as a means of correcting some geometrical imperfections in a drive pulley system, admitting that cambered pulleys would be detrimental in a perfect web line. He discusses the concept of a couple developed in a web approaching a tapered or crowned roller and the resulting steering of the web (corrective in this case). He looks at the problems of: misaligned shafts (co-planar), twisted shafts (out of plane), staggered pulleys, and oblique drives. In accordance with each system, he suggests the minimum amount of crown or taper that should be employed to control the web with minimum interference of stresses in the web. Experimental results are given in support of his suggestions of corrective measures. One of the most important developments to this paper is the concept of normal

entry. Swift provides the first reference (found by this author) to state that a belt running under steady state conditions must enter the roll perpendicular to its axis of rotation (offset by the radius of the roller).

Another early work was conducted by Lorig [24] in 1950. His work focused on self centering rollers. He discussed the steering action of a web due to cylindrical, crowned, concave, and jointed self centering rollers. He explains the theory of steering due to each type of roller but stops short of producing formulae and models for prediction of lateral behavior.

In 1968, Shelton [37] discussed the lateral steering of a web due to various forms of web guides. Shelton first lists most of the common forms of web guidance systems at the time, and provides a thorough study of the underlying principles behind each type. The work is then applied to a discussion of optimal applications of these devices.

In his development of theory for web steering, Shelton [37] primarily focuses his attention to modeling the steering effects of a misaligned roller. He presents a model for web deflection based on a web being treated as a beam. He then establishes the boundary conditions on a web span encountering a downstream misaligned roller. An important development was the concept of zero moment in the web as it approached the downstream misaligned roller. Also significant, was the modeling of a developing slack edge in a web. Shelton discussed the use of normal entry of a web to a roller. Shelton stated that the concept of normal entry had been used previously in the drive belt industry

(mentioned above) but was as yet unknown to most people involved in web guiding systems.

Shelton built a test apparatus to provide experimental verification for his models. In testing a web, he described procedures of determining web material properties and coefficients of friction. Tests were conducted to support the theories presented which include, web to roller friction, dynamic response of steering guides and their control, and multiple web span interactions.

Gehlbach, et al. [12] applied plate buckling criteria to a web in a free span. This was done to predict the onset of shear wrinkles (which they defined at that time). This work suggested that shear stresses coupled with a web line tension could result in a compressive 2^{nd} principal stress capable of buckling the web. The paper focused on experimental verification, in the case of the misaligned downstream roller. Experimental results support the proposed model for the ranges and web line parameters tested. The length to width ratio of the web span was tested from 1.5 to 4.33, resembling common span ratios. The work assumed isotropic web properties.

Gopal and Kedl [18] worked to apply finite element analysis to the prediction of wrinkle formation due to a downstream misaligned roller. Their goal was to predict wrinkle formation, even after the formation of troughs and possibly a slack edge in the web. Additionally, they stated that the buckled deformation not be constrained to sine wave troughs uniformly distributed across the width of the web. They utilized two

approaches, the first being a 2-D FE (finite element) model that used wrinkling membrane elements (which could not sustain any compression) to model a web span. The model did predict the deformations of a web encountering a misaligned roller.

Next, they attempted to predict wrinkle formation by increasing the shear force applied until an unstable equilibrium equation occurred. The model was unable to predict wrinkle formation. A second model, utilizing regular plate elements, was more successful in predicting wrinkles. It applied both shear force and an out of plane perturbation to the web. If this out of plane perturbation resulted in a sustained out of plane deformation even after the perturbation was removed, then a wrinkle was said to have formed. Limited verification accompanied this work. They did not link their model to any classic shell-buckling theory. Also, the web taking on a shell form while on the roller was not modeled in any way.

The forgoing wrinkling membrane elements mentioned were developed to their current state by Miller and Hedgepeth [26]. They proposed a method of FE analysis for partly wrinkled membranes. They modify the stiffness of elements based on their current strain. Elements can have linear elastic behavior when taut in two directions, wrinkled when taut in only one direction with a modified stiffness, or slack, where the stiffness is set to zero. The method works by assuming a stiffness for an element and then calculating its stress state. Next, a modified stiffness is calculated from the strain developed in the first iteration and the process is repeated until convergence. It is important to note that the load is applied in steps and that convergence must be achieved

at each load step. They applied this process to classic problems, to which approximate solutions existed, and achieved satisfactory agreement. One problem they modeled was that if a rotating shaft in a hub.

Papandreadis [30] also discussed wrinkling behavior in webs. He presented a FE code that incorporates membrane behavior into elements that cannot support either bending or compression. He then applied lateral forces to his model and characterized the effects of material properties and web thickness on web wrinkling, as well as predicting lateral contraction of the web width. He did not simulate the boundary conditions of an actual web passing over a roller. Also, presented is a buckling analysis of panels using NASTRAN and a characterization of the resulting mode shapes, including the number of waves present and wavelength of the corrugations.

Shelton [33] discussed the buckling of webs in the free span and on rollers. He reported a critical strain associated with plates and shells and suggests their use in determining web buckling. Something similar had previously been applied by Gehlbach et al. [12] in 1989. In modeling a web as a buckled plate or a shell, Shelton predicted the wavelength of the buckled form and provided some experimental data. Shelton went on to suggest models for the compressive strain developed in a web as it passes over a roller and enters a different tension, temperature, or moisture zone. The case of a varied web tension across a roller is considered as a potential source for compressive strain. Shelton also discussed possible compressive strains due to a viscoelastic memory in webs, and

due to a web entering a deflected roller. The latter case would be similar to a curved axis roller. Other topics included web to roller traction, and pressurized shell buckling.

Benson et al. [5] developed a FE code based on tension field theory. Their self titled code FEWA was derived from the "Wrinkle Strain Method". The code was applied to theoretical cases, and proposed trough lines were characterized by the web model. The main purpose of the code, therefore, was to predict locations of compressive stresses and likely locations where troughs would form, not to predict the onset of these troughs.

Delahoussaye and Good [9, 10] presented works using FE to model the effects of contoured rollers interacting with webs. The first reference was concerned with the spreading capabilities of a concave roller. The later reference similarly dealt with the spreading effects of a curved axis roller on a web. Experimental verification was not presented.

Dobbs and Kedl [11] studied web to roller traction and the possibility of interaction between web spans. They looked at how a misaligned roller could cause slippage of the web at the upstream roller and the influence that may have on wrinkle formation. They presented models to predict when slippage would occur and provided experimental data.

Good [13] also looked at the possible interaction of multiple web spans due to a downstream shear force. Traction was discussed as a factor to web slippage and the

ensuing moment transfer between web spans. A velocity dependent traction model was developed. It focused on air entrainment between a moving web and a transport roller and its effect on web to roller traction. Good also incorporated the effect of a slack edge into his model for a downstream misaligned roller in a multi-span system. Experimental verification was provided.

Good et al. [16] presented another work dedicated to shear wrinkles in isolated web spans. There was discussion of regime 1 (velocity independent) and regime 2 (velocity dependent) wrinkles. Models were developed for the prediction of both regime 1 and regime 2 wrinkles (in retrospect, the models may have been better suited to predicting trough formation). In the case of regime 2 wrinkles, a traction algorithm, which was velocity dependent, was applied to the downstream misaligned roller itself to see if sufficient traction was available to cause enough steering to induce instability. Extensive experimental support was provided.

Shelton [35] discussed the issue of web camber and its effect on web handling. One of the first methods of qualifying web camber was established in what he termed "sweep tests". He proposed a critical tension required to pull a cambered web taut. He went on to analyze behavior of a straight web on a tapered roller and the resulting steering of the web. This was then compared to the similar case of a cambered web on a cylindrical roller. Additionally, Shelton discussed the concept of steering a cambered web.

Another paper related to web camber came from Wang [44]. He proposed models for the behavior of cambered webs and their resultant machine tension variations across the width of the web. He discussed cambered webs approaching both aligned and misaligned rollers. Of most interest, is the experimental procedures used to experimentally measure tension variation across the web. He developed a technique of exciting a tensioned moving web with a pulse of air that induced an out of plane vibration in the free span. Two microphones were then used to measure the speed of wave propagation in order to determine the tension in that locality of the web. The present author has used this technique, it does work for large tension variation, but the resolution is outside the range of most studies concerning contoured rollers.

Swanson [38], also discussed the issue of cambered webs. He defined three boundary conditions, the upstream deflection being constant, the slope of the web at the upstream roller is equal to zero, and the slope of the web at the downstream roller is equal to zero. He bracketed the 4^{th} boundary condition, which is the moment at the downstream roller, but does not quantitatively define it. He suggested that the effect of camber be quantified by shear, deflection, and moment measurements. He also argued against Shelton's tapered roller analogy as a model for a cambered web.

The topic of cambered webs was later picked up by Olsen in [27]. He developed models based on beam theory to describe the lateral behavior of the web. His model considered varying stiffness properties and frozen-in strains. He characterized the

deformations but provided no experimental support. Olsen included shear effects in his model in [29] and focused on cambered webs experiencing low tensions in [28].

Good and Straughan [17] investigated wrinkling due to the downstream roller being twisted in a CMD plane, that is perpendicular to the webs regular orientation. The model made use of an Airy's stress function to predict the stresses in the web span. They linked these stresses to shell instability theory to predict wrinkle formation. Experimental support was provided.

Markum and Good [25] studied the spreading potential of concave and bowtie rollers. In their analysis, each half of the web was essentially modeled as a beam. The downstream contoured rollers impose a moment on each half of the web. A shear force and correlating deformation were predicted. In order to test the shear force developed at the concave roller, Markum and Good devised an experiment that slit the web as it left the upstream roller. The two halves of the web were now free to steer away from each other. The deflection was measured to verify that the correct shear force was predicted.

Good and Beisel [4, 15] readdressed the issue of wrinkling due to a downstream misaligned roller. Previous wrinkling models were generalized by the inclusion of shear and tension effects. In addition, the model was derived with consideration of orthotropic material properties. Experimentation revealed distinct differences between trough and wrinkle formation in the case of the misaligned roller. The study showed that a closed form solution could be found for the prediction of trough formation, but the wrinkle

formation would require a post-buckling analysis. Previous efforts to predict trough formation had been limited to typical length to width ratios, but here both short and long spans were tested. The shorter spans revealed the importance of modeling shear effects, while tension effects were more critical in the longer spans. Orthotropic materials were characterized and tested to verify those inclusions in the model (newsprint and a proprietary non-woven).

It was later noticed that the critical angle of roller misalignment for wrinkle phenomenon was nearly twice that of trough formation. This was further investigated by Webb [45]. He tested a large number of materials and consistently found the same correlation between trough and wrinkle formation. Webb presents an expression for wrinkle formation based on the model developed for trough formation in [4], but with an empirical factor derived from experiment. He then attempted to model wrinkle formation using finite element techniques. He used wrinkling membrane elements that cannot sustain any compressive stress to model the web with corrugations due to troughs. Acceptable agreement was achieved but only after the rotations from the FE analysis were added to the rotations needed to form troughs per [4].

Good and Beisel [15] investigated the formation of troughs due to tapered rollers to see if a procedure similar to that employed for misaligned rollers would the applicable to the case of a downstream tapered roller. Their paper was a direct result of this dissertation and will not be discussed further here.

Shelton [34] presented an unpublished paper for an internal board review which discussed misaligned and tapered rollers; however most consideration was given to multiple web span interactions and moment transfer. No experimental support was provided. Shelton's models pertaining to tapered rollers will be included in section 3.4 for comparison.

In 2005 Hashimoto [19] presented a paper on roller misalignment. It was mainly concerned with paper webs and therefore orthotropic properties. The models and conclusions presented were very similar to previous works such as [4, 15, 16].

Brown [6, 7] presented two papers in 2005. He proposed models for the lateral mechanics of webs encountering misaligned, tapered, concave, crowned, and cambered webs. He suggested two modifications of the web boundary conditions. One was a generalization of the normal entry rule and the other was the addition of what he called the normal strain rule. Nonlinear two dimensional plane stress equations were solved with a numerical partial differential equations solver and the results were compared to other previously developed models, but not to experimental results.

Shelton [36] again addressed the multi-span effects of misaligned rollers. He simultaneously solved a two span system and discussed the influence on preceding web guides. He gave recommendations for prevention and tolerances of misalignment to prevent inter-span influence. Experimental data is provided.

Jones [22] specifically addressed the issue of webs wrinkling on rollers. He stated that webs wrinkling on rollers are most similar to shells buckling on a rigid support, in an outward-only mode. This rigid support is claimed to increase the buckling load by 1.73 times that for an unsupported shell. Also, presented was a model for single ring buckling with and without consideration of friction. No experimental support was provided.

An early paper concerned with thin shell buckling was that of Weingarten et al. [46]. Their work focused on the effect of internal pressurization on critical shell loading. Careful experimentation was carried out with consideration of end effects. They found that internal pressure would bring experimental buckling data up to the value predicted for instability in an un-pressurized shell. They also qualified experimentally what pressure would be required to fully stabilize the shell structure. Their conclusion was that internal pressure only limited premature buckling due to shell imperfections and that a pressurized shell would buckle at the critical load predicted for an unpressurized shell.

Experiments related to shell buckling are carried out in this dissertation. Critical information about dimensions and materials were provided by Hosford and Duncan [20]. Their paper described the manufacture and properties of modern aluminum beverage cans, including loads the cans must endure during the filling process.

A recent discussion of wrinkle elements and tension field theory as applied to thin membranes was given by Iwasa et al. [21]. The paper discussed the limitations of said theories and evaluated their performance. Special attention was given to a comparison of

tension field theory and bifurcation theory. The differences were suggested to arise from compressive stresses that remain in the membrane after wrinkling has occurred. This paper focused on the case of a circular membrane resisting a rotating hub. No direct application to web handling was discussed.

Discussions of material properties, including shear modulus, were given by both Cheng [8] and Szilard [40]. Szilard presented an expression for the shear modulus dependent on orthotropic Young's Modulus and Poisson's Ratio. The equation is not verified and presented without derivation. Cheng presented the same expression and goes on to reveal it was originally presented by St. Venant. Cheng then derived a new expression dependent on the same variables. It should be noted that both expressions reduce to the expected isotropic forms.

2.1 Relevant texts

Timoshenko and Goodier [42] provided a basis of original work and a collection of existing works of others in their "Theory of Elasticity". Also helpful was the work by Timoshenko and Gere [41] on "Theory of Elastic Stability". Beam stiffness matrices were developed in Przemieniecki's [31] "Theory of Matrix Structural Analysis". Orthotropic materials and their inclusion in analysis were discussed by Lekhnitskii [23] in "Anisotropic Plates".

Finite elements and related boundary conditions are covered in Reddy's [32] "Finite Element Method". Allen and Bulson [3] provided an insight into shell buckling. They proposed two separate buckling modes, ring and chessboard buckling. They showed that internal pressure stabilizes the shell and ring buckling, as predicted by classical analysis, may be achieved. Un-pressurized shells may buckle prematurely and assume the chessboard buckling mode. Finally, additional materials for stress analysis were presented in "Advanced Strength of Materials and Applied Elasticity" by Ugural and Fenster [43].

2.2 Summary of Current State of Wrinkling Analysis

The early contributions of Swift [39] (normal entry) and Shelton [37] (M_j=0 at misaligned roller) have led to the current developments in wrinkle prediction. Gelbach et al. [12] showed that plate buckling criteria could be linked to beam theory to predict trough formation in typical free spans, due to misaligned rollers. Good et al. [16] discussed the effects of traction, and its dependence on web velocity, on web wrinkling. The generalization of existing models for prediction of trough formation, due to a downstream misaligned roller, was carried out by Good and Beisel [4, 15]. This generalization included consideration of shear effects, tension effects, and orthotropic web properties. It extended the application of existing theories.

Prior attempts have been made to model webs after troughs have formed in them, by use of wrinkling membrane elements incorporated into FE analysis. The most commonly used wrinkle element was developed by Miller and Hedgepeth [26]. These elements were applied to a web approaching a simulated-misaligned-downstream roller by Gopal and Kedl [18]. They did not link their model to a classic instability criterion; neither did they achieve success with the wrinkling membrane elements. They did claim success in predicting the wrinkle phenomenon with a second model by using regular membrane elements but verification was limited. The later model did not link wrinkle formation to a shell buckling criterion nor did it attempt to model the web on a roller.

The most recent attempt to model wrinkle formation, due to a misaligned roller, was by Webb [45]. His model used wrinkling membrane elements in an FE analysis that

was linked to a shell buckling criterion. He achieved agreement with experimental data but only after adding the rotation required by his model to the rotations required to produce trough formation as described by Beisel [4]. The model Webb employs is not considered valid by this author, and will be discussed later. Had the model been correct, the rotations predicted by the FE analysis would have been equivalent to the observed rotations that caused wrinkles to form in the web.

2.3 Research Objectives

The research objectives of this dissertation include:

1.0 The effective prediction of trough formation due to a tapered downstream roller in a closed form solution with consideration of shear effects, tension effects, and orthotropic web properties. This method must be consistent with other cases of shear troughs and is presented along with the case of a misaligned roller.

2.0 The modeling of wrinkle phenomenon on rollers by use of wrinkling membrane elements linked to classic shell buckling criteria for the cases of both the misaligned and tapered rollers in one consistent method.

3.0 The study of boundary conditions of webs approaching crowned rollers, the study of trough formation due to crowned rollers, the modeling of wrinkle formation due to a downstream crowned roller by use of FE analysis, application of this model to other cases of machine direction wrinkles, specifically the case of a roller with an enlarged section.

From the literature survey these objectives are known to be novel. Wrinkling or web instability research has been supported by the corporate sponsors of the Web Handling Research Center since 1985, when the WHRC began conducting research. Through Input given by each sponsor, it is known that a significant economic loss occurs due to web wrinkling [2].

CHAPTER III

Prediction of Troughs Due to Shear

3.0 Modeling Webs as Beams (Deflection Due to Taper)

To effectively reach the goal of predicting instabilities in webs, many steps must be undertaken and ultimately combined. The first of these steps is the ability to accurately describe the behavior of a web encountering a contoured roller. The case to be studied is that of a downstream tapered roller.

Tapered rollers are commonly encountered in web handling. The process of roller manufacture will almost certainly result in a roller with a slight taper. These tapered rollers are produced unintentionally and their use in web lines will be detrimental. Machining techniques involving feedback could help resolve this problem but economy prevents such measures. If the effect of taper is better understood then guidelines and tolerances may be used to evaluate roller manufacturing processes as well as the quality of the rollers produced.

A tapered roller is defined as a roller with a linearly varying radius across its width. A diagram of a tapered roller is shown below in Figure 1.

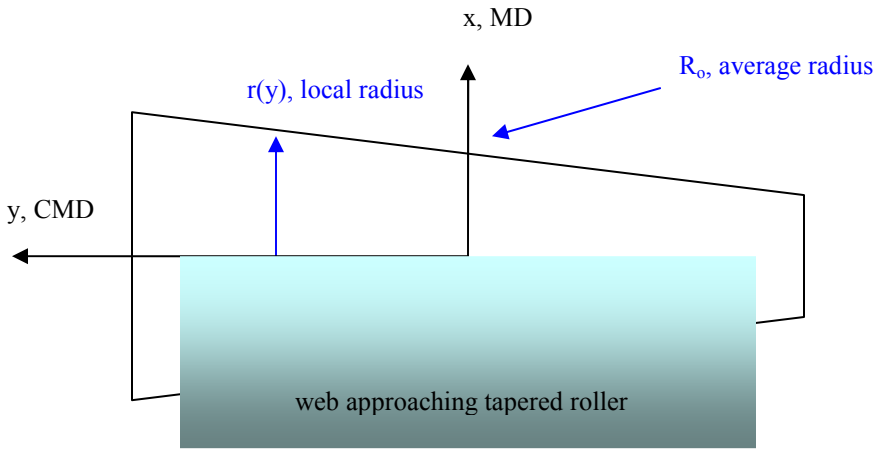

Figure 1 – Tapered Roller Profile

As a web comes into contact with a tapered roller, it is assumed to stick to the surface of the roller and travel with the same speed as the roller surface while in contact with the roller. The radius of the roller at any point across its width is:

$$r(y) = my + R_o \tag{1}$$

where m is the slope of the roller in terms of change in radial in./ in. width. The velocity of the web is:

$$V(y) = r(y)\omega = (my + R_o)\omega \tag{2}$$

where ω is the angular velocity of the roller. The average web velocity may be found using the average roller radius.

$$V_{avg} = R_o\omega \tag{3}$$

The local velocity of the web may now be related to the strain at that location as seen in eq. (4).

$$\varepsilon(y) = \frac{V(y) - V_{avg}}{V_{avg}} = \frac{r(y) - R_o}{R_o} \tag{4}$$

A uniaxial version of Hook's Law has been commonly used in web spans to estimate the MD stress as in eq. (5).

$$\sigma(y) = E_x \varepsilon(y) = \frac{E_x m y}{R_o} \tag{5}$$

Integrating the stress multiplied by the incremental area and its y position across the width of the web yields the total moment acting on the web at the tapered roller.

$$M_{tot} = \int_{\frac{-W}{2}}^{\frac{W}{2}} \sigma(y) \cdot t \cdot y \cdot dy = \int_{\frac{-W}{2}}^{\frac{W}{2}} \frac{E_x m t y^2}{R_o} \cdot dy = \frac{m E_x t W^3}{12 R_o} \tag{6}$$

Equation (6) gives the total moment developed at the tapered roller in terms of roller taper (m), average roller radius (R_o), Young's Modulus (E_x), web thickness (t), and web width (W).

In modeling a web span as a beam it is assumed that the web is planar before troughs form in the span and that linear elastic theory may be used. The positive sign conventions are shown below in Figure 2.

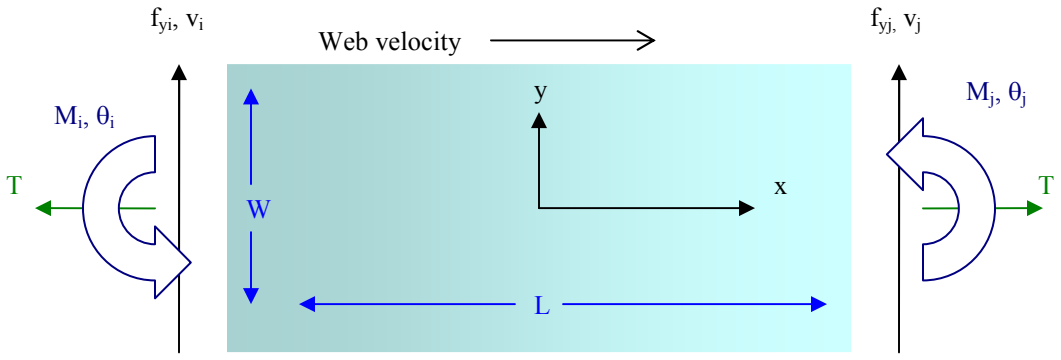

Figure 2 – Positive Sign Conventions for a Beam

As seen in the above figure, the upstream boundary conditions are denoted with the subscript $_i$, and the downstream end of the web is denoted with the subscript $_j$. The other terms are; shear force ($f_{yi,j}$), moment ($M_{i,j}$), web deflection ($v_{i,j}$), end rotation ($\theta_{i,j}$), web line tension (T), span length (L), and web width (W).

The boundary conditions imposed on the web span are as follows. A web guide keeps the location of web entry constant, therefore, we may arbitrarily set $v_i = 0$. Shelton [37] had previously shown the importance of normal entry in application to webs which suggests we set dv/dx = 0, and from elementary mechanics [31] we have:

$$\theta_{i,j} = \frac{\partial v}{\partial x} + \gamma_{xy} = -\frac{f_{yj}}{GA_s} \tag{7}$$

Where G is the shear modulus and A_s is the area reacting shear, which for a rectangle is:

$$A_s = \frac{5}{6}A = \frac{5}{6}tW \tag{8}$$

The fourth boundary condition is the moment at the tapered roller, as given by equation (6), and due to the coordinates and sign conventions chosen, $M_j = -M_{tot}$.

$$M_j = \frac{-mE_x tW^3}{12R_o} \tag{9}$$

With the boundary conditions determined, beam theory may now be applied to the web span. Equation (10) is a beam stiffness matrix derived from Przemieniecki [31] that incorporates both shear and tension effects as well as orthotropic material properties.

$$\begin{pmatrix} f_{yj} \\ M_i \\ f_{yj} \\ M_j \end{pmatrix} = \begin{bmatrix} \frac{12E_xI}{L^3(1+\phi)}+\frac{6T}{5L} & \frac{6E_xI}{L^2(1+\phi)}+\frac{T}{10} & \frac{-12E_xI}{L^3(1+\phi)}-\frac{6T}{5L} & \frac{6E_xI}{L^2(1+\phi)}+\frac{T}{10} \\ \frac{6E_xI}{L^2(1+\phi)}+\frac{T}{10} & \frac{E_xI(4+\phi)}{L(1+\phi)}+\frac{2TL}{15} & \frac{-6E_xI}{L^2(1+\phi)}-\frac{T}{10} & \frac{E_xI(2-\phi)}{L(1+\phi)}-\frac{TL}{30} \\ \frac{-12E_xI}{L^3(1+\phi)}-\frac{6T}{5L} & \frac{-6E_xI}{L^2(1+\phi)}-\frac{T}{10} & \frac{12E_xI}{L^3(1+\phi)}+\frac{6T}{5L} & \frac{-6E_xI}{L^2(1+\phi)}-\frac{T}{10} \\ \frac{6E_xI}{L^2(1+\phi)}+\frac{T}{10} & \frac{E_xI(2-\phi)}{L(1+\phi)}-\frac{TL}{30} & \frac{-6E_xI}{L^2(1+\phi)}-\frac{T}{10} & \frac{E_xI(4+\phi)}{L(1+\phi)}+\frac{2TL}{15} \end{bmatrix} \cdot \begin{pmatrix} v_i \\ \theta_i \\ v_j \\ \theta_j \end{pmatrix} \tag{10}$$

where ϕ is an introduced shear parameter defined by:

$$\phi = \frac{12E_xI}{GA_sL} \tag{11}$$

and I is the area moment of inertia given by:

$$I = I_z = \frac{tW^3}{12} \tag{12}$$

Using equation (10) and the boundary conditions mentioned on the previous page; v_i=0 and equations (7) and (9), a model for describing the behavior of a web encountering a tapered roller may be developed. Expanding the 3rd row in equation (10) and solving for f_{yj} gives the following expression

$$f_{yj} = \frac{-6GA_s}{L} \cdot \frac{10E_xI + TL^2(1+\phi)}{60E_xI + L^2(T-5GA_s)(1+\phi)} \tag{13}$$

Similarly, expanding the 4th row of equation (10) yields:

$$f_{yj} = \frac{-GA_s}{L} \cdot \frac{10L^2(1+\phi)M_j + [60E_xI + TL^2(1+\phi)]v_j}{60E_xI + TL^2(1+\phi)} \tag{14}$$

Equations (13) and (14) may be set equal and solved for v_j, if equation (9) is used for the moment, the result may be solved for v_j.

$$v_j = \frac{mE_xtW^3}{6R_o} \cdot \frac{-60E_xI + L^2(5GA_s - T)(1+\phi)}{[60E_xI + TL^2(1+\phi)](T+GA_s)} \tag{15}$$

Equation (15) provides an expression for the lateral steering of a web due to a downstream tapered roller. By following a similar procedure, the shear force that causes this lateral steering may be found. Again, by expanding the 3rd row of the stiffness matrix but now solving for v_j yields:

$$v_j = \frac{-Lf_{yj}}{6GA_s} \cdot \frac{60E_xI + L^2(T - 5GA_s)(1+\phi)}{10E_xI + TL^2(1+\phi)} \tag{16}$$

Expanding the 4th row of the matrix and solving for v_j:

$$v_j = \frac{-L}{GA_s} \cdot \frac{10LGA_s(1+\phi)M_j + [60E_xI + TL^2(1+\phi)]f_{yj}}{60E_xI + TL^2(1+\phi)} \tag{17}$$

If equations (16) and (17) are equated, equation (9) is substituted for moment, and equation (12) is substituted for the area moment of inertia, the shear force may be found.

$$f_{yj} = \frac{mE_xtW^3}{LR_o} \cdot \frac{GA_s\left[10E_xI + TL^2(1+\phi)\right]}{[60E_xI + TL^2(1+\phi)](T + GA_s)} \tag{18}$$

Equations (18) and (15) yield the shear force generated at a downstream taper roller and the resulting deflection of the web, respectively, in terms of web properties and web line conditions. One factor limiting the use of equations (15) and (18) is the possible development of a "slack" edge in the web. A slack edge occurs when a portion of the web develops zero web line tension. When the MD stress due to moment becomes greater and opposite to the MD stress due to web line tension, zero web line tension will develop at that location in the web line. The onset of a slack edge due to a tapered roller is given by:

$$T_{slack} = \frac{mE_xtW}{288R_o} \tag{19}$$

The above equations require Shear Modulus as an input. These equations may also be used for orthotropic webs, requiring the use of orthotropic material properties. Below are two equations for Shear Modulus in terms of Young's Modulus and Poisson's Ratio. The first was presented by Szilard [40] without derivation, which was originally proposed by St. Venant, as Cheng [8] reveals.

$$G = \frac{\sqrt{E_x E_y}}{2(1+\sqrt{\upsilon_{xy}\upsilon_{yx}}} \tag{20}$$

Another expression was presented by Cheng [8] and was supported by a derivation.

$$G = \frac{E_x E_y}{E_x(1+\upsilon_{yx}) + E_y(1+\upsilon_{xy})} \tag{21}$$

The validity of these expressions is not considered here, perhaps the five material properties associated with a web in plane stress conditions should be considered entirely independent. These expressions are convenient in that the measurement of shear modulus in webs is inhibited by the subject of this dissertation, wrinkling. If orthotropic material properties are required in modeling another useful relation regarding inputs is Maxwell's Reciprocal Theory.

$$\frac{\upsilon_{xy}}{E_x} = \frac{\upsilon_{yx}}{E_y} \tag{22}$$

3.1 Experimental Verification of Deflection due to Taper

An experiment was designed and constructed to verify the deflections predicted by equation (15). Initially, these tests were to be conducted with the web remaining planar. This constraint required the use of extremely slight tapers. Tapers on the order of 0.0005 radial in. / in. of width were required for use with the 92 ga polyester tested. In order to conduct these experiments, tapered rollers needed to be constructed and accurately qualified.

These slight tapers were beyond the capabilities of typical taper cutting attachments on the lathes available for use, so an alternative method was employed. By holding one end of the roller in the lathe chuck and the other in the tail stock, slight tapers may be produced by small misalignments of the tailstock. The process was iterative with an evaluation of the roller after each pass and a corresponding readjustment of the tailstock. When the rollers were considered to be "close enough" to their target taper, they were removed from the lathe and qualified for their actual taper.

The tapered rollers were qualified on a special piece of equipment developed in house by the current author at the WHRC named the "roll profiler". The apparatus consisted of two Keyence laser micrometers mounted on the tool post of an old lathe bed. The micrometers could then be moved along the roller axis while recording roller diameter. The position along the roller axis was monitored with a yo-yo potentiometer. Both readings were simultaneously recorded on a computer equipped with a National

Scientific data acquisition board and a program written in Labview. The setup is shown below in Figure 3.

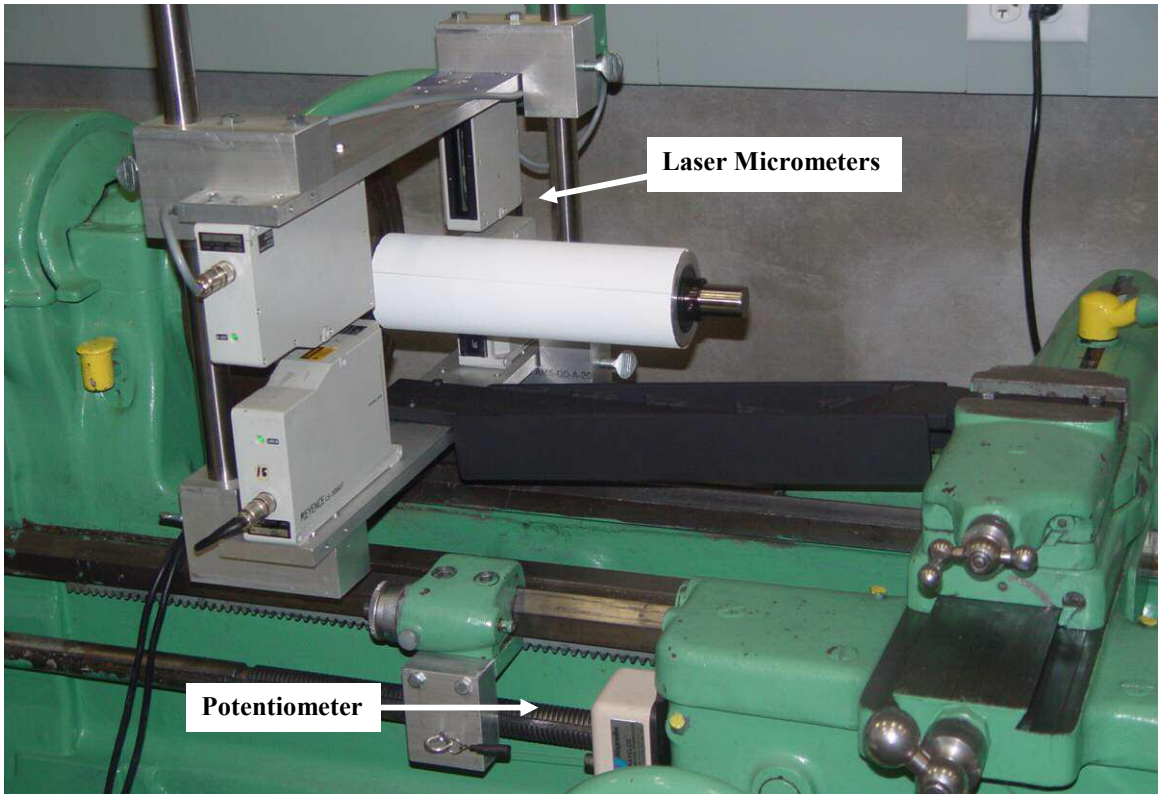

Figure 3 – Roller Profiler

An example output from the roller profiler is shown below in Figure 4.

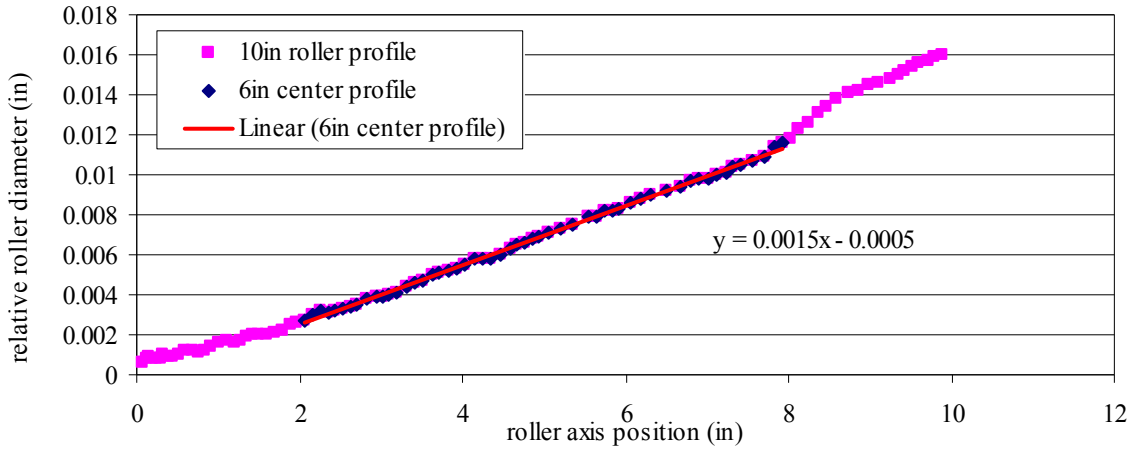

Figure 4 – Sample Output for Taper Qualification

Imperfections in the machining process can be clearly seen above in Figure 4. The taper is not uniform or even symmetric from end to end of the roller. This is likely caused by flexure of the roller shell while being machined. The clamping of the roller may be loosely described as fixed – pinned beam boundary conditions, allowing more rotation at one end of the roller than at the other. In determining the taper of the roller, it is important to consider only the portion of the roller that is in contact with the web. In this case a 6" wide web was used. It will be shown that deflections are less than 0.1" in these experiments. Therefore, only the central 6" portion of the roller was considered in determining the taper of a roller. The dark blue diamonds in Figure 4 show this central 6" portion of the roller. The red line is a linear fit to this region of the roller, the slope of which is used to determine the radial taper of the roller.

A total of 8 rollers were produced with tapers of 0.00028, 0.00056, 0.00066, 0.00075, 0.0010, 0.00113, and 0.00144 (radial in. / in. roller width). The profiles of the central 6" portions of these rollers are plotted below in Figure 5 and Figure 6.

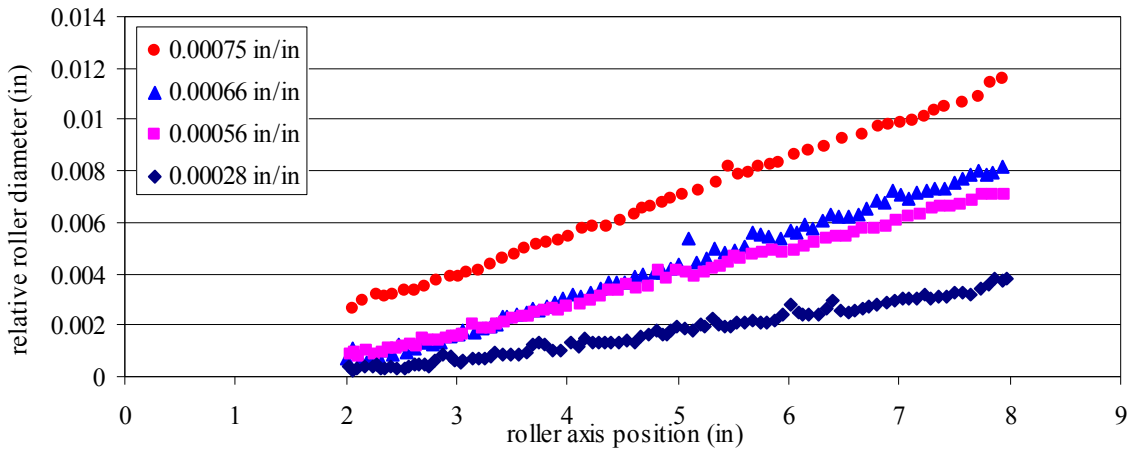

Figure 5 – Low Taper Roller Profiles

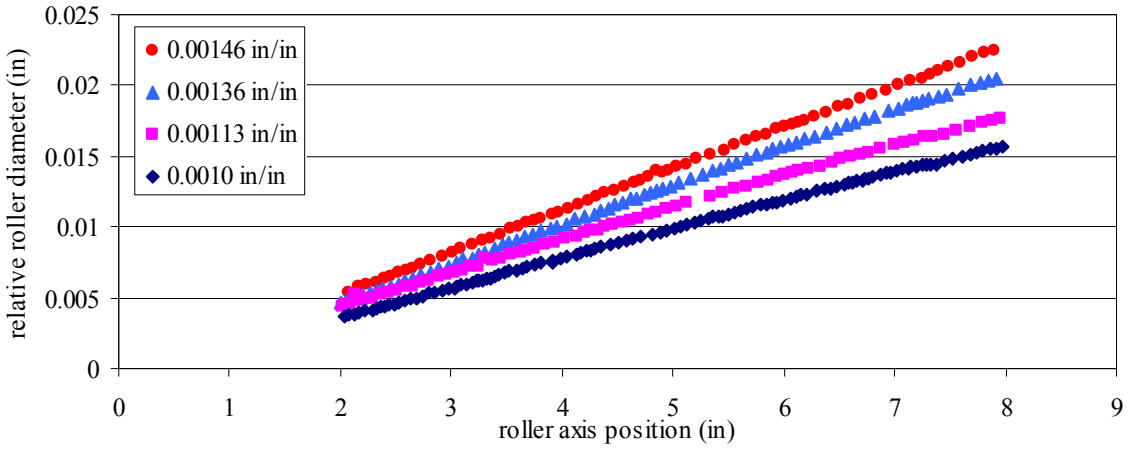

Figure 6 – High Taper Roller Profiles

With the tapered rollers qualified and in hand, an experiment was designed to measure the deflection of the web due to a downstream tapered roller. The measurement apparatus consisted of a frame to hold rollers parallel at four different web span lengths, while maintaining a constant angle of wrap at each span length. The tapered rollers, or any contoured roller, may be inserted downstream of a cylindrical upstream roller. In order to measure deflection, two Keyence laser micrometers were used. One was placed in the web span preceding the test span, and the other was placed in the post span. Since normal entry requires the web to enter a roller perpendicular to the roller axis, and the assumption was made that there was no slippage between the web and roller, the locations of the micrometers in the pre and post spans were not critical.

The laser micrometers required the use of an opaque web. A polyester web, 6" wide, 92 ga. in thickness, embedded with titanium dioxide, named Melinex 377 (a DuPont film) was used. The Young's Modulus was measured to be 712,000 psi in an axial stretch test. The Poisson's Ratio was assumed to be 0.3, and the web was

considered to be isotropic. The axial stretch test just mentioned requires a web length of 50 feet to be subjected to various levels of tension down its length while simultaneously recording the resulting deformations. The data from this test is used to construct charts of stress vs. strain where the slope determines the MD Young's modulus. This test was developed in house at the WHRC to minimize grip effects that have been observed in modulus tests on films conforming to the ASTM specification D882 [1]. The results of the stretch test for the 92 ga polyester are shown in Figure 7. The below data are the results of 5 independent tests with error bars representing the maximum and minimum values measured. As expected, the polyester begins to leave the realm of linear elasticity at approximately 7000 psi.

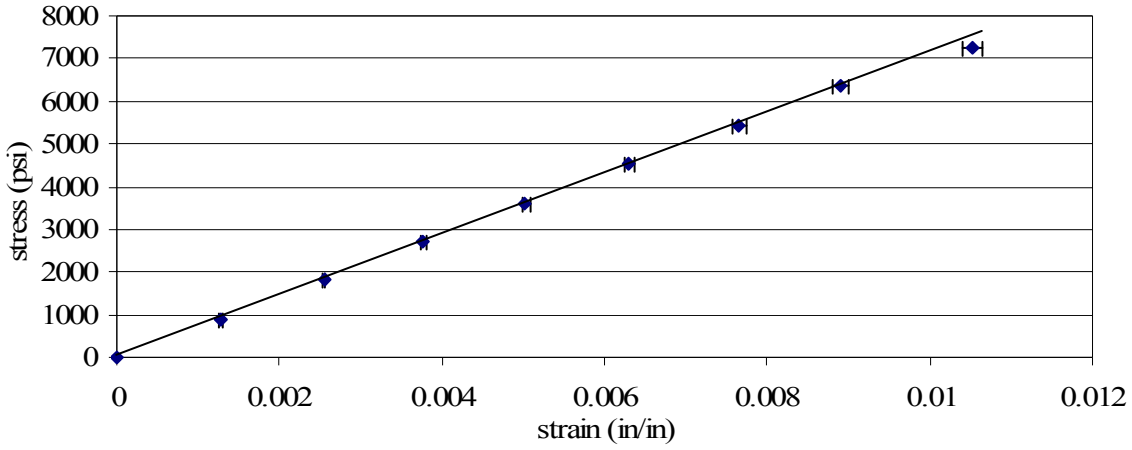

Figure 7 – Data From Stretch Test, 92 ga Polyester, E_x = 712000 psi

Web deflection was measured for three different web span lengths, five different web line tension levels, and four different roller tapers. The tension was monitored by use of load cells located just prior to entry to the test span and controlled by use of a magnetic break. Web speed was low and the rollers in the test span were covered with a

high traction tape to ensure the assumed no-slip condition between the web and rollers. The experimental set-up is shown below in Figure 8.

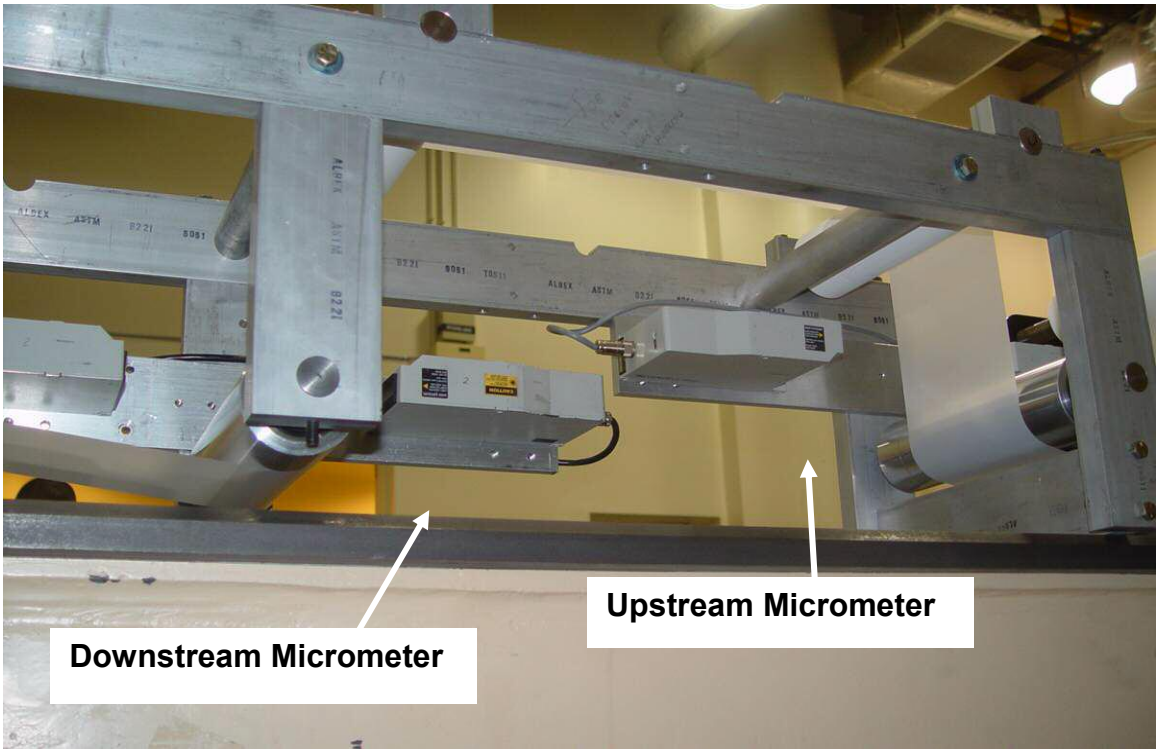

Figure 8 – Apparatus for Deflection Experiment

The deflection data obtained form the experiment depicted in Figure 8 were plotted against the values for deflection predicted by equation (15) and is presented below in Figure 9 - Figure 13. The data were plotted as open and filled triangles. The filled triangles represent a planar web, while the open triangles indicate the presence of troughs in the test span. Each data point was obtained by first running the web over a cylindrical roller to determine the normal position of the web in the machine. Then a tapered roller was exchanged for the downstream cylindrical roller. Once the web reached steady state, the position of the web was recorded. The slope of the taper was then reversed in the machine and another position measurement was recorded. This

reversal of the taper served to reduce the possible effects of web camber on the experiment.

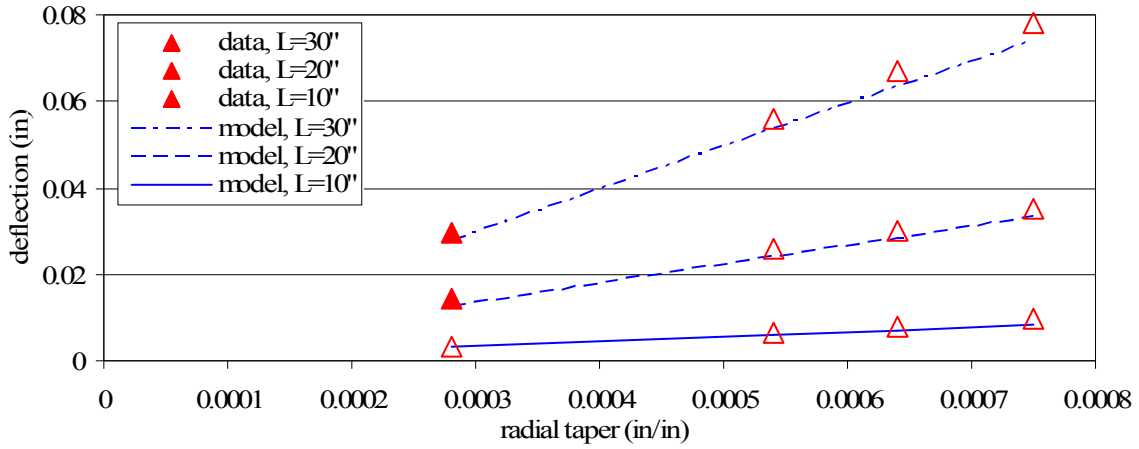

Figure 9 – Deflection Due to Taper, T = 10lbs

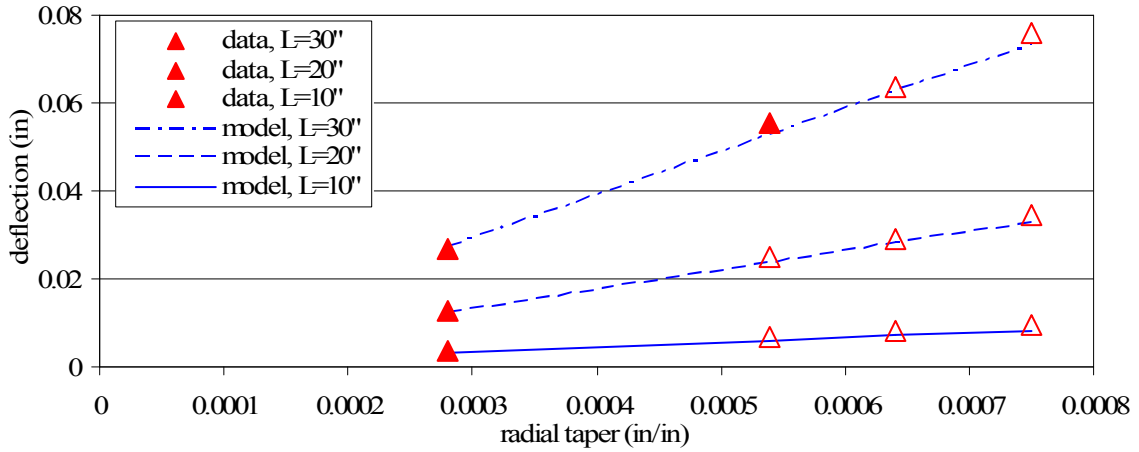

Figure 10 – Deflection Due to Taper, T = 15lbs

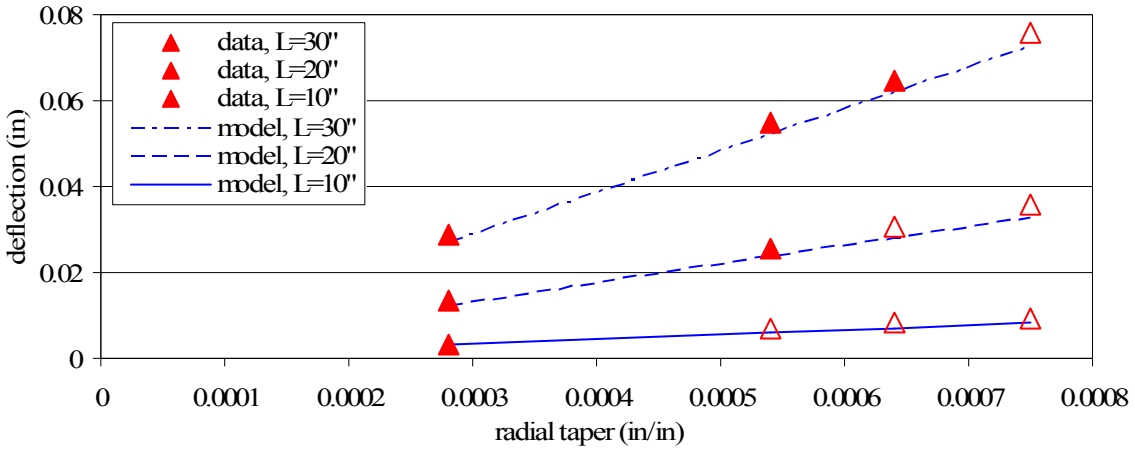

Figure 11 – Deflection Due to Taper, T = 20lbs

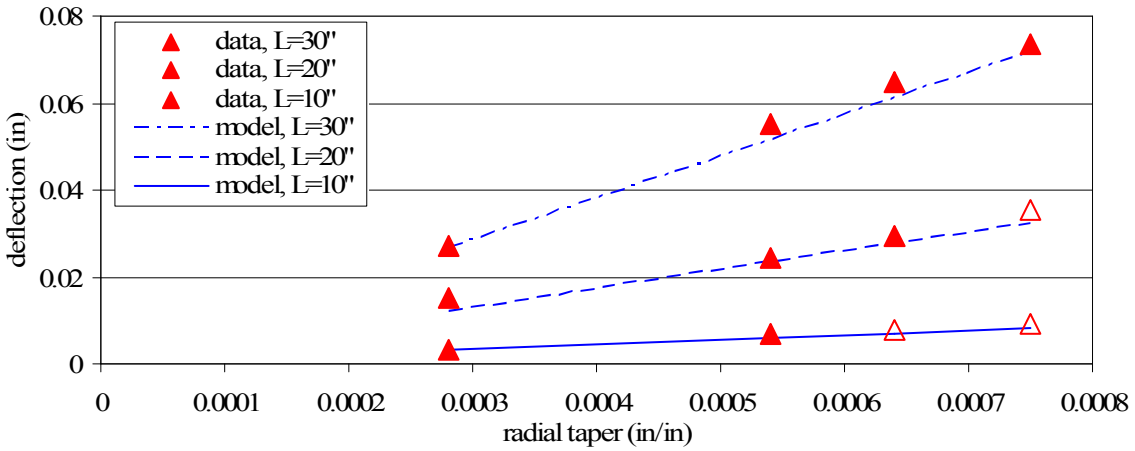

Figure 12 – Deflection Due to Taper, T = 25lbs

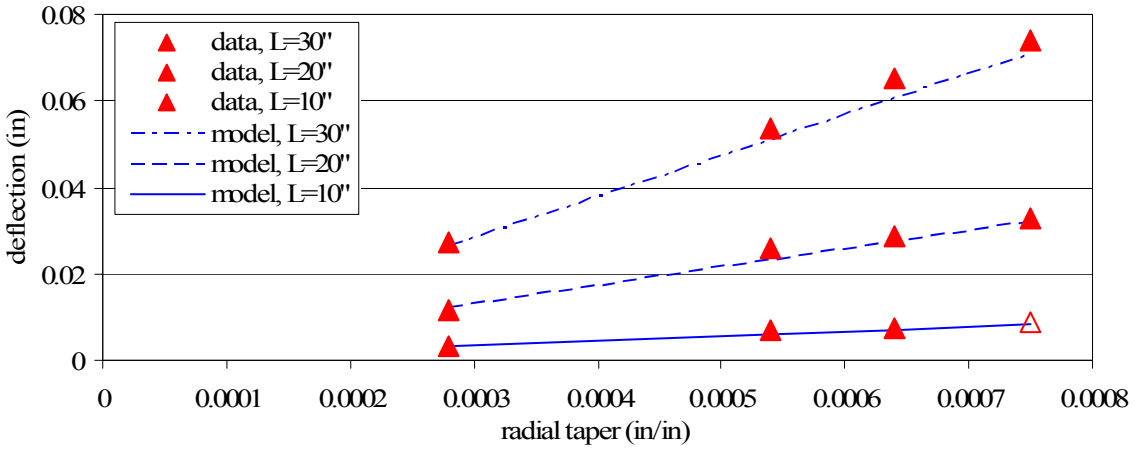

Figure 13 – Deflection Due to Taper, T = 30lbs

The preceding graphs display agreement between the proposed model, equation (15), and experimental values over all conditions tested. The conclusion was reached that a web can effectively be modeled as a beam over a typical range of web line parameters, providing a convenient closed form expression for deflection of a web due to a downstream tapered roller. Two points were worthy of note in the experimental data. In comparing values from the data taken at different tension levels, the effect of web line tension on deflection appears to be small. Tension did however seem to stabilize the web from a buckling point of view. Most data points taken at 30 lbs web line tension were planar as compared to the mostly troughed data points taken at 15 lbs tension.

The other point is that the presence of troughs in the test span did not affect the steering of the web. Equation (15) provided accurate deflection predictions even when troughs were present in the test span. This was not necessarily anticipated since once troughs form in the web span, the web takes on an out-of-plane component to its geometry. This second point increases the generality of equation (15) by suggesting it may provide an estimate of lateral steering even when troughs are present in a web encountering a downstream tapered roller.

3.2 Trough Formation in Web Spans; Instability Criteria

In the previous sections, webs have been successfully modeled as beams. The next step in modeling instabilities in webs was the development of a buckling criterion for trough formation in a free span. Timoshenko and Gere's [41] plate buckling criterion was employed but with orthotropic material properties included in this analysis. The guidelines for the orthotropic material properties were found in Lekhnitskii [23]. The positive sign conventions used by both Timoshenko and Gere [41] and Lekhnitskii [23] are given in Figure 14.

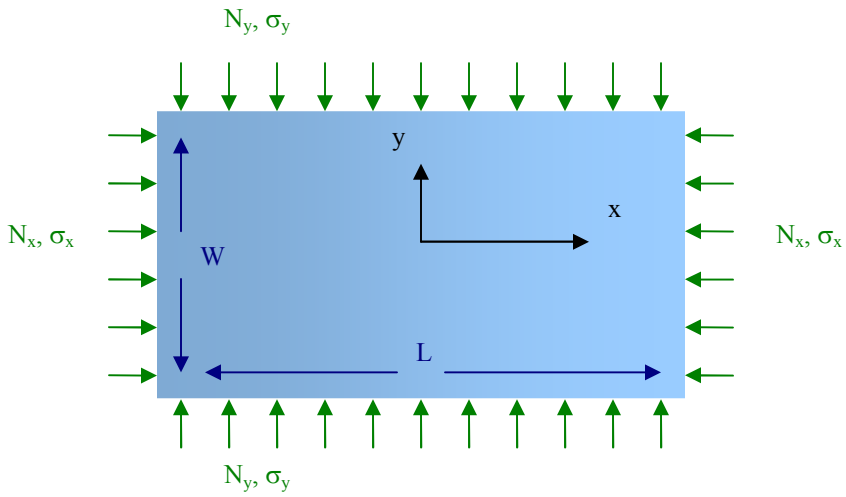

Figure 14 – Positive Sign Conventions for Loaded Plate

N_x and N_y represent the forces acting per unit length along the edge of the coupon. It should be noted that the forces are positive when compressing the coupon. The equilibrium equation for this rectangular coupon-shaped plate was presented by Lekhnitskii [23].

$$D_1 \frac{\partial^4 w}{\partial x^4} + 2D_3 \frac{\partial^4 w}{\partial x^2 \partial y^2} + D_2 \frac{\partial^4 w}{\partial y^4} + N_x \frac{\partial^2 w}{\partial x^2} + N_y \frac{\partial^2 w}{\partial y^2} = 0 \qquad (23)$$

Where w is the out of plane deformation and D_1, D_2, and D_3 are defined by the following equations:

$$D_1 = \frac{E_x t^3}{12(1-\upsilon_{xy}\upsilon_{yx})} \tag{24}$$

$$D_2 = \frac{E_y t^3}{12(1-\upsilon_{xy}\upsilon_{yx})} \tag{25}$$

$$D_3 = D_1\upsilon_{xy} + 2D_k \tag{26}$$

$$D_k = \frac{Gt^3}{12} \tag{27}$$

Poisson's Ratio can be defined from the following constitutive relations:

$$\varepsilon_x = \frac{\sigma_x}{E_x} - \frac{\upsilon_{yx}\sigma_y}{E_y} \tag{28}$$

$$\varepsilon_y = \frac{\sigma_y}{E_y} - \frac{\upsilon_{xy}\sigma_x}{E_x} \tag{29}$$

$$\gamma_{xy} = \frac{\tau_{xy}}{G} \tag{30}$$

The general form of the solution to the equilibrium equation is also presented by Lekhnitskii [23].

$$w = A_{kn}\sin\left(\frac{k\pi x}{L}\right)\sin\left(\frac{n\pi y}{W}\right) \tag{31}$$

If the proper partial derivatives are taken of equation (31) and then plugged into equation (23), the following result is obtained.

$$D_1\left(\frac{k\pi}{L}\right)^4 + 2D_3\left(\frac{kn}{LW}\right)^2\pi^4 + D_2\left(\frac{n\pi}{W}\right)^4 = N_x\left(\frac{k\pi}{L}\right)^2 + N_y\left(\frac{n\pi}{W}\right)^2 \tag{32}$$

Equation (32) can be written in terms of stress by dividing through by t, which is web thickness. In addition, multiplying through by L^2/π^2 leads to the following result:

$$\sigma_x k^2 + \sigma_y \left(\frac{Ln}{W}\right)^2 = \frac{\pi^2}{t}\left[D_1 \frac{k^4}{L^2} + 2D_3\left(\frac{kt}{W}\right)^2 + D_2 L^2\left(\frac{n}{W}\right)^4\right] \tag{33}$$

Most practical applications in the web handling industry require tension in the machine direction. The presence of machine direction tension excludes the possibility of troughs forming oriented with the cross machine direction in a free span. This sets our half wave number k equal to 1. Another term is now introduced for algebraic simplicity, an equivalent stress.

$$\sigma_e = \frac{\pi^2 \sqrt{D_1 D_2}}{L^2 t} \tag{34}$$

Making use of this expression and solving equation (33) yields:

$$\sigma_y = \frac{-W^2}{L^2 n^2}\left(\sigma_x - \sigma_e \sqrt{\frac{D_1}{D_2}} - 2\sigma_e \frac{L^2 n^2}{W^2} \cdot \frac{D_3}{\sqrt{D_1 D_2}} - \sigma_e \frac{L^4 n^4}{W^4}\sqrt{\frac{D_2}{D_1}}\right) \tag{35}$$

Equation (35) gives the CMD stress required to buckle the web span for a particular half wave number (n).

Determination of the half wave number can be a tedious process and is not included here. Shelton [33] first proposed the idea of allowing for a continuous half wave number in web spans. Timoshenko [41] gives an example of this for the wave number in cylindrical shells in compression. This concept will now be employed. If the partial derivative of σ_y is taken with respect to n and the result is set to equal zero, the resulting expression may be solved for an n that requires the minimum compressive force. The only positive and real root is given by:

$$n = \frac{W}{L\sqrt{\pi}} \cdot \sqrt[4]{\frac{\pi^2 D_1 - \sigma_x t L^2}{D_2}} \tag{36}$$

For typical web handling materials and conditions, it can be shown that $\pi^2 D_1 << \sigma_x t L^2$ (typically 2-3 orders of magnitude). Thus, neglecting the first term, substituting for D_2, and realizing $\sigma_x = -\sigma_{md}$, results in the following expression:

$$n = W\sqrt{\frac{2}{\pi L t}} \cdot \sqrt[4]{\frac{3\sigma_{md}\left(1 - \upsilon_{xy}\upsilon_{yx}\right)}{E_y}} \tag{37}$$

Equation (37) may now be substituted into equation (35) yielding:

$$\sigma_{ycr} = \frac{2\pi}{L^2 t} \cdot \frac{\pi^2 D_1 \sqrt{D_2} + L^2 t \sigma_{md} \sqrt{D_2} + \pi D_3 \sqrt{\pi^2 D_1 + L^2 t \sigma_{md}}}{\sqrt{\pi^2 D_1 + L^2 t \sigma_{md}}} \tag{38}$$

In comparing the terms in equation (38), some simplifications may again be made. For typical web handing conditions, we can neglect terms one and three in comparison to term two in the numerator and the first term in the radical in the denominator is small in comparison to the second term. Also, the definition for D_2 is applied resulting in:

$$\sigma_{ycr} = \frac{t\pi}{L}\sqrt{\frac{\sigma_{md} E_y}{3(1 - \upsilon_{xy}\upsilon_{yx}}} \tag{39}$$

Equation (39) provides us with a simple expression to predict the compressive stress that will result in buckling of a tensioned coupon loaded across its length. If equation (39) is applied to webs, it should yield the compressive stress required in a free web span that will result in troughs forming in that span.

In the case of webs experiencing a net lateral steering force at a downstream roller, the source of the required compressive must be determined. In the case of shear troughs, the shear stress at the downstream roller combined with the tension induced machine direction stress, τ and σ_{md} respectively, cause a compressive second principle stress.

$$\sigma_2 = \frac{\sigma_{md}}{2} - \sqrt{\left(\frac{\sigma_{md}}{2}\right)^2 + \tau^2} \tag{40}$$

In addition, a relation for the direction of the second principle stress is given by:

$$\alpha = \frac{1}{2}\tan^{-1}\left(\frac{2\tau}{\sigma_{md}}\right) \tag{41}$$

In the experimental cases studied, this angle was small and therefore, σ_{cmd} was approximated to be equal to σ_2. This assumption may not be valid for extremely short spans. The induced compressive CMD stress, equation (40), may now be equated to the critical compressive stress required to buckle the web, equation (39), and solved for the critical shear stress.

$$\tau_{cr} = \sqrt{\left(\frac{\pi}{L}\right)^2 \frac{tE_yT}{3W\left(1-\upsilon_{xy}\upsilon_{yx}\right)}} + \frac{\pi}{L}\sqrt{\frac{E_yT^3}{3tW^3\left(1-\upsilon_{xy}\upsilon_{yx}\right)}} \tag{42}$$

The shear stress in equations (40), (41) and (42) may be calculated from one of the following two expressions.

$$\tau_{avg} \approx \frac{f_{yj}}{tW} \qquad \text{(“short” plates)} \tag{43}$$

$$\tau_{max} \approx \frac{3}{2}\cdot\frac{f_{yj}}{tW} \text{(rectangular cross section beams)} \tag{44}$$

Whether equation (43) or (44) should be used is based on the expected shear stress distribution in the web. Experimentation with a particular class of shear troughs may suggest the use of one equation over the other. However, if a conservative analysis is needed the maximum shear stress should be used. In the next few sections, this instability criterion for trough formation in webs experiencing shear forces will be applied consistently to two common causes of shear troughs. Those cases are misaligned and tapered downstream rollers.

3.3 Troughs Due to Misaligned Rollers

Roller alignment has always been a critical issue in the web handling industry. All web lines need to be "trammed" which is the process of aligning all the rollers such that their axis are parallel. Good roller alignment is required to keep the web positioned laterally in web processes but also to prevent trough and wrinkles from forming which interfere with those processes. Roller alignment can be a challenging and time consuming process. Improved guidelines and the ability to set realistic tolerances for this procedure would be helpful to web handling.

The most recent works concerned with roller misalignment come from Beisel [4] and Webb [45]. The work by Webb is concerned with wrinkle formation and will be discussed more in the next chapter. Earlier models had been proposed by Good et al. [16] and Shelton [33]. The earlier efforts did not include tension effects, shear effects, or consideration of orthotropic material properties. The model proposed by Beisel [4] does include these additions and will be presented here for completeness. Additionally, one of the current goals is to show that all shear troughs may be modeled with one consistent method, with boundary conditions representative of each particular case. Therefore, the same method of analysis will be applied to troughs due to misaligned rollers in this section and to tapered rollers in the next.

Similar to the previous deflection experiments with tapered rollers, the misaligned roller will be modeled as a beam with conventions as in Figure 2. The beam stiffness

matrix, equation (10), will be used to describe the behavior of the web. For the case of the downstream misaligned roller, the boundary conditions are:

$$v_i = 0 \tag{45}$$

$$\theta_i = \frac{f_{yj}}{GA_s} \tag{46}$$

$$M_j = 0 \tag{47}$$

$$\theta_j = \theta_{misaligned\_roller} \tag{48}$$

The first condition is due to the upstream web guide holding an arbitrary but constant entry point which is set to zero. The rotation at the upstream roller is due to shear deformation. The zero moment at the downstream roller was proposed by Shelton [37] and others. The rotation of the downstream end of the beam will equal the angle of roller misalignment.

The boundary conditions in equations (45-48) are applied to the stiffness matrix of equation (10). The 3rd and 4th rows of equation (10) may be expanded and solved for v_j. The resulting two equations may then be set equal and solved for the steering or shear force developed at the misaligned roller.

$$f_{yj} = \frac{GA_s\left[240E_x{}^2I^2 + 3T^2L^4(1+\phi) + 8E_xITL^2(13+3\phi)\right]}{240E_x{}^2I^2 + 2TL^4(2GA_s + T)(1+\phi) + 8E_xIL^2\left[15GA - T(2-3\phi)\right]} \cdot \theta_j \tag{49}$$

Similarly, the 3rd and 4th rows of equation (10) may be solved for f_{yj}. If the resulting equations are equated, the result may be solved for the deflection of the web due to a misaligned roller.

$$v_j = \frac{L}{3} \cdot \frac{720E_x{}^2I^2 + 4L^2E_xI\left[15GA_s(40+\phi)+3T(6+\phi)\right]+\left(T^2L^4+8GA_sTL^4\right)(1+\phi)}{240E_x{}^2I^2+8E_xIL^2\left[15GA_s-T(2-3\phi)\right]+TL^4(T+2GA_s)(1+\phi)} \cdot \theta_j \qquad (50)$$

In order to predict instability in web approaching a downstream misaligned roller, the equations describing the behavior of the web must be linked to the instability criterion developed in equation (39). In the case of shear troughs, equation (39) was set equal to the compressive 2nd principle stress, equation (40), and the result was solved for the critical shear stress, equation (42). Equation (42) may now be equated to the shear stress developed due to the shear force at the misaligned roller through the use of equation (43). Subsequent substitution of equation (49) for shear force results in an expression for critical rotation of a downstream misaligned roller, which will cause troughs to form in a free web span.

$$\theta_{cr} = bh\frac{240E_x{}^2I^2+TL^4(2GA_s+T)(1+\phi)+8E_xIL^2\left[15GA_s-T(2-3\phi)\right]}{GA_s\left[240E_x{}^2I^2+3T^2L^4(1+\phi)+8E_xITL^2(13+3\phi)\right]}\sqrt{\left(\frac{\pi}{L}\right)^2\frac{tET}{3W(1-\upsilon_{xy}\upsilon_{yx})}}+\frac{\pi}{L}\sqrt{\frac{T^3E}{3tW^3(1-\upsilon_{xy}\upsilon_{yx})}} \qquad (51)$$

Equation (51) was developed with an assumption of uniform or average shear stress distribution. If a maximum value of shear stress is desired and a parabolic distribution is assumed then:

$$\theta_{cr,\tau_{max}} = \frac{2}{3}\theta_{cr,\tau_{avg}} \qquad (52)$$

Equation 50 was compared to experimental data taken over a range of typical web line conditions, by varying span length at different tensions. The material used in testing was 6" wide 92 gauge clear polyester. The polyester was isotropic with a Young's Modulus of E_x = 725000 psi. The Poisson's Ratio was assumed to be ν = 0.3. More

details related to these experiments were given by Beisel in [4]. He studied the effect of the assumed Poisson's ratio on the model, concluding that Poisson's Ratio has little impact on the model. He also gives statistics for the experimental data.

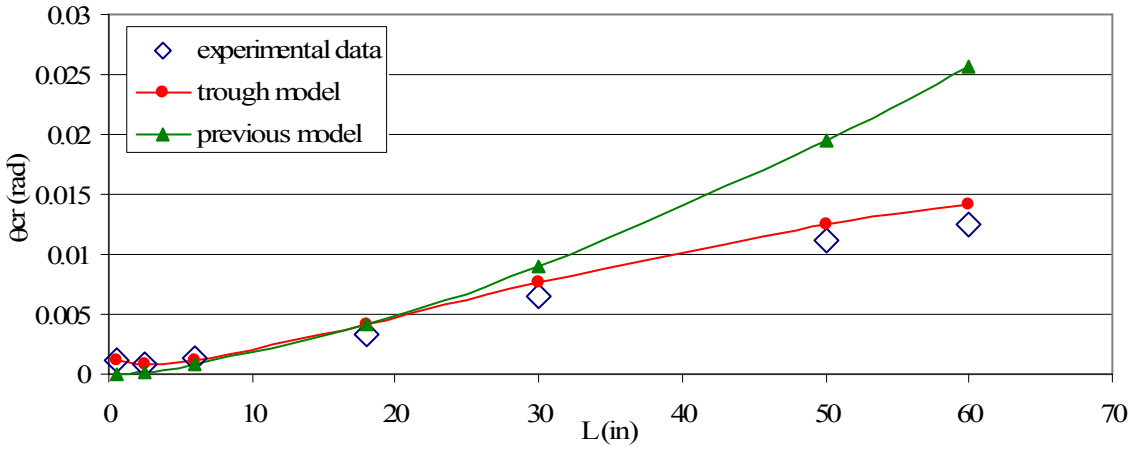

Figure 15 – Troughs Due to Misalignment, Polyester, T = 6.3 lbs

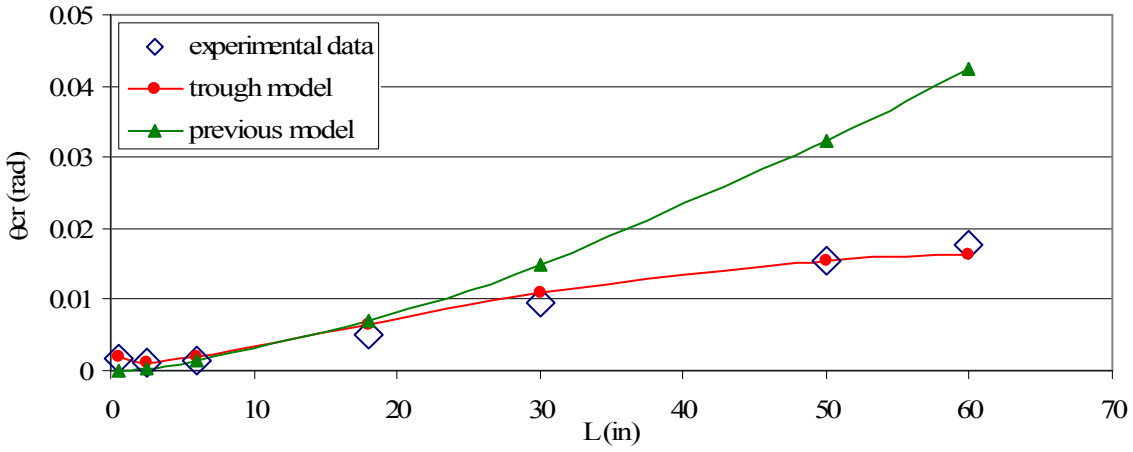

Figure 16 – Troughs Due to Misalignment, Polyester, T = 12.3 lbs

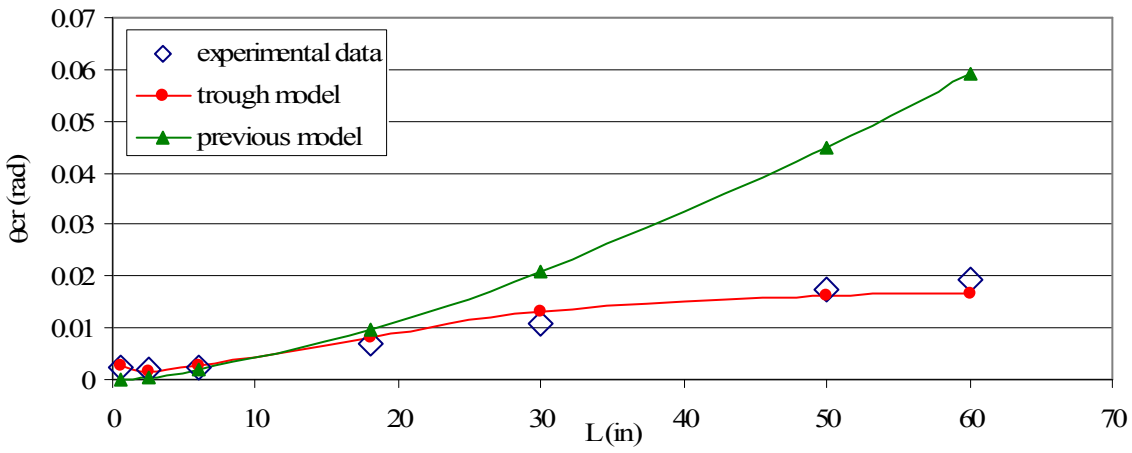

Figure 17 – Troughs Due to Misalignment, Polyester, T = 19.2 lbs

Figure 15 - Figure 17 show a comparison of equation (51) to experimental results obtained by misaligning the downstream roller until troughs were observed in the web span. The "previous model" line on the graph refers to an earlier effort by Good [16] that did not take into account tension nor shear effects. Each datum point was an average of three misalignments in either direction to reduce the effects of web camber. It can be seen that for short and long spans shear and tension effects are critical.

Equation (51) also accepts orthotropic web properties as inputs. Two materials with measurably orthotropic (newsprint and a non-woven) were also tested. Their properties are listed below in Figure 18.

Newsprint		Non-woven	
L =	variable	L =	variable
W =	6.2"	W =	4.17"
t =	0.0028"	t =	0.005"
Ex=	630,000 psi	Ex=	8000 psi
Ey=	401,000 psi	Ey=	1200 psi
νxy=	0.3	νxy=	0.3
νyx=	0.19	νyx=	0.045
G=	199,000 psi	G=	968 psi

Figure 18 – Properties of Orthotropic Materials

Comparisons of equation (51) to experiment are presented below in Figure 19 and Figure 20.

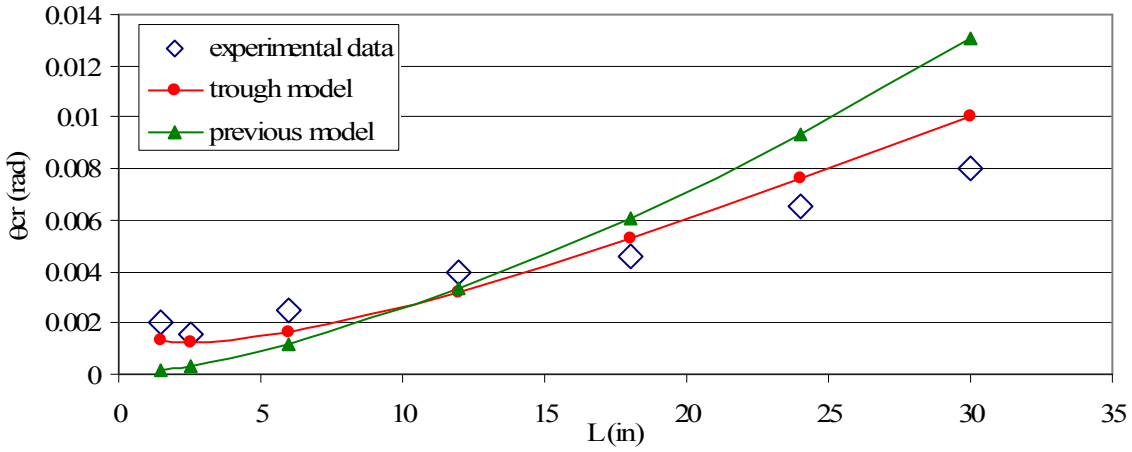

Figure 19 – Troughs Due to Misalignment, Newsprint, T = 15 lbs

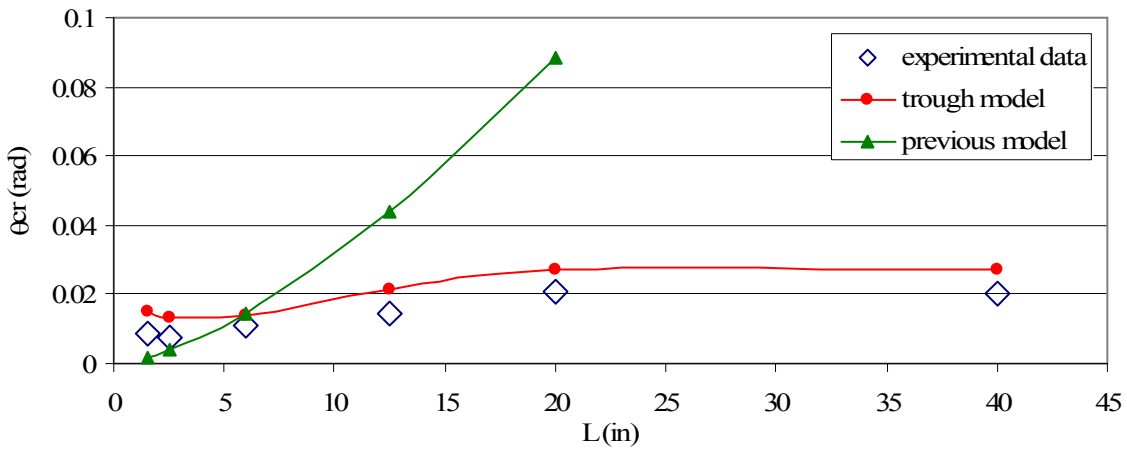

Figure 20 – Troughs Due to Misalignment, Non-woven, T = 1.5 lbs

The agreement achieved in Figure 19 and Figure 20 was not as good as that achieved for the polyester web. Newsprint and the non-woven material are difficult materials to characterize. Their material properties are difficult to measure in the cross machine direction. Additionally, these materials are non-homogeneous on a local scale and the proposed model only accounts for macroscopic properties. Never the less, the model did yield the general trend of the data and noticeable improvements were made due to the inclusion of tension and shear effects.

3.4 Troughs Due to Tapered Rollers

The prediction of troughs forming in a web approaching a tapered downstream roller will be accomplished with a method consistent to that applied to the misaligned roller of the previous section. In section 3.0, the boundary conditions for a web encountering a tapered roller were established. These boundary conditions were then used to develop a model for web behavior, based on beam theory. This resulted in expressions for web deflection, equation (15), and shear force, equation (18), developed at the tapered roller.

Previously, this shear force and resulting shear stress have been shown to cause a compressive stress across the web when coupled with web line tension, equation (40). Expression (39) has been developed to yield the compressive stress that the web in a free span can withstand before troughs form. Equation (42) gives the result of setting the compressive stress developed equal to the critical compressive stress required to buckle the web, which is then solved for a critical shear stress. If equation (18) is then inserted into equation (42) through use of equation (43), the result may be solved for the critical taper required to cause troughs to form in a web span approaching a tapered roller.

$$m_{cr} = \frac{LR_o}{W^2 E_x} \frac{\left[60E_x I + TL^2(1+\phi)\right](T + GA_s)}{GA_s\left[10E_x I + TL^2(1+\phi)\right]} \sqrt{\left(\frac{\pi}{L}\right)^2 \frac{tE_y T}{3W\left(1-\upsilon_{xy}\upsilon_{yx}\right)}} + \frac{\pi}{L}\sqrt{\frac{E_y T^3}{3tW^3\left(1-\upsilon_{xy}\upsilon_{yx}\right)}} \qquad (53)$$

If a maximum shear stress with a parabolic distribution is assumed, equation (44), then a more conservative estimate is given by:

$$m_{cr,\tau_{max}} = \frac{2}{3} m_{cr,\tau_{avg}} \qquad (54)$$

Equation (53) provides a guide for how much radial taper a roller can have before it causes buckling problems in a web line. Shelton [34] had previously proposed a model for tapered rollers in an unpublished document. He also used the Timoshenko buckling criteria, but without a development for orthotropic web properties. Additionally, his deflection equation did not account for tension or shear effects. His model was never verified experimentally, so it will be included here for completeness. Shelton similarly proposed two equations, equation (55) for L/W < 2 ("short" beams) and equation (56) for L/W > 2 ("long" beams).

$$m_{cr} = 1.39\frac{R_o}{W}\sqrt{\frac{t}{W}}\cdot\left(\frac{L}{W}\right)^{-\frac{3}{2}}\varepsilon^{-\frac{1}{4}}\frac{K_e L\left(\left(1+\left(\frac{E}{G}\right)\varepsilon\right)\left(\cosh\left(K_e L\right)\right)-1\right)}{\sinh\left(K_e L\right)} \tag{55}$$

$$m_{cr} = 0.928\frac{R_o}{W}\sqrt{\frac{t}{W}}\cdot\left(\frac{L}{W}\right)^{-\frac{3}{2}}\varepsilon^{-\frac{1}{4}}\frac{K_e L\left(\left(1+\left(\frac{E}{G}\right)\varepsilon\right)\left(\cosh\left(K_e L\right)\right)-1\right)}{\sinh\left(K_e L\right)} \tag{56}$$

where K_e is given by:

$$K_e = \sqrt{\frac{T}{EI\left[1+1.2\left(E/G\right)\varepsilon\right]}} \tag{57}$$

3.5 Measurement of Troughs Due to Tapered Rollers

Experimental verification was needed for equation (53-54). The trough-due-to-taper experiment utilized the same setup as that constructed for the case of deflection due to a tapered roller. The eight tapered rollers previously constructed and qualified were used with two web thicknesses over four different span lengths.

Since the tapered rollers were of fixed geometry, tension was used as the variable condition in the tests. The tests were conducted by starting at a relatively high web line tension, since tension increases web stability in free spans. Tension was then slowly decreased until instability occurred in the web. The onset of instability was determined visually. The visibility of this occurrence was assisted by the use of a plane of laser light at a very low angle of incidence with the web. A planar web will show a straight line across the web, where a web with any out of plane deformations will show a similar pattern in the laser light across the web. A typical web span with developed troughs will show the laser light incident with the web as a wavy sinusoidal line. Furthermore, as the troughs move across the web, the wavy line will dynamically move or "wiggle" creating a noticeable visual effect. An example of the incident laser on a web span with developed troughs is shown in Figure 21.

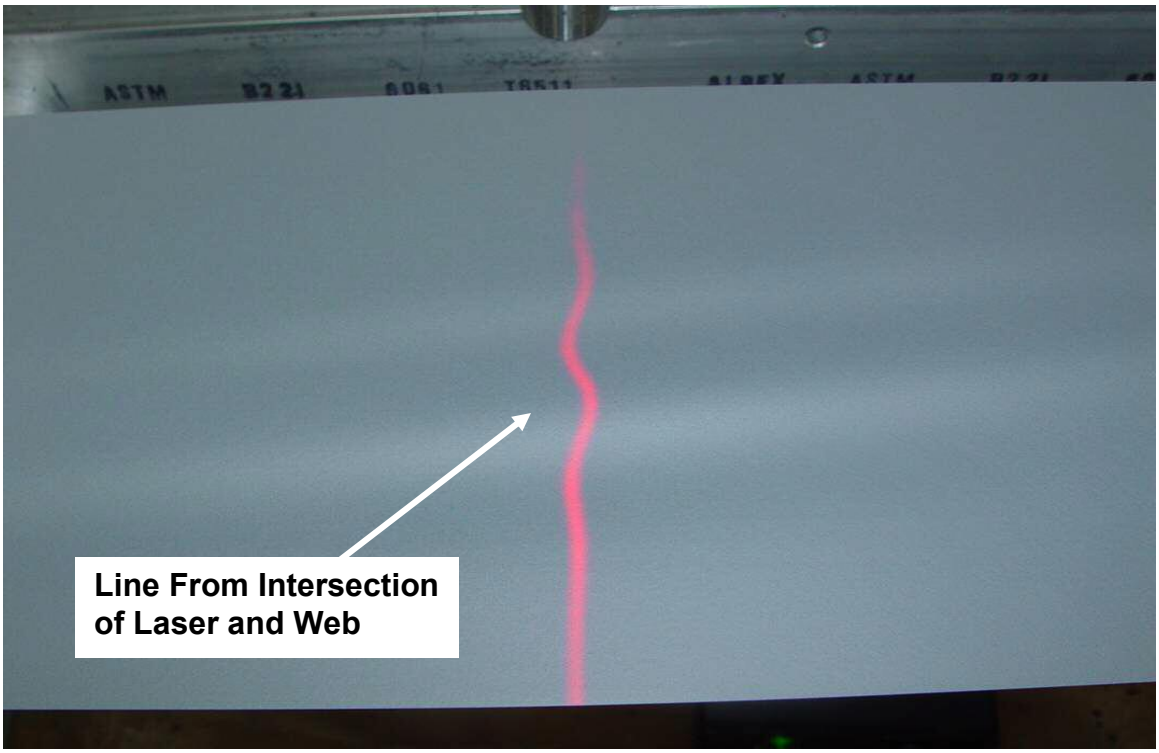

Figure 21 – Trough Visualization

The first web tested was the same isotropic 92 ga. polyester used in the deflection experiments. It had a width of W = 6", a Young's Modulus of E_x = 712000 psi, and a Poisson's Ratio of ν = 0.3. Each data point is the result of an average of three measurements. In addition, each measurement was based on the web being deflected in either direction. This was accomplished by reversing the roller taper by flipping over the roller in the test stand. The purpose of this was to reduce the possible effects of web camber. The test results were plotted against the values predicted by equation (54). Through out this paper error bars, where given, represent a maximum and minimum value measured, unless specifically stated otherwise.

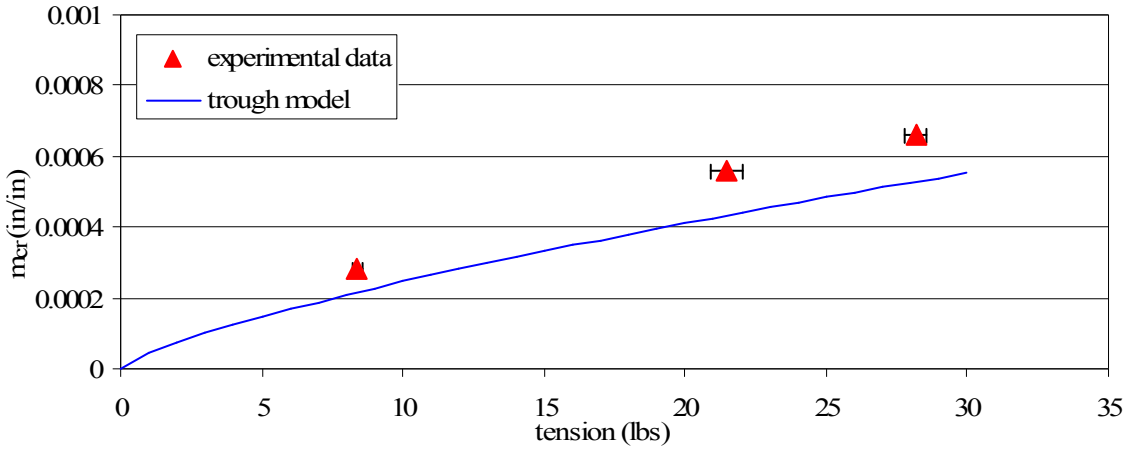

Figure 22 – Troughs Due to Taper, 92 ga Polyester, L = 10”

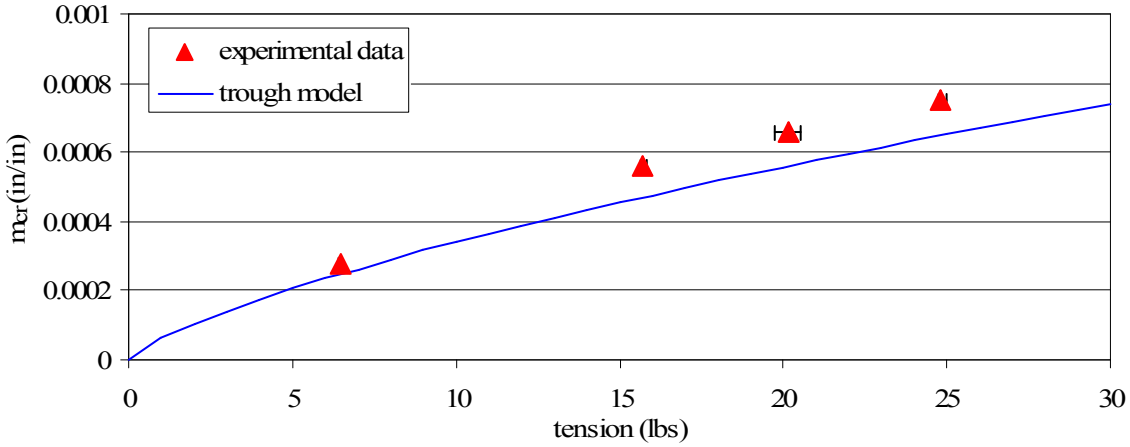

Figure 23 – Troughs Due to Taper, 92 ga Polyester, L = 20”

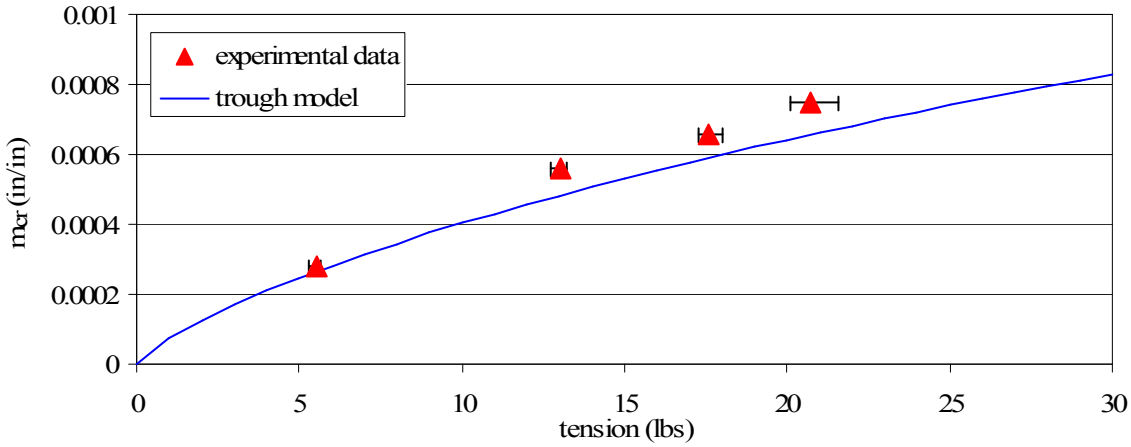

Figure 24 – Troughs Due to Taper, 92 ga Polyester, L = 30”

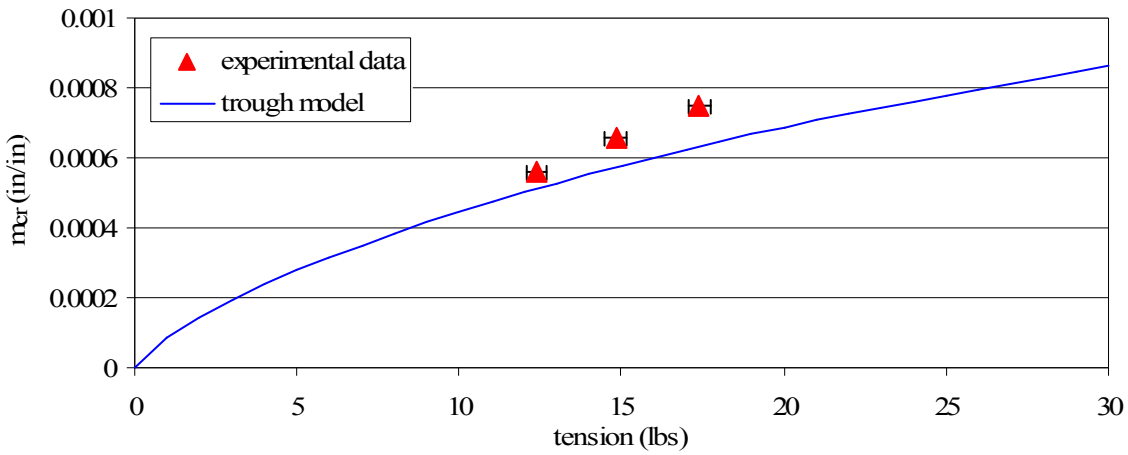

Figure 25 = Troughs Due to Taper, 92 ga Polyester, L = 40”

For the range of conditions tested, the experimental results fairly closely followed the trend established by equation (54). It is interesting to note that the data points representing troughs in the web were all above the line predicted by the model. This was expected since the data points were based on the observation of troughs that had already formed in the web. All the span lengths exhibited similar behavior. The tests also suggest that even the 10 inch span for a 6 inch wide web should be considered a “long” beam. Due to the nature of the test apparatus, shorter spans were not tested to determine exactly when equation (53) should be used instead of equation (54).

An additional web thickness was tested. This web was a clear polyester with a width of W = 6”, a thickness of t = 0.00056”, a Young’s Modulus of E_x = 658000 psi, and a Poisson’s Ratio of ν = 0.3. The results are shown below in Figure 26 - Figure 28. The data for the 56 ga polyester represents a single measurement due to the difficulties associated with the thin web.

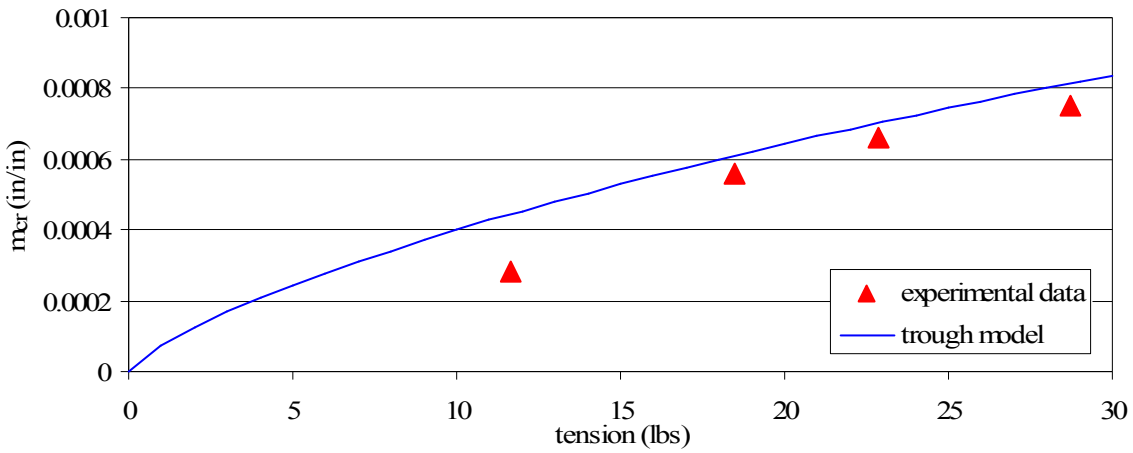

Figure 26 – Troughs Due to Taper, 56 ga Polyester, L = 20”

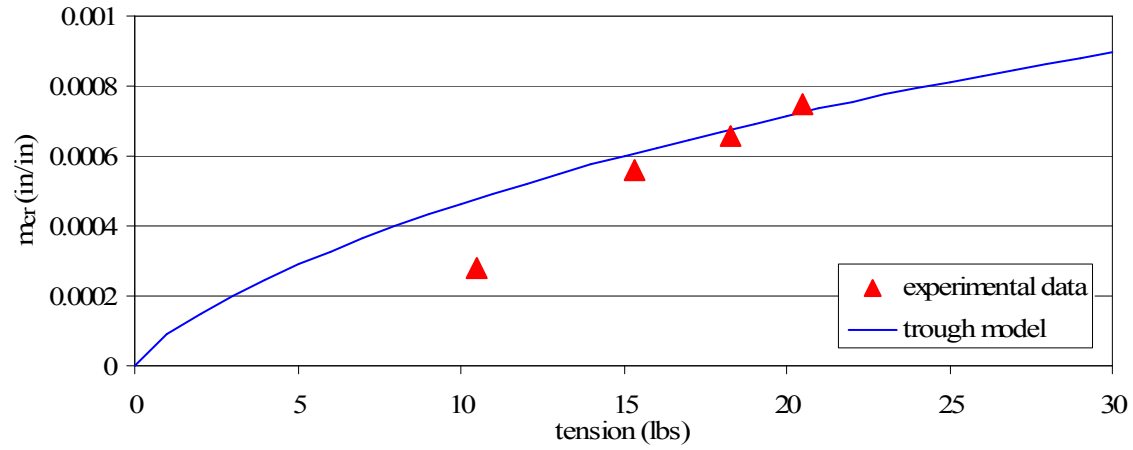

Figure 27 – Troughs Due to Taper, 56 ga Polyester, L = 30”

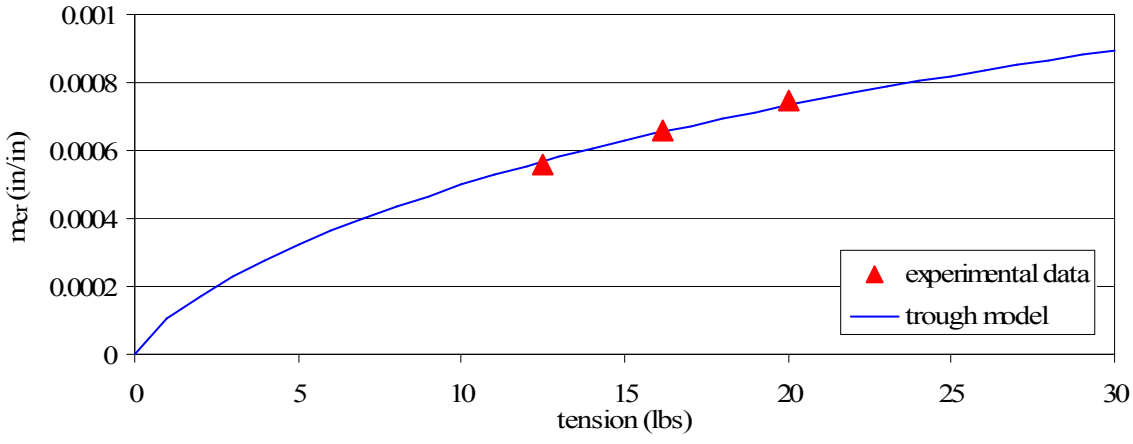

Figure 28 – Troughs Due to Taper, 56 ga Polyester, L = 40”

We can see from the results of the thinner web that the model does not follow as closely as it did for the 92 gauge case. There is good agreement on the 40 inch span as well as in the higher tensions for all spans. It is interesting to note that the trough data on the 20 and 30 inch spans do not appear, if extrapolated, to intersect the origin of the graph, which would be expected behavior from any model. One possible reason for the experimental data's low tension deviation may be in the geometry of the thin web itself. If manufacturing controls over variables, such as web thickness, are more crucial on thin webs, then the seemingly premature instabilities may be due to local variations in stress caused by local defects in the web itself.

3.6 Misaligned – Tapered Rollers

The prediction of trough formation due to either roller taper or roller misalignment has been successfully achieved in closed form models in the previous sections. A model is now presented for the combined effects of a downstream misaligned *and* tapered roller. This condition of roller error may occur accidentally and guidelines for tolerances would be desirable. Another possibility for this condition might be to correct the effect of either misalignment or taper by use of the other parameter. Shear troughs in a web look similar in the web line independent of whether they were generated by roller misalignment or tapered rollers. Operators will find they can misalign a tapered roller and make troughs disappear. Hence, it is important to understand the combined effect.

When considering this case, there are two possible orientations of a misaligned and tapered roller. The roller can be oriented such that the shear force due to taper is aligned with the shear force due to misalignment, or the roller can be oriented such that the shear forces are opposed. These two distinct orientations are shown below in Figure 29.

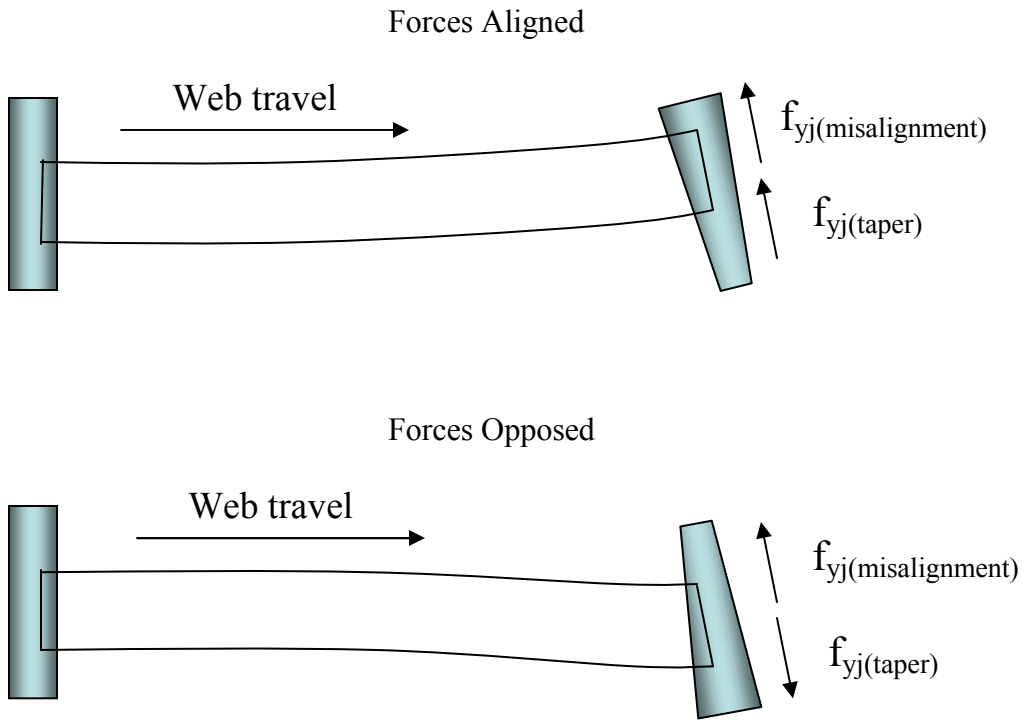

Figure 29 – Orientations of a Misaligned-Tapered Roller

For the case of the aligned shear forces we have:

$$f_{yj} = f_{yj(misalignment)} + f_{yj(taper)} \tag{58}$$

and for the case of opposed shear forces:

$$f_{yj} = f_{yj(misalignment)} - f_{yj(taper)} \tag{59}$$

If the appropriate equation is used from above, equations (49) and (18) supply the values for shear forces, and finally, equation (43) or (44) can be used to relate shear stress. Here, equation (44) was used for maximum shear stress in a rectangular cross section. The shear stress generated is then set equal to the critical shear stress required to buckle the web in a free span, as given in equation (42). The resulting expression may then be solved for critical misalignment for a roller with a particular taper, as seen in

equations (60) and (61). Conversely, the critical taper for a roller with a particular misalignment might have been found. For the case of aligned shear forces:

$$\theta_{cr} = \frac{\frac{2Wt}{3}\sqrt{\left(\frac{\pi}{L}\right)^2 \frac{tE_yT}{3W(1-\upsilon_{xy}\upsilon_{yx})}} + \frac{\pi}{L}\sqrt{\frac{E_yT^3}{3tW(1-\upsilon_{xy}\upsilon_{yx})}} - \frac{mtW^3E_x}{LR_o}\frac{GA_s\left[10E_xI+TL^2(1+\phi)\right]}{\left[60E_xI+TL^2(1+\phi)\right](T+GA_s)}}{\frac{GA_s\left[240E_x{}^2I^2+3T^2L^4(1+\phi)+8E_xITL^2(13+3\phi)\right]}{240E_x{}^2I^2+TL^4(2GA_s+T)(1+\phi)+8E_xIL^2\left[15GA_s-T(2-3\phi)\right]}} \quad (60)$$

and for the case of opposed shear forces:

$$\theta_{cr} = \frac{\frac{2Wt}{3}\sqrt{\left(\frac{\pi}{L}\right)^2 \frac{tE_yT}{3W(1-\upsilon_{xy}\upsilon_{yx})}} + \frac{\pi}{L}\sqrt{\frac{E_yT^3}{3tW(1-\upsilon_{xy}\upsilon_{yx})}} + \frac{mtW^3E_x}{LR_o}\frac{GA_s\left[10E_xI+TL^2(1+\phi)\right]}{\left[60E_xI+TL^2(1+\phi)\right](T+GA_s)}}{\frac{GA_s\left[240E_x{}^2I^2+3T^2L^4(1+\phi)+8E_xITL^2(13+3\phi)\right]}{240E_x{}^2I^2+TL^4(2GA_s+T)(1+\phi)+8E_xIL^2\left[15GA_s-T(2-3\phi)\right]}} \quad (61)$$

Equations (60) and (61) represent the maximum shear stress if a parabolic distribution is assumed. If an average shear stress distribution is assumed then as before, equation (43) must be used in the derivation instead of equation (44).

In order to verify this additive model for a misaligned and tapered roller, an experiment was conducted to determine the onset of trough and wrinkle phenomena. The rotating yoke from the misaligned roller experiment was fitted with a tapered roller from the tapered roller experiment. At a given web line tension, with a set span length, using a particular tapered roller, the downstream roller was misaligned to the right and then to the left. The onset of troughs and then wrinkles were determined in each direction. Next, the tapered roller was flipped end for end in its yoke and the entire process was repeated. This was done to reduce possible effects of web camber. Each data point was the average of three attempts to identify the first evidence of either trough or wrinkle formation in the web. By rotating both right and left as well as reversing the tapered roller, data were

simultaneously collected for the case of aligned shear forces and for the case of opposed shear forces. The onset of trough and wrinkle formation were again determined visually.

The material used for testing was, again, the 92 gauge opaque polyester, with a Young's Modulus of E_x= 712000 psi, a Poisson's Ratio of $\nu = 0.3$, and a width of W = 6 inches. The material was considered to have isotropic properties. The results of these tests are compared to equations (60) and (61) below in Figure 30 - Figure 32.

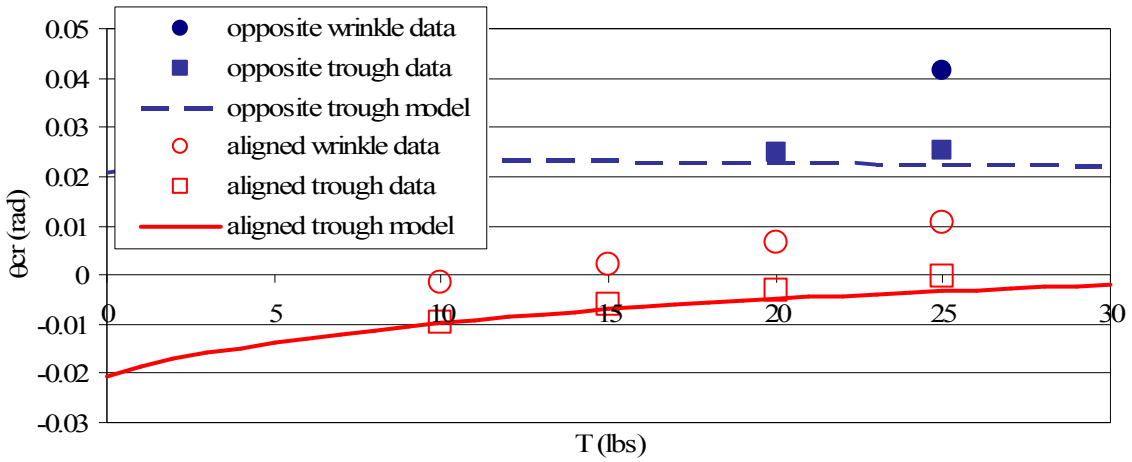

Figure 30 – Misaligned-Tapered Roller, m = 0.0010 radial in/in, L = 30"

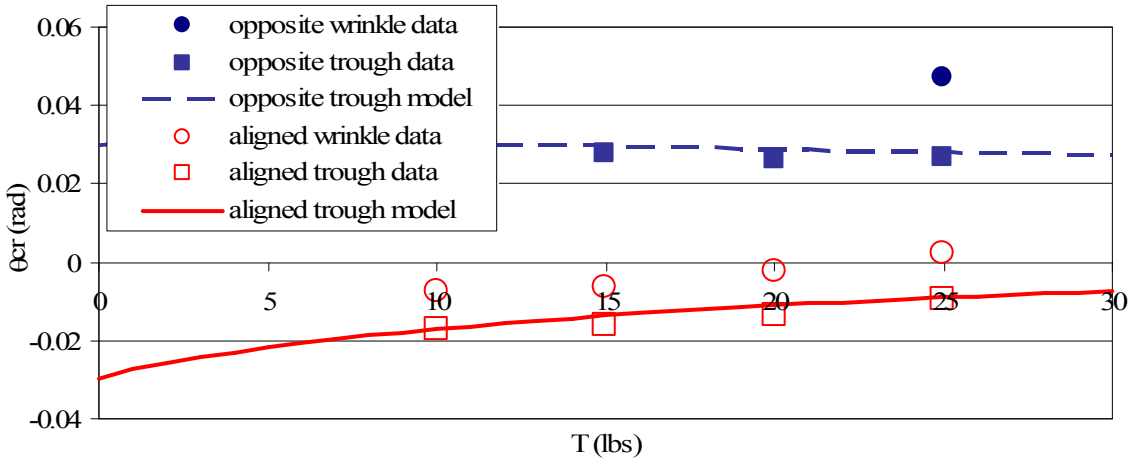

Figure 31 – Misaligned-Tapered Roller, m = 0.00144 radial in/in, L = 30"

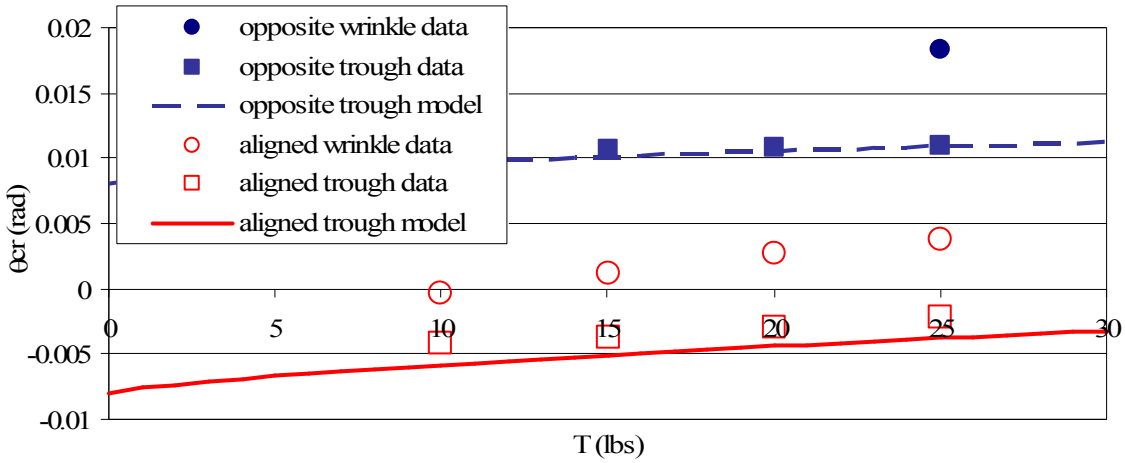

Figure 32 – Misaligned-Tapered Roller, m = 0.0010 radial in/in, L = 10”

The preceding graphs show a comparison of equations (60) and (61) and data that represent the formation of troughs in the web span. Limited wrinkle data are also displayed but no modeling attempts were made. Two different tapers were tested at a span length of L = 30” and a relatively “short” web span of L = 10” was also tested. The agreement between the model and corresponding data was acceptable in all cases. The graphs clearly exhibit the two distinct orientations of the misaligned-tapered roller. The results demonstrate that the forces due to a misaligned and tapered roller can in fact be modeled adequately in an additive manner for typical web spans.

3.7 Introduction to the Use of Finite Elements in Webs

In order to successfully predict wrinkles in webs finite elements were needed. The first step in applying finite elements to webs was to successfully model a known case of instability in webs. The case chosen was that of troughs forming in webs due to a downstream tapered roller. In predicting troughs, the web remains planar up to the point of trough formation, thus, regular elastic elements may be used to model the web. The main development to be achieved through this exercise is the correct establishment of the boundary conditions for the finite element wrinkling model.

The web was modeled in five sections. Three of these sections represent the web on rollers and the other two sections represent the web in free spans. A diagram is given in Figure 33. It should be noted that a traveling web would not behave this way. This configuration is used to impose the correct boundary conditions on the left side of the model. The right side of the model is symmetric to the left side. The force applied to the model is therefore $2*f_{yj}$ in the y direction. Since the nodes are locked together in the y direction across the middle, roller it does not matter where on the roller section the shear load is applied. Rows of nodes are locked together in order to achieve normal entry at the rollers.

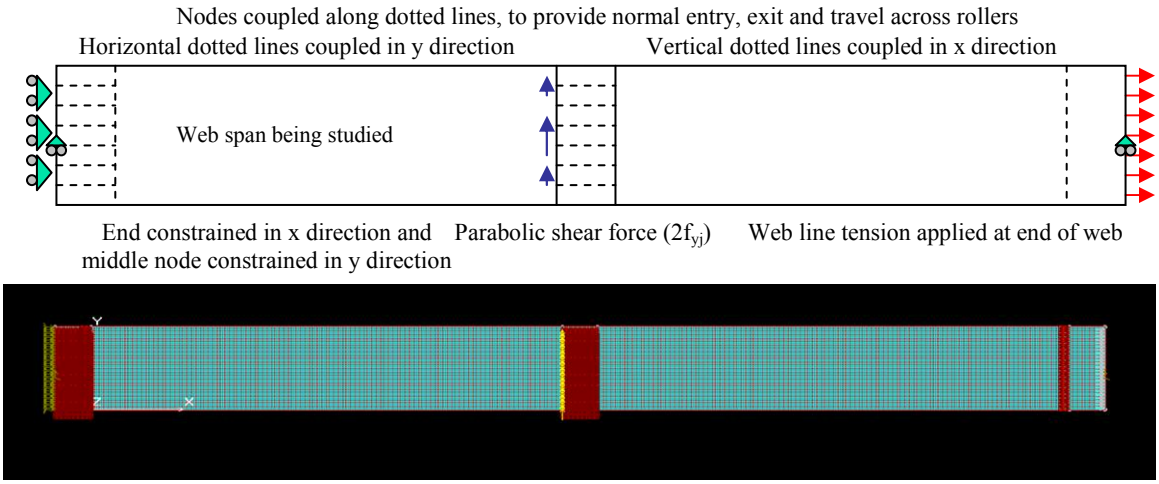

Figure 33 – FE Trough Model, Tapered Roller

Figure 34 shows a typical stress output for the FE model.

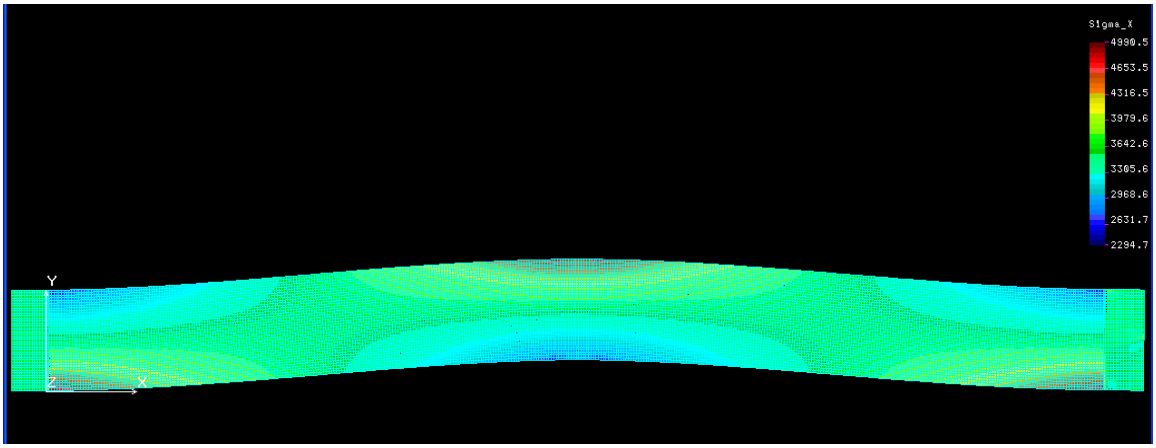

Figure 34 – FE Trough Model, σ_x Stress Output

The MD stress behaves as expected, developing equal moments at each end of the web span. What is of more interest to our stability studies are the compressive CMD stresses. It has been shown previously that the combination of a MD stress and a shear stress will result in a compressive second principle stress across the web. Figure 35 shows this principal stress.

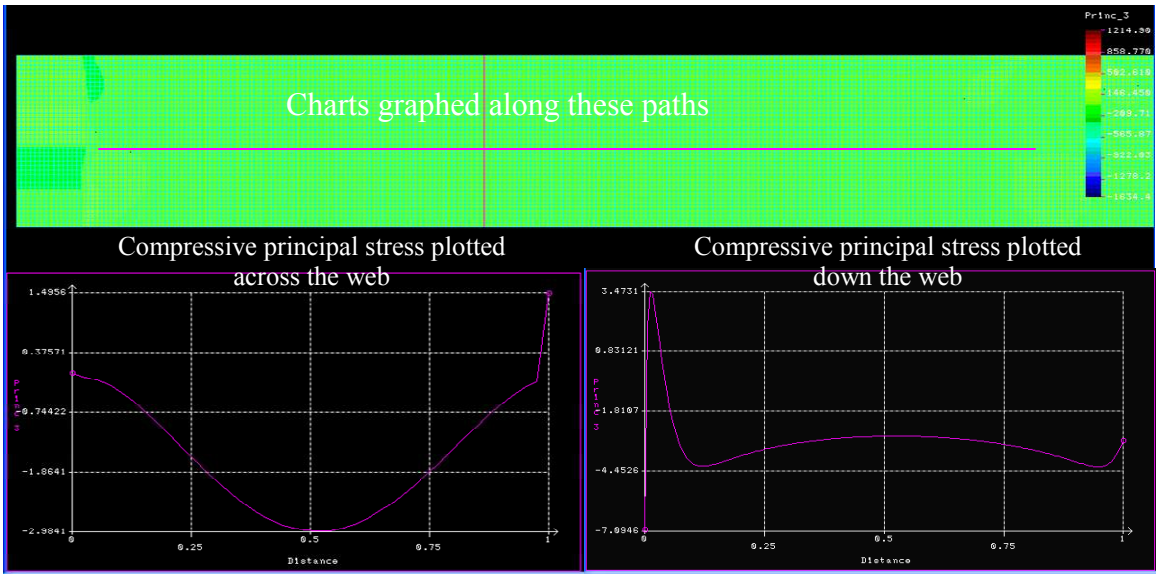

Figure 35 – FE Trough Model, Compressive Principle Stress

Figure 35 shows a region of developed compressive stress across the web span. At near the center of the web span, a saddle point of compressive stress can be seen. Once the compressive stress at this point reaches the critical stress needed to buckle a tensioned plate, there will be nothing to prevent the formation of troughs in the web.

The process of modeling trough formation in a web span begins by starting with a relatively low shear force, f_{yj}. If the resulting CMD compressive stress was less in magnitude than the required critical stress, given by equation (39), then the applied shear force was increased. Once the critical CMD stress is reached, the downstream moment was calculated by integrating the MD stresses multiplied by their positions and incremental areas across the web. The taper required to induce this moment can be found through use of equation (9). Results of this method are shown below compared to data previously shown in Figure 22, Figure 24, and Figure 27.

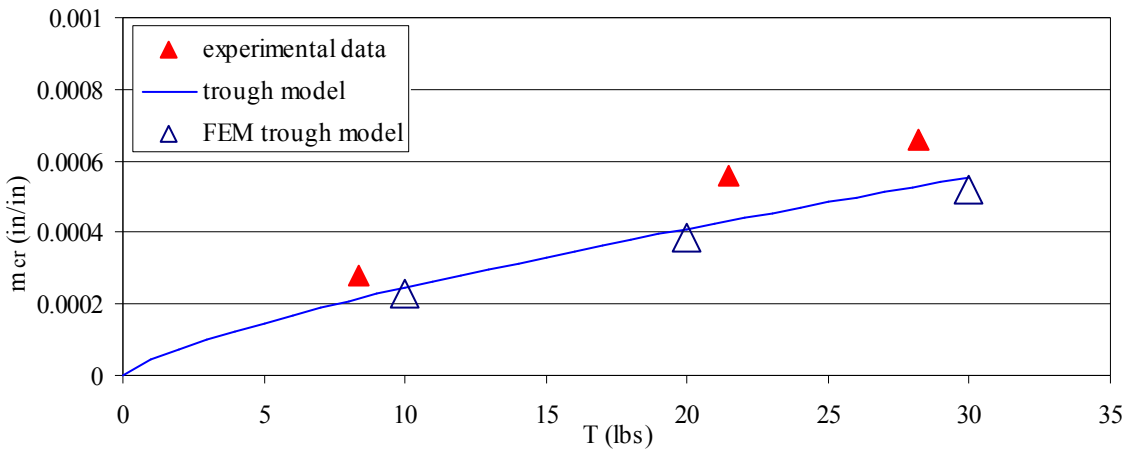

Figure 36 – Troughs Due to Taper, 92 ga Polyester, L = 10”

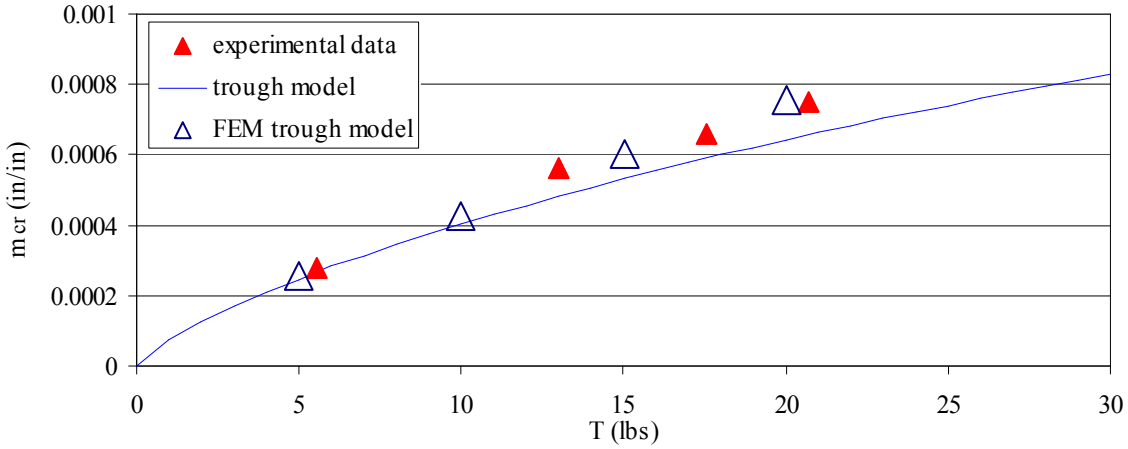

Figure 37 – Troughs Due to Taper, 92 ga Polyester, L = 30”

Figure 36 and Figure 37 show comparisons of experimentally determined values for critical taper at a given tension to analytical as well as FE models. Figure 36 gives the results for a relatively short span while Figure 37 represents a longer span. In both cases, the FE model was acceptable in predicting the onset of trough in a web span due to a tapered roller. To further examine the model, a thinner web was again tested.

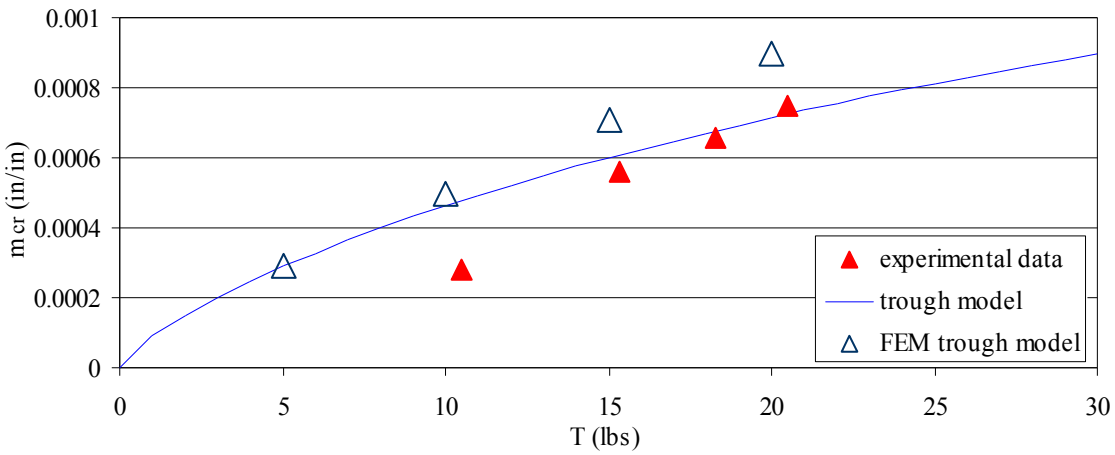

Figure 38 – 56 ga Polyester, L = 30”

The relatively thin web represented in Figure 38 shows the experimental values dropping out early so as not to intersect with the origin as previously mentioned on page 58. We can see the FE model following the analytical model, equation (54), in this respect.

3.8 Conclusions of Troughs Due to Shear

Webs encountering misaligned and tapered rollers have been consistently modeled as beams. The models considered tension effects, shear effects, as well as orthotropic web properties. In the case of the tapered roller, experimental verification was provided for web deflection. An interesting observation was the fact that the deflection equation accurately predicted the deflection of the web even after a trough had formed in the free span.

A buckling criterion suitable to webs was presented and linked to the respective beam models. This produced equations for critical misalignment and also for critical roller taper that would induce troughs to form in the web. Experiments were conducted and the proposed models were compared to resulting experimental data. Of importance, is that the models were developed with consistent methodology and were successful for both the cases of the misaligned roller and the tapered roller. The implication is that this same method is likely to be successful in predicting trough formations in any webs experiencing steering forces at a roller. An example is that of a web encountering a set of rubber covered rollers with uneven nip pressure.

A final point is the successful modeling of the case of combined effects due to misalignment *and* taper. Experiments verified that the shear forces generated by each case may be combined additively. The methodology mentioned in the previous paragraph was applied and a model predicting trough formation due to a misaligned-tapered roller was developed and verified.

CHAPTER IV

Prediction of Wrinkles Due to Shear

4.0 Wrinkle Formation on Rollers, Instability Criteria

A web is considered wrinkled when a trough from the free span traverses a roller. As a web travels over a roller, it changes from the plate it was in the free span into a cylindrical shell on the roller. The shell geometry has a substantially higher buckling stress than that of the same web in the tensioned plate form. In order to predict wrinkling of webs, the instability criterion for the web in this shell form is now developed. This work has been previously presented by Good and Beisel [15].

Others have shown that the buckling load for a sector of a cylinder is the same per unit circumferential length as that of a complete cylinder [41]. Figure 39 shows such a sector in the strip jk. Figure 39 also shows coordinate directions as well as forces per unit length N_x and N_y.

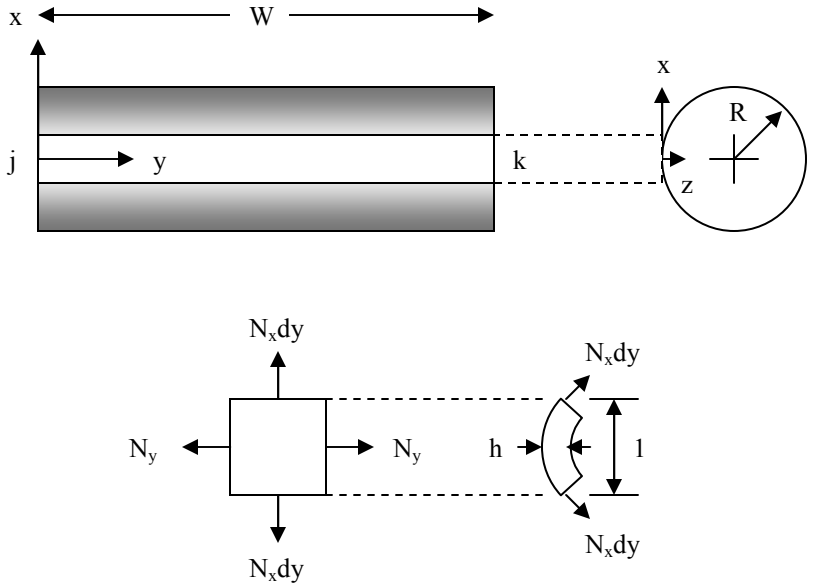

Figure 39 – Shell Instability Conventions

The constituent relations of equations (28) and (29) can be solved simultaneously and expressed in terms of stresses:

$$\sigma_x = \frac{E_x}{\left(1 - \upsilon_{xy}\upsilon_{yx}\right)}\left(\varepsilon_x + \upsilon_{yx}\varepsilon_y\right) \tag{62}$$

$$\sigma_y = \frac{E_y}{\left(1 - \upsilon_{xy}\upsilon_{yx}\right)}\left(\varepsilon_y + \upsilon_{xy}\varepsilon_x\right) \tag{63}$$

Equations (62) and (63) can be used to relate the membrane forces to the strains in the shell by dividing through by the shell thickness, t. In addition, for an axisymmetric object subject to an axisymmetric load, the circumferential strain is $\varepsilon_x = -w/R$. The variable w represents the out of plane deformation of the shell. After this substitution, equations (62) and (63) can be written as:

$$N_x = \frac{tE_x}{1 - \upsilon_{xy}\upsilon_{yx}}\left(-\frac{w}{R} + \upsilon_{yx}\varepsilon_y\right) \tag{64}$$

$$N_y = \frac{tE_y}{1-\upsilon_{xy}\upsilon_{yx}}\left(\varepsilon_y - \upsilon_{xy}\frac{w}{R}\right) \tag{65}$$

By comparing equations (64) and (65) and making use of Maxwell's reciprocal theorem, equation (22):

$$N_x = E_x\left(\frac{N_y\upsilon_{yx}}{E_y} - t\frac{w}{R}\right) = N_y\upsilon_{xy} - tE_x\frac{w}{R} \tag{66}$$

If we consider the strip jk from Figure 39, the forces have a component in the z direction, which per unit length is:

$$\frac{N_x}{R} = \frac{1}{R}\left(N_y\upsilon_{xy} - tE_x\frac{w}{R}\right) \tag{67}$$

Further, summing all the loads per unit length in the z direction in strip jk yields:

$$q + \frac{N_y\upsilon_{xy}}{R} - tE_x\frac{w}{R^2} + N_y\frac{\partial^2 w}{\partial y^2} \tag{68}$$

where q is the potential pressure acting on the strip. The last term represents the component of transverse load due to the membrane load N_y acting through the out-of-plane deformation w. Thus, the differential equation for the bending of strip jk is:

$$D_2\frac{d^4w}{dy^4} = q + \frac{N_y\upsilon_{xy}}{R} - tE_x\frac{w}{R^2} + N_y\frac{d^2w}{dy^2} \tag{69}$$

In the application of equation (69), q is set to zero and w is measured from the middle of the cylinder after the uniform compression N_y is applied. Therefore, w is replaced by:

$$w \Rightarrow w + \frac{N_y\upsilon_{xy}R}{tE_x} \tag{70}$$

Substituting into the differential equation and assuming N_y is positive when in compression gives:

$$D_2 \frac{d^4 w}{dy^4} + N_y \frac{d^2 w}{dy^2} + tE_x \frac{w}{R^2} = 0 \tag{71}$$

The cylindrical shell is expected to buckle into axisymmetric modeshapes that can be represented by the waveform:

$$w = -A \sin \frac{n\pi y}{W} \tag{72}$$

If equation (72) is substituted into equation (71) and like terms are eliminated:

$$\frac{R^2 t^3 n^4 \pi^4 E_y + 12W^2 \left(tW^2 E_x - R^2 n^2 \pi^2 N_y\right)\left(1 - \upsilon_{xy}\upsilon_{yx}\right)}{12R^2 W^4 \left(1 - \upsilon_{xy}\upsilon_{yx}\right)} \tag{73}$$

Solving equation (73) for Ny yields:

$$N_y = \frac{tW^2 E_x}{R^2 n^2 \pi^2} + \frac{t^3 n^2 \pi^2 E_y}{12W^2 \left(1 - \upsilon_{xy}\upsilon_{yx}\right)} \tag{74}$$

Equation (74) gives us an expression that relates the axial load per unit length to the half wave number n. The minimum value of N_y for any buckled shape needs to be determined. A new variable is substituted into equation (74), $\lambda = n\pi/W$, yielding:

$$N_y = \frac{tE_x}{R^2 \lambda^2} + \frac{t^3 \lambda^2 E_y}{12\left(1 - \upsilon_{xy}\upsilon_{yx}\right)} \tag{75}$$

If the assumption is made that λ can be a continuous variable, equation (75) may be minimized with respect to N_y by setting the derivative equal to zero.

$$\frac{\partial N_y}{\partial \lambda} = -\frac{2tE_x}{R^2 \lambda^3} + \frac{t^3 \lambda E_y}{6\left(1 - \upsilon_{xy}\upsilon_{yx}\right)} = 0 \tag{76}$$

Equation (76) yields four roots, only one of which is real and positive.

$$\lambda = \frac{n\pi}{W} = \sqrt{\frac{2}{Rt}} \cdot \sqrt[4]{\frac{3E_x\left(1-\upsilon_{xy}\upsilon_{yx}\right)}{E_y}} \tag{77}$$

Equation (77) may be solved for n, and if the result is substituted back into equation (74) then the critical buckling load may be found.

$$N_{ycr} = \frac{t^2}{R}\sqrt{\frac{E_x E_y}{3\left(1-\upsilon_{xy}\upsilon_{yx}\right)}} \tag{78}$$

Finally, equation (78) was divided by the web thickness to yield the critical stress:

$$\sigma_{ycr} = \frac{t}{R}\sqrt{\frac{E_x E_y}{3\left(1-\upsilon_{xy}\upsilon_{yx}\right)}} \tag{79}$$

Equation (79) gives the value of the critical buckling stress of an orthotropic cylinder. It is assumed that the web will buckle when compressive stresses in the web on the roller reach the stresses given by equation (79). If the associated half wave number is desired it may be found from equation (77).

4.1 Stabilized Shell Buckling, Experimentation

In the previous section, the critical buckling stress for an unsupported orthotropic cylinder was presented. Whether or not equation (79) is appropriate for use in describing webs buckling on rollers has been debated [22]. Experimental studies have been undertaken to determine whether the use of equation (79) in cases involving pressurized and internally supported shells is appropriate.

A web traversing a roller is not the same situation as an unsupported cylindrical shell in regards to buckling. As previously mentioned, it has been shown that a sector of a shell buckles at the same compressive stress that would cause a complete shell to buckle. However, the web line tension gives rise to a hoop stress around the shell and a normal pressure similar to an internally pressurized cylinder. Additionally, the web pulled around the roller provides a rigid support against the internal wall of the cylinder.

Traditional studies of unsupported shell buckling typically include a large scatter in data and the loads that cause failure usually fall short of expected critical levels. In addition, the mode of buckling is not always as expected, for a cylindrical shell, diamond buckling is normally what is observed instead of circumferential buckling modes. Most studies blame this on non-uniformities of the shell or eccentricity of the loading, resulting in uneven stress distributions. These uneven stresses cause buckling to occur locally and then spread throughout the shell. Allen and Bulson [3] show that the ring and diamond shape buckles can occur a similar compressive loads. Diamond buckles are uncommon in webs on web lines. They are seen only when web tension levels are low. Allen and

Bulson also show that internal pressurization will stabilize ring buckling. Since web tension effectively induces an internal pressure between the web and roller, the behavior observed in web lines appears to agree with their observations of pressurized shells.

Weingarten [46] and others also suggest that a pressurized cylinder will approach the theoretical value of critical stress predicted by thin shell stability theories. These studies have been reviewed previously and provided the justification for using these classical theories, thus far, in modeling webs buckling on a roller. Although there are many similarities between webs traversing a roller and a pressurized shell, the case of a web on a roller seems to have one difference. The roller provides not only a pressure on the inner surface of the web but also a rigid support. The presence of a rigid support means the web must buckle entirely outward. This outward buckling of the web is considered by some to be a different buckling mode than the normal sinusoidal mode currently being used to model wrinkling. This leads to the proposition that the outward only buckling mode may require a higher critical stress. In a recent paper, Jones and McCann [22] propose that since only outward buckling may occur on a rigid roller, equation (72) may be inadequate to describe the buckled shape. They are concerned that the web buckling away from the roller causes a rise in machine direction stress that affects the onset of instability. These concepts were presented without verification. Due to the various theories associated with stabilized shell buckling, experimentation was conducted herein.

An experimental setup was designed to test thin shell elastic buckling for cylinders. The tests were meant to determine specifically whether cylinders that were rigidly supported internally would buckle at a higher level than cylinders that were internally pressurized (which approach values predicted by classical analysis). In order for the tests to represent elastic buckling the shells used in the experiment needed to be very thin. Machining a shell of the required thickness accurately would be beyond the capabilities of most machining practices, however, a suitable shell might be accurately drawn. It was realized that aluminum beverage cans might be potential candidates.

A typical beverage can has a diameter of 2.59" with an average thickness of 0.0039". Cans used in experiments were measured with a hand micrometer. The cans ranged in measured thickness from 0.0038"-0.0040", however, multiple measurements on the same location on a can averaged the expected 0.0039". This led to the assumption that cans were more uniform than our measurement techniques were accurate. The sides of beverage cans are drawn from an aluminum alloy consisting of 1% magnesium, 1% manganese, 0.4% iron, 0.2 % silicon, and 0.15% copper, Hosford [20]. Inserting these dimensions into equation (79) along with the material properties of aluminum and then distributing the stress around the can gives a critical buckling load of nearly 580 lbs.

The tests were conducted on two distinct configurations. One was the case of an internally pressurized cylinder buckling under an axial loading. The other was the case of a cylindrical shell supported by an internal rigid foundation buckling under an axial

loading. For the internally pressurized shell, mandrels were made to support the inside of the ends of the shell as shown below in Figure 40.

Figure 40 – Mandrel Supports for Internally Pressurized shell

The test samples were placed in an Instron machine and then crushed while simultaneously monitoring load and displacement. The first test was conducted on an un-pressurized sample ($P_{internal}$ = 0 psi). The result was a buckling load far below the

expected value to 580 lbs. The mode of buckling was also diamond shaped instead of circumferential rings. The diamonds first appeared in one location on the can surface and then grew around the can as the applied axial load was continually increased. The result is shown in Figure 41.

Figure 41 – Pressurized shell, $P_{internal}$ = 0 psi

The next tests were conducted with internal pressure = 70 psi. The cans again buckled short of the 580 lb critical load predicted. However, the cans did buckle at the very outer lip of the can where it was in contact with the mandrel; edge effects were suspected.

Figure 42 – Buckling at Outer Edge of Shell

Figure 42 shows a can where the edge is folded over onto itself. In order to get away from the possible interference of edge effects, additional restraints were required. The ends of the shell which were supported internally by the mandrels were also loosely clamped on the outside to ensure that the shell could not buckle at the very ends. These clamps are shown below in Figure 43.

Figure 43 – Clamps to Prevent Shell Buckling Near End of Can

Cans were constrained as shown above and collapsed in the Instron. The tests were conducted at three different pressures to see if internal pressure had any effect on shell buckling load. The cans were loaded to an initial axial preload to help seal the ends of the shell. Next, internal pressure was applied and controlled by a regulator. The amount of load reacted by the internal pressure was calculated by subtracting the preload from the force reading after the internal pressure was applied. The axial loading was increased until buckles formed in the cans. A computer equipped with a National data acquisition board recorded the loads and displacements. The data was reviewed and the highest load was found. This maximum reading minus the pressure effects, as

determined previously, resulted in the critical buckling load observed in experiments. Two tests were conducted at 30 psi internal pressure with critical loads of 561 and 582 lbs. One test at 50 psi resulted in a maximum axial load of 576, and three tests at 75 psi yielded critical loads of 627, 592, and 586.

It appears that the magnitude of internal pressure is not a major factor in shell stability. The internal pressure primarily seems to stabilize the cans to give more uniform buckling results. If all data points are averaged, a critical buckling load of 587 lbs was obtained experimentally compared to a predicted value of nearly 580 lbs from equation (79). Under the circumstances this seems to be very good agreement. One standard deviation of the data is 22.1. Even though the scope of this study was limited, initial conclusions are favorable of equation (79) providing accurate axial buckling stress for internally pressurized cylindrical shells.

The next case examined was that of an internally, rigidly supported shell. A mandrel was machined to match the inside diameter of our test cans. The cans must be able to slide onto the mandrel with a snug fit. A cap was then machined to slide over the top of the mandrel to compress the cans. The clamps used in the internally pressurized tests were again used here to prevent end effects and provide a built end condition at the ends of the cans. The experimental setup is shown below in Figure 44. In Figure 43 and Figure 44 we can see fully formed circumferential buckles away from the ends of the shell as evidence of the benefit of the sliding clamps.

Figure 44 – Rigidly Supported Shell Buckling

Fifteen cans were compressed to buckling, giving an average critical load of 562 lbs as compared to the expected value of nearly 580 lbs. The maximum load recorded was 665 lbs and the minimum load was 469 lbs. One standard deviation was 63.3. The spread of the data seems high but during the experiments notes were taken that may give

insight to the test results. The test notes indicated that in certain cases the cans were difficult to remove from the mandrel. This suggests that frictional forces may have contributed to the higher loads attributed to these cases. In the case of the lower buckling loads, it was observed that the cans fit the mandrel very loosely. The result was diamond shaped buckles forming in the cans first.

Results obtained from experimentation with both internally pressurized cylinders and rigidly supported cylinders indicate that equation (79) may indeed be appropriate to use in modeling a web buckling on a roller. Tests did indicate that both a pressurized cylinder and an internally, rigidly supported cylinder buckle very near the predicted value. The test samples were small and larger test samples would be recommended for future studies. The case of the internally, rigidly supported cylinder might be further improved by using a 3 piece mandrel instead of the two piece mandrel currently used. The three piece mandrel would allow a load cell to be placed underneath the internal mandrel and effectively measure the frictional force between the can and its internal support. This frictional force could then be subtracted from the overall buckling load. This procedure would also help to lower the deviation in the test values since loose fitting cans would no longer be used in testing procedures.

4.2 Wrinkling and Finite Elements; Previous Efforts

The first effort to model a web with troughs formed in the span, with finite elements, was by Webb [45]. Webb addressed the issue of wrinkles developing on a downstream misaligned roller. It was at this time that a linear relationship between θ_{trough} and $\theta_{wrinkle}$ was first observed. Data collected by Beisel [4] was plotted in Figure 45.

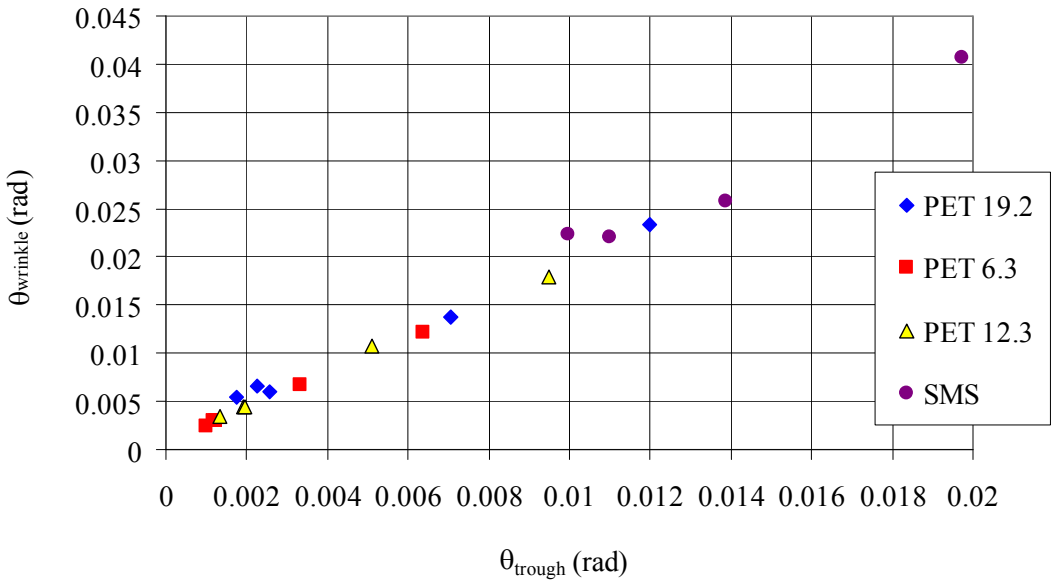

Figure 45 – Correlation Between Troughs and Wrinkles

Webb then proceeded to collect trough and wrinkle data for a larger number of materials which yielded similar results. Webb conducted experiments to measure deflection due to a misaligned roller similar to the tapered roller deflection experiments presented earlier. The following chart was produced.

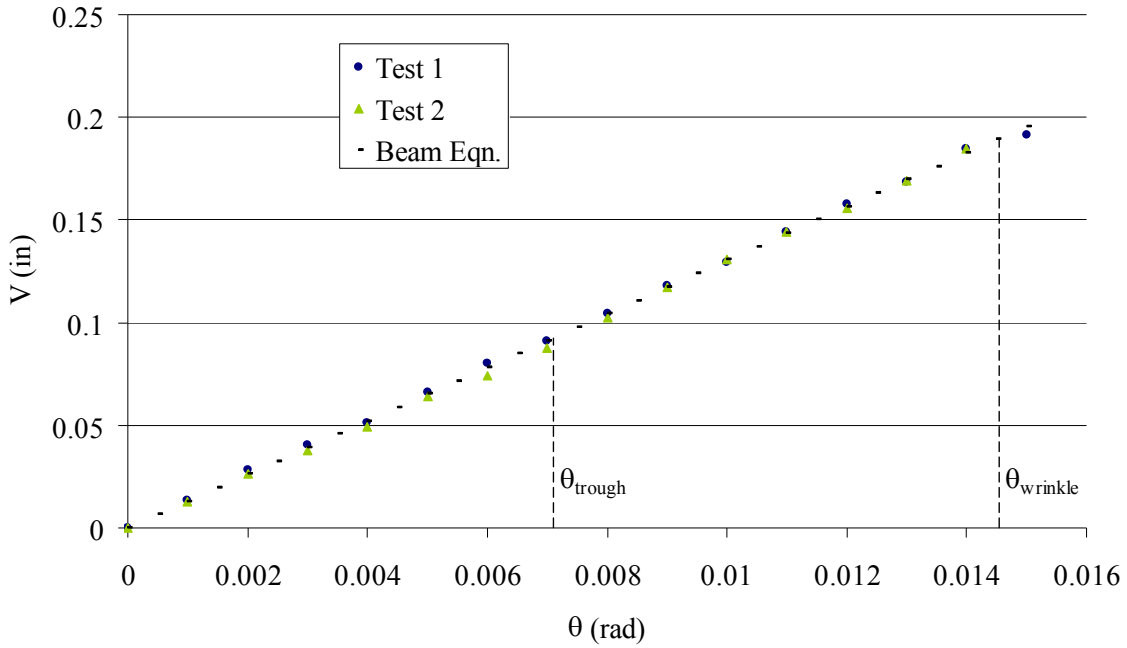

Figure 46 – Deflection Due to a Misaligned Roller; 92 ga Polyester, L = 18”

Figure 46 demonstrates the same behavior as seen previously in the case of the tapered roller. The deflection remains linear after troughs have formed in the web span. Webb also investigated the relationship between web buckling (trough and wrinkle) and width reduction of the web.

Modeling a web span with developed troughs until the point of wrinkling with finite elements was the effort of Webb most relevant to this study. Figure 47 shows a diagram of boundary conditions and applied loads used by Webb.

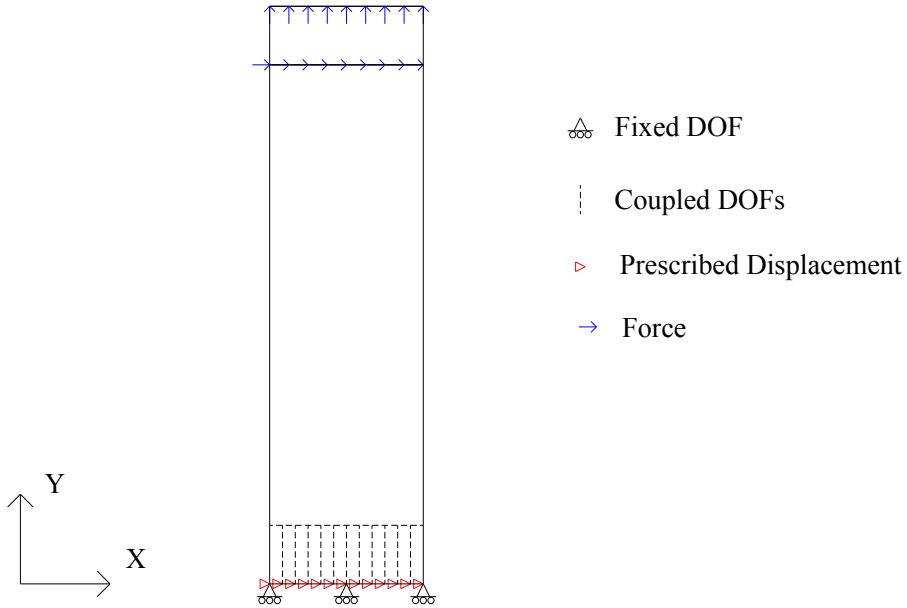

Figure 47 –Boundary Conditions and Applied Loads as Used by Webb

Webb's model incorporated the no-compression elements in the web span and regular elastic elements for the web on the rollers. He increased the shear force until the critical shell buckling stress was reached, as given in equation (79). Once the critical compressive CMD stress was reached Webb determined the rotation of the downstream roller from the displacement output from the analysis. The results seemed to suggest that the rotations developed by the FE model were not as great as those observed in experiment. It was then proposed that the rotation should be the addition of the angle needed to cause trough formation, equation (51), and the angle of rotation needed to cause wrinkles per FE analysis.

$$\theta_{cr,misalignment} = \theta_{cr,trough} + \theta_{cr,wrinkle} \tag{80}$$

Comparison of equation (80) to experimental data is given in Figure 48. Webb's error bars in this graph represent a 95% confidence for his 3 tests.

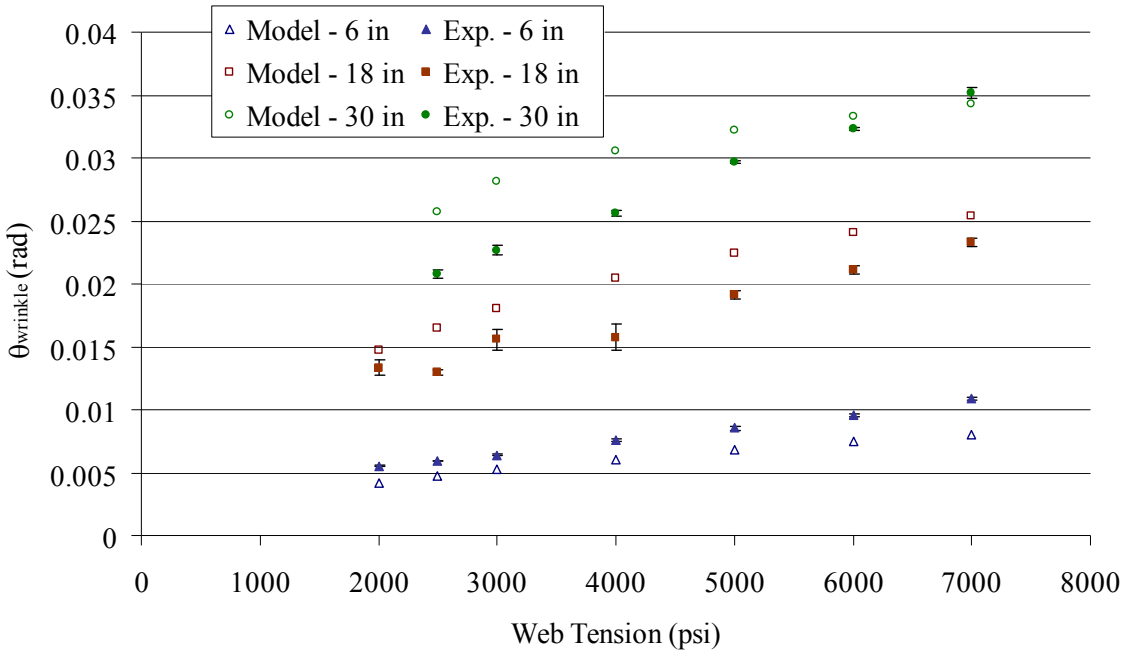

Figure 48 – Webb's FE Model and Experiment, 92 ga Polyester, R_o = 1.45"

Figure 48 shows relative agreement with experiment. The largest discrepancies occur at the longer web spans with lower tensions. Of concern, is the model itself, equation (8080) is not considered here to be valid and lacks theoretical basis. If this model gives the correct formulation for a misaligned roller then the same procedure should be applicable to the case of the tapered roller. The two cases are very similar with only downstream boundary conditions being different. In light of this, the case of the misaligned roller and the development of wrinkles on the downstream roller will be investigated further. A satisfactory solution method must be found that can be consistently applied to both the misaligned and the tapered roller cases.

4.3 Wrinkles Due to Misaligned Rollers; Finite Elements

The method for the determination of wrinkle formation due to a downstream misaligned roller is now developed. This method should be applicable to other types of shear wrinkles in a consistent manner. The basic model developed is similar to that presented by Webb, where wrinkling membrane elements are used to determine the stresses in the web after troughs are assumed to have formed in the web span. The misalignment is then increased until the compressive CMD stress at the tangent point to the roller reaches the critical stress determined by equation (79).

The wrinkling membranes used to handle the post buckled state of the web in the free span were developed to their most common form by Miller and Hedgepeth [26]. When thin membranes are buckled, it is assumed that the bending stiffness associated with additional compression of the membrane is negligible. The elements used to handle this buckled condition may take on one of three possible states each with a different associated stiffness matrix. Each state is determined by the stress present in the element. If it is determined that there is slack in any direction then the stiffness matrix corresponding to the stack direction is then set to equal zero. In essence, wrinkling membrane elements cannot withstand compression. This process therefore required a non linear iterative process to handle the state dependent properties associated with the wrinkling membrane elements. The possible states of the wrinkling membrane elements are shown below in Figure 49.

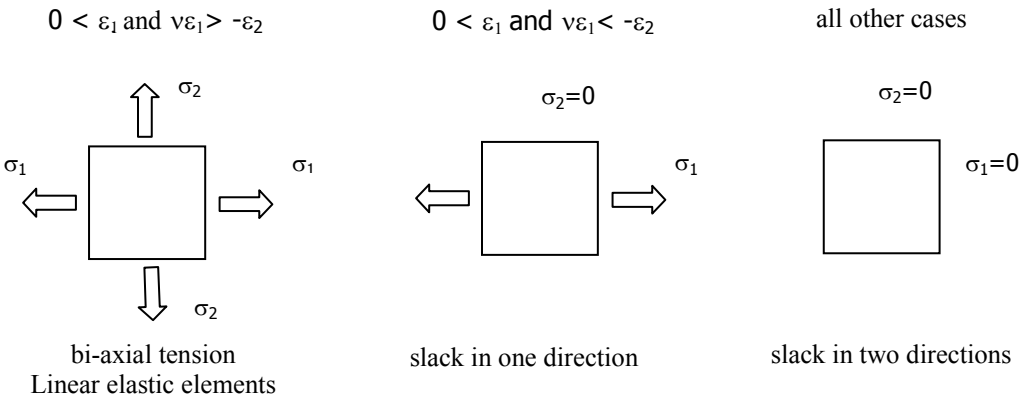

Figure 49 – States of Wrinkling Membrane Elements

The boundary conditions presented for the case of a downstream misaligned roller as given in equations (45-48) are now implemented in an FE model. These boundary conditions are shown below in Figure 50.

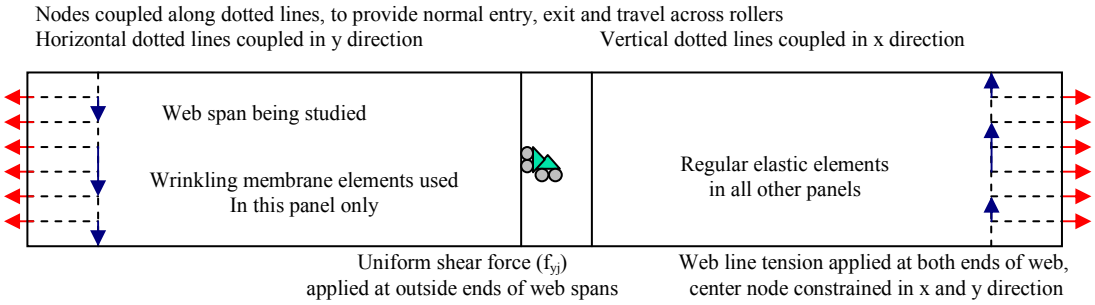

Figure 50 – FE Wrinkle Model, Misaligned Roller

The model shown above in Figure 50 is divided up into five panels. The first represents the web on the upstream roller. This web may contract with Poisson effects due to applied tension but the exit of the roller assumes no slippage until the web leaves the roller. The coupled nodes in panels representing web on rollers helps enforce normal entry and exit on upstream rollers. The second panel is the span where web with developed troughs is being simulated and is the only span to make use of the wrinkling membrane elements; all other spans use regular elastic elements. The third panel represents, to a limited extent, the web on the downstream misaligned roller. The fourth

and fifth panels are used only to help achieve the desired boundary conditions in the left hand side of the model; they are not representative of the web behavior downstream of a misaligned roller. Additionally, the elastic material on the right hand side of the model also, resists compression. A sample σ_y stress output from this model is displayed in Figure 51.

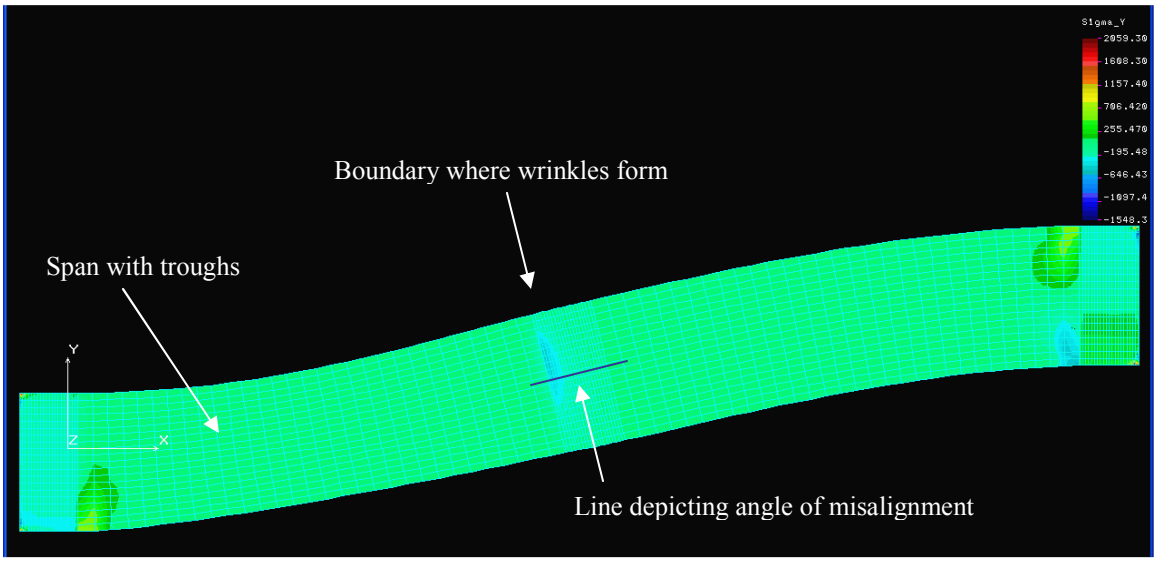

Figure 51 – Deformed Model (10x) Depicting σ_y Stress

The model presented above shows the deformed shape (10X) of the FE model. If the MD stress (not shown) is analyzed, we can see a large moment developing at the upstream roller boundary and decreasing linearly as we head toward the downstream roller. At the misaligned roller boundary the moment across the web is reduced by approximately 95% and shortly afterwards reached zero before a moment in the opposite direction linearly increases in the right side of the model. Also, if deformations are studied across the misaligned roller, the web deforms linearly across this region suggesting compliance with normal entry and transport. These deformations are plotted below in Figure 52.

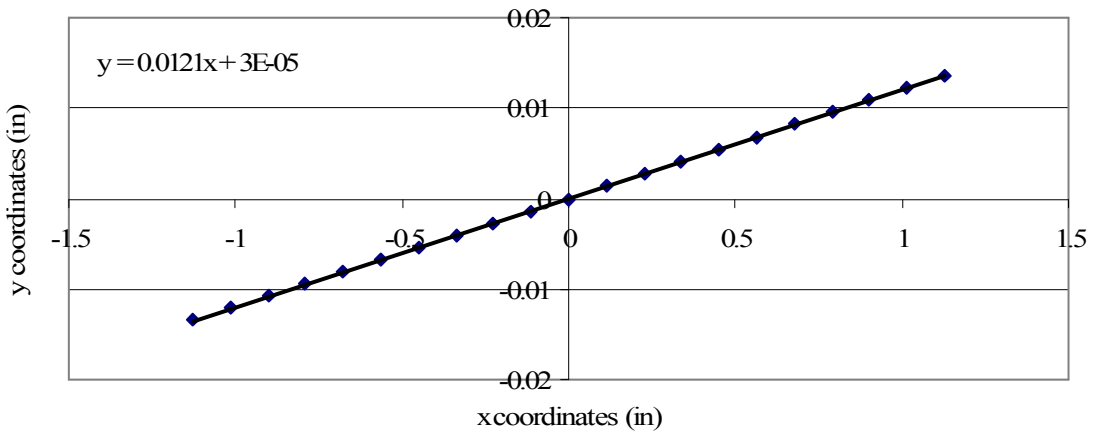

Figure 52 – Deformed Nodal Coordinates

The rotation of the misaligned roller is determined by the slope (dv/dx) of the deformed nodes across the third panel of the web.

Execution of the proposed model began with the application of the desired web line tension. Next, shear force was applied. This shear force was increased until the critical compressive stress required by equation (79) was achieved in the first row of elastic nodes. This first row of elastic nodes represents the boundary between the troughed web span and the web that is forming a shell on the roller. At this point, the web was considered to have reached the onset of wrinkle formation. The slope could now be determined from nodal deformations, as previously mentioned. The output of the compressive principal stress across the web is shown below in Figure 53.

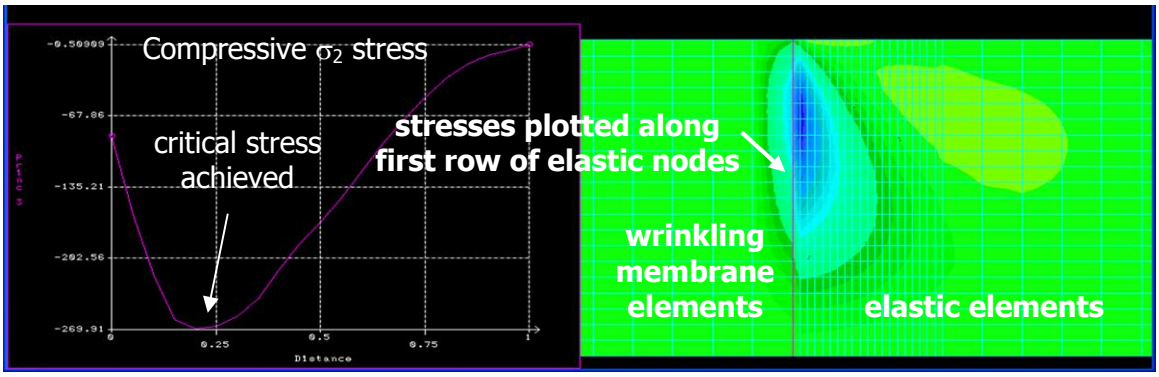

Figure 53 – Critical σ_2 Stress Developed in FE Analysis of Misaligned Rollers

Experiments determining the onset of wrinkle formation due to a misaligned downstream roller have been previously performed by both Beisel (which have never been presented) and Webb [45]. The experiments were conducted in the same manner as described earlier for trough formation due to misaligned rollers. Here, the data presented by Webb is again used to verify the currently proposed model in the following figures. The material is, again, an opaque 92 ga polyester, with a width of W = 6", a MD Young's Modulus of E_x = 712000 psi and a Poisson's Ratio of ν = 0.3. The misaligned roller had a radius of 1.45". Equation (79) yields a critical compressive stress for this case of approximately 270 psi.

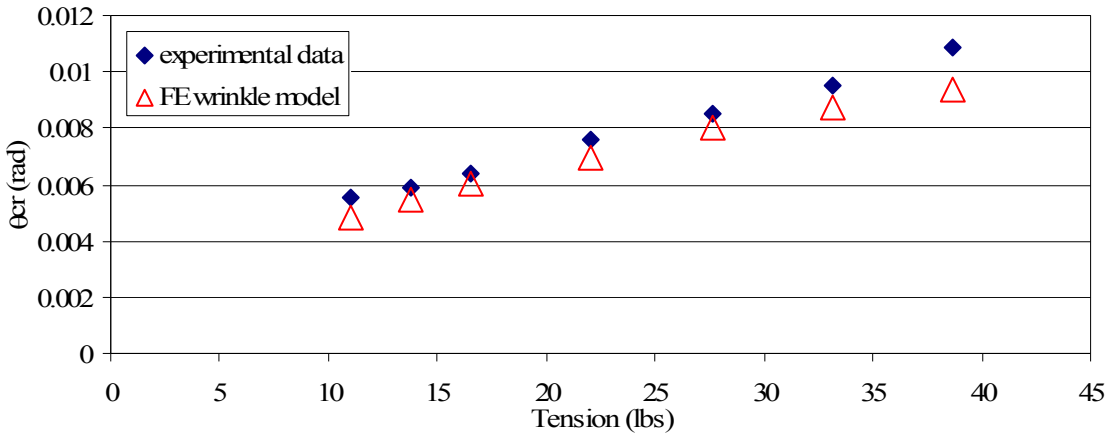

Figure 54 – Wrinkles Due to Misalignment, 92 ga Polyester, L = 6"

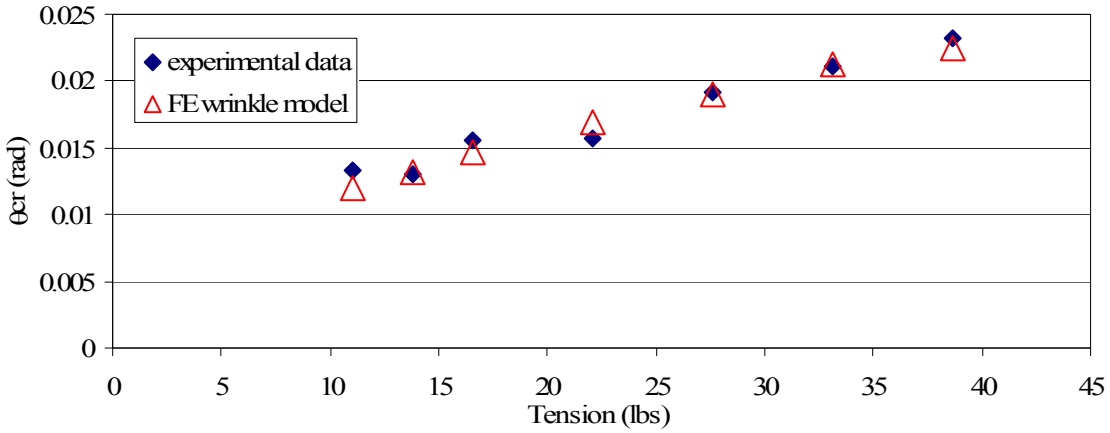

Figure 55 – Wrinkles Due to Misalignment, 92 ga Polyester, L = 18”

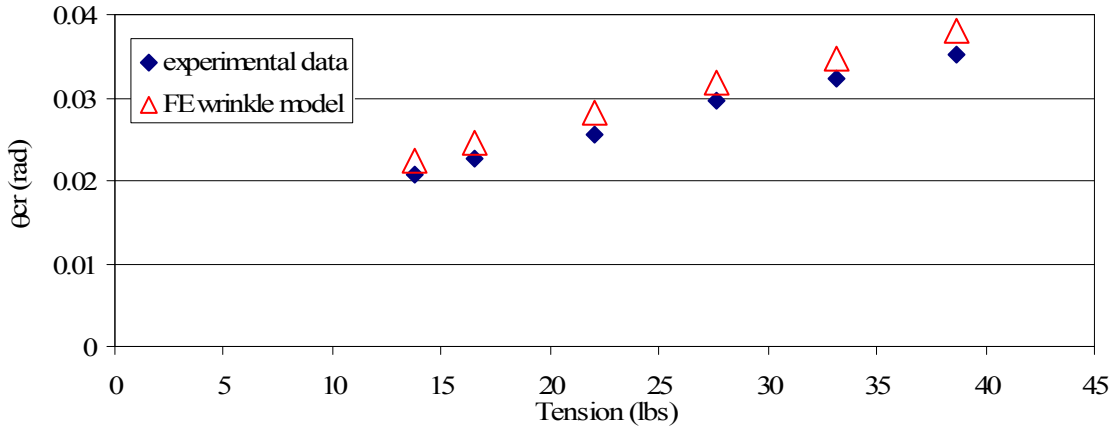

Figure 56 – Wrinkles Due to Misalignment, 92 ga Polyester, L = 30”

Figure 54 - Figure 56 show relative agreement between the FE model and experimental results over the range of parameters tested. Whether the proposed model would be applicable in extremely short or long web spans remains uncertain. However, the model is capable for predicting an estimate of wrinkle formation for a typical web span. Of interest is a comparison between the current FE model and that previously

proposed by Webb [45] as shown below in Figure 57. Again, Webb's error bars represent a 95% confidence.

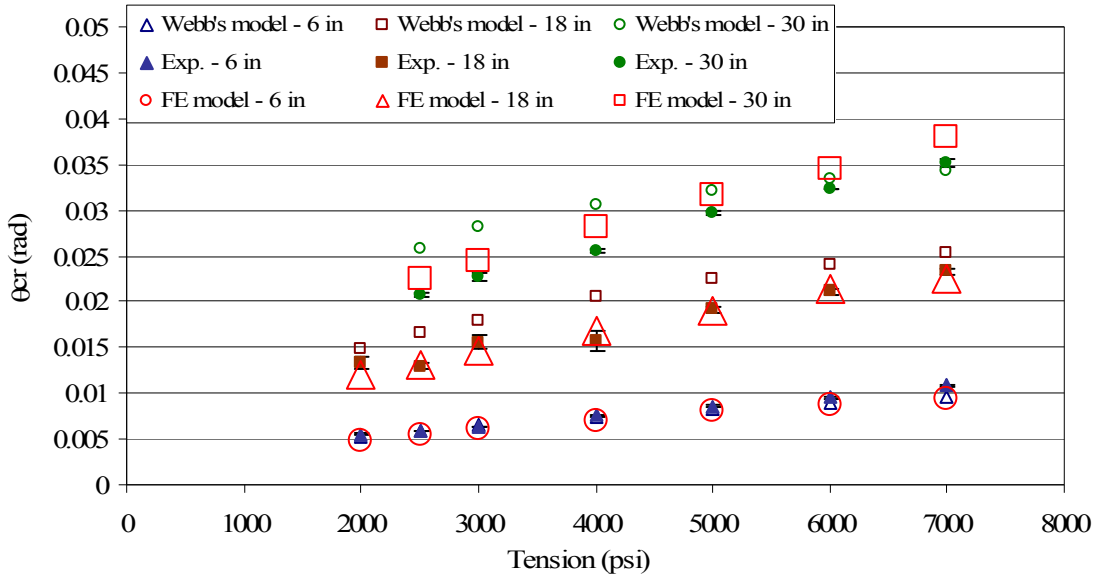

Figure 57 – Comparison of Webb's Model to Current FE Model

Figure 57 shows comparable performance between the current model and Webb's model in the 6 in span. However the proposed model provides better results in the longer spans. Of greater importance is the currently proposed model does not rely on the use of equation (80) which is not considered here to be valid. It is assumed the improved model was the result of a better implementation of the proposed boundary conditions in the FE analysis, namely the additional elastic material on the right hand side of the model, which also resisted compression. Moreover, the results achieved in Figure 54 - Figure 57 support the concept of modeling webs with developed troughs, using wrinkling membrane elements in an FE analyses coupled with a shell buckling criteria, equation (79), to predict the formation of wrinkles due to a downstream misaligned roller. In this,

and other FE analyses, the software package used was COSMOS 2.8. Appendix A discusses particulars of the inputs used in the analyses.

4.4 Wrinkles Due to Tapered Rollers; Finite Elements

The model for the determination of wrinkle formation due to a downstream tapered roller is similar to the model presented in the previous section. The buckling criterion for a shell, equation (79), yields the compressive stress that the web on the tapered roller can withstand before a wrinkle forms. The boundary conditions presented in equation (7), equation (9), and $v_i = 0$ are then implemented in a FE model, making use of the wrinkling membrane elements to model sections of the web where troughs are considered to have formed. This FE model generates the stress distributions in the web which can then be related to the required critical compressive stress in the web on the roller.

The boundary conditions are implemented into the FE model, as shown in Figure 58.

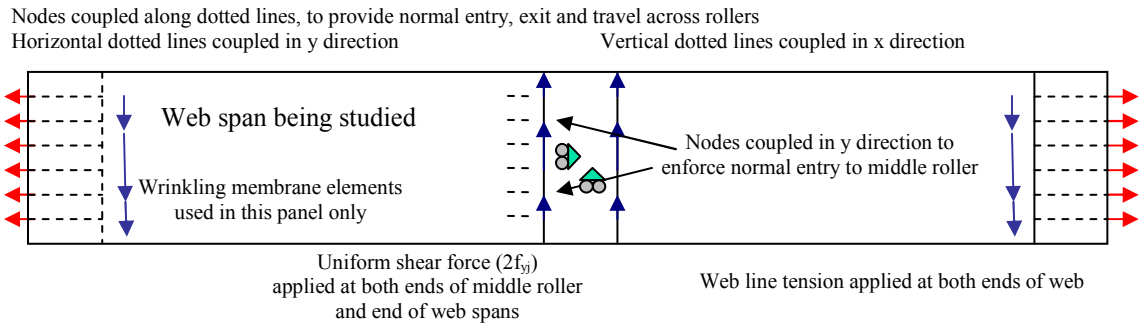

Figure 58 – FE Wrinkle Model, Tapered Roller

The model is again divided up into five panels. The first panel represents the web on the upstream roller. The nodes on this panel are locked along horizontal lines. Each node on the line must move with the same y displacement as the rest of the nodes on the same line. This allows for Poisson contraction due to web line tension but requires a zero

slope at the beginning of the troughed web span. The nodes at the exit of the upstream roller (right side of first panel) are locked in the x direction along a vertical line to simulate the roller gripping the web in a no-slip condition. The second panel makes use of the wrinkling membrane elements that simulate web with developed troughs. Along the right edge of the second panel the nodes are again locked along horizontal lines in the y direction for a very short distance. This ensures normal entry of the web to the tapered roller. The third panel is the elastic web on the tapered roller. The right hand side of the model is only used to help enforce the boundary conditions on the left side of the model and is not representative of the web downstream of a tapered roller.

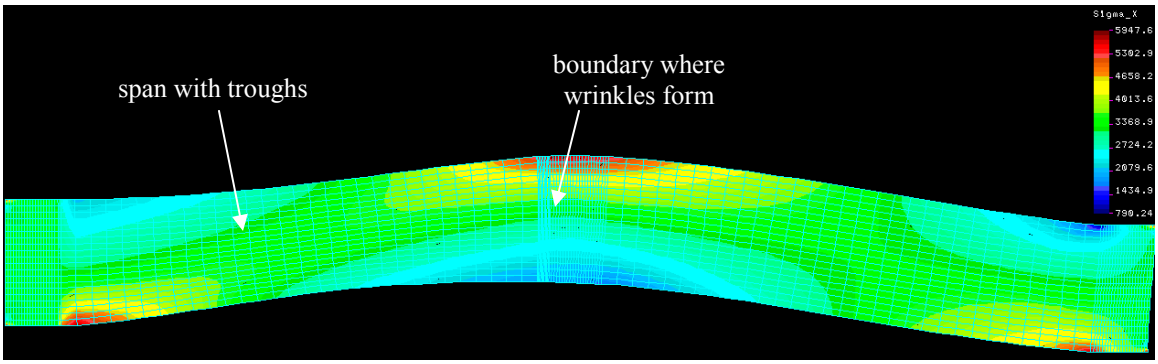

Figure 59 – Deformed Model (25X) Depicting σ_x Stress

Figure 59 depicts the deformed shape (25X) of the FE model. We can see a moment developed at the upstream end of the troughed web span. The moment decreases linearly until reaching a net value of zero at the middle of the span then increasing to the middle panel. We see the compressive σ_y stresses at the free span - roller boundary in Figure 60.

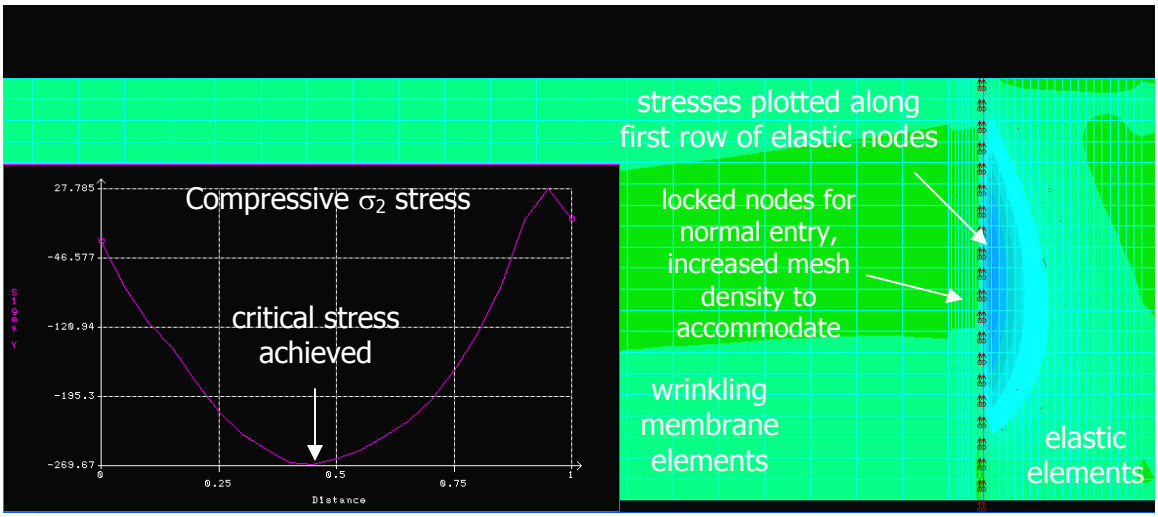

Figure 60 – Critical σ_y Stress Developed in FE Analysis of Tapered Roller

In the case of the downstream tapered roller, the mesh density of the wrinkling membrane elements is increased just before the boundary with the elastic elements. This was not done for reasons of convergence but rather to allow for minimal interference of the nodes coupled in the y direction. In fact, it was found that the length of coupled nodes was not critical and the same results were achieved whether the first two, first three, or second and third nodes from the boundary were coupled. Placing the y constraints in the elastic elements creates interference with the development of compressive stress and should be avoided.

The model was executed by first applying web line tension and then increasing shear force until the compressive stress across the first row of elastic nodes on the elastic-wrinkling membrane element boundary reached the critical value predicted by equation (79). Whether the compressive σ_y stress or the compressive principal stress is used, the results are the same for the case of the tapered roller.

Experimental results for the onset of wrinkles due to a downstream tapered roller were obtained at the same time as the results for trough formation due to taper. The experimental method employed was the same as described earlier with the exception of wrinkle formation being determined visually instead of troughs. Also, no laser was used for enhancement of visual effects. The first web tested was a 92 ga opaque polyester with a Young's Modulus of E_x = 712000 psi, a Poisson's Ratio of $\nu = 0.3$, and a width of W = 6". The nominal radius of any tapered roller was R_o = 1.49". The compressive stress required by equation (79) was approximately 265 psi for this case. Comparison between the proposed FE model and experimental results are given below. The experimental data represents the average of three tests with error bars again representing the minimum and maximum values measured.

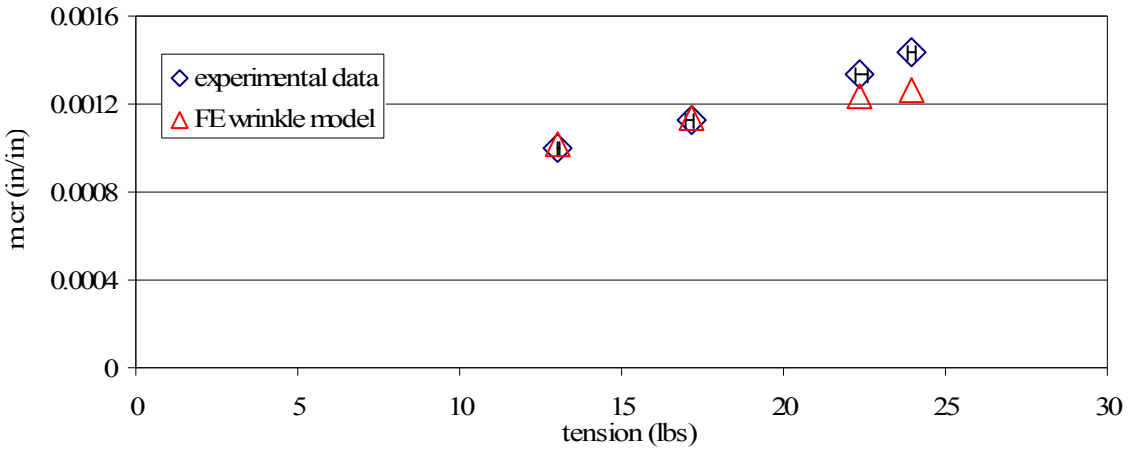

Figure 61 – Wrinkles Due to Taper, 92 ga Polyester, L = 10"

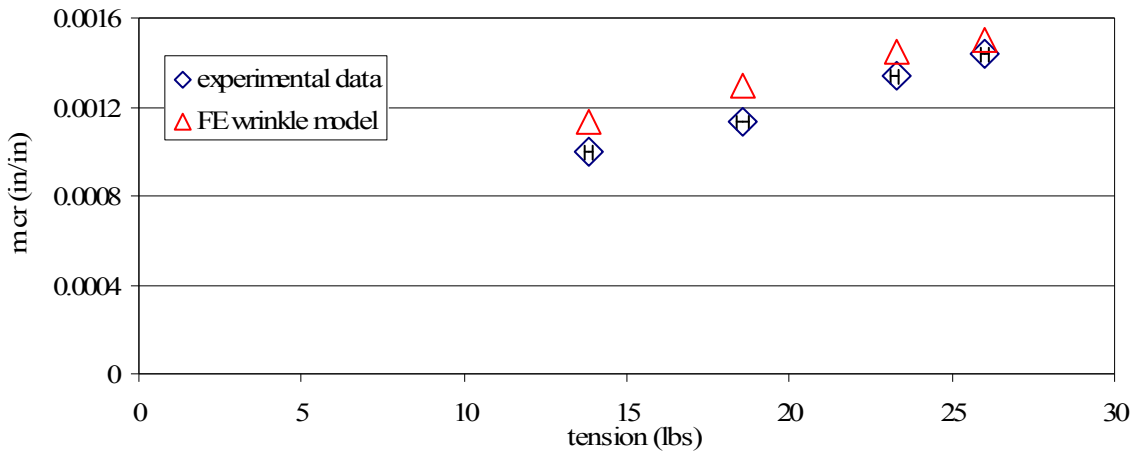

Figure 62 – Wrinkles Due to Taper, 92 ga Polyester, L = 20”

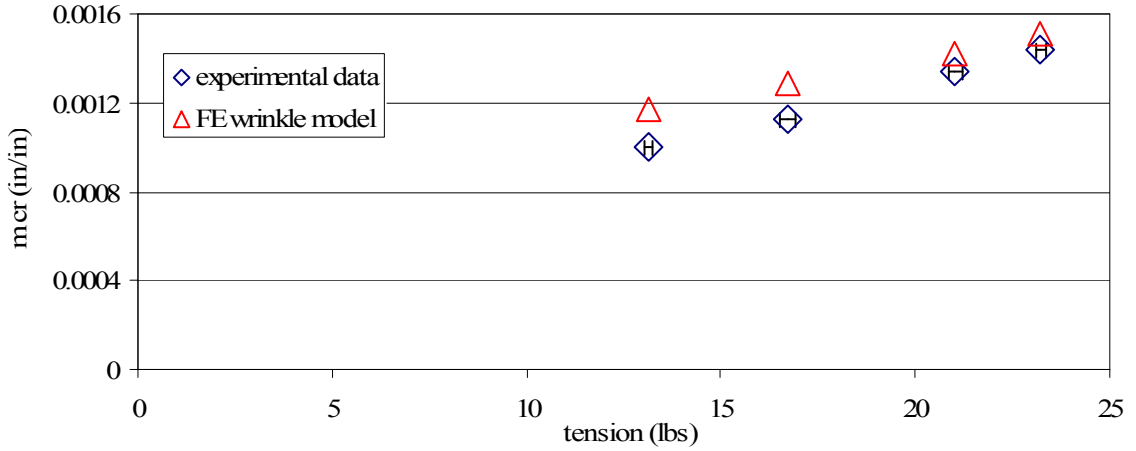

Figure 63 – Wrinkles Due to Taper, 92 ga Polyester, L = 30”

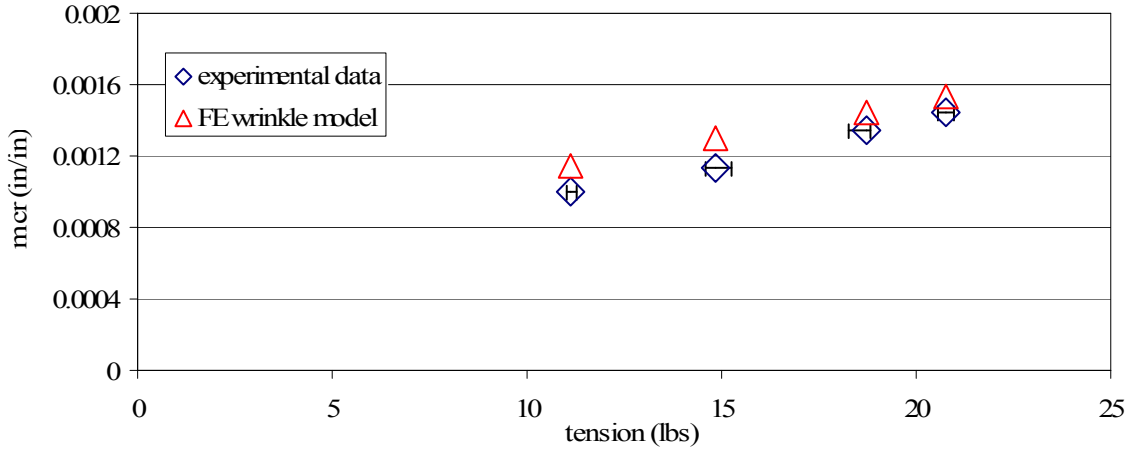

Figure 64 – Wrinkles Due to Taper, 92 ga Polyester, L = 40”

Figure 61 - Figure 64 show good agreement between the FE model and experimental values. The shortest span studied was 10" and some drift from the data due to span may be detectable. While 10" is longer than the shortest span studied for case of a misaligned roller (6"), is should be noted that the case of the misaligned roller is very nearly ½ of the model for a tapered roller with moment reversals occurring in about ½ of the span length. The longer spans tested (20", 30", and 40") show the model tracking correctly with changes in span length.

Also tested was a relatively thin web, a 56 ga Polyester, with a Young's Modulus of E_x = 658000 psi, an assumed Poisson's Ratio of $\nu = 0.3$, and a width of W = 6". Since only one set of data was collected for this case, error bars are not shown. The critical stress required by equation (79) is 150 psi.

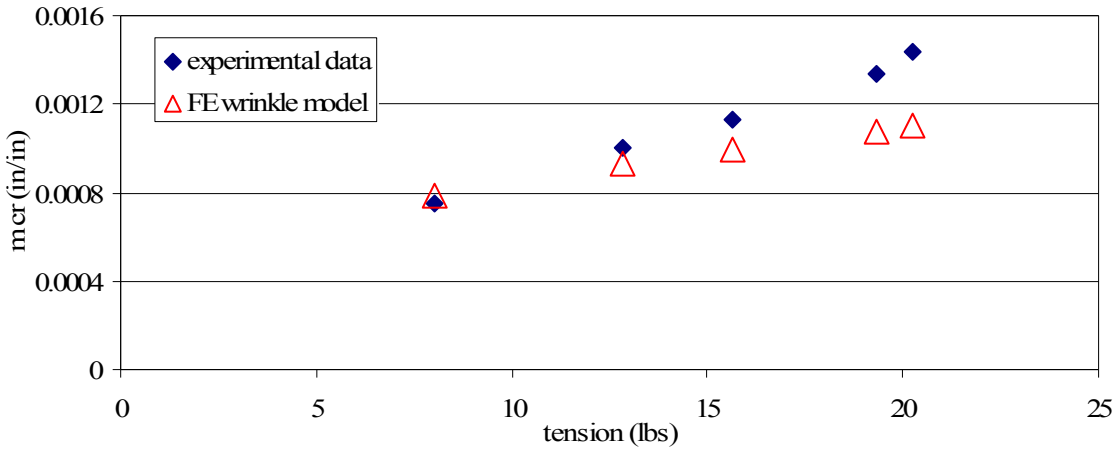

Figure 65 – Wrinkles Due to Taper, 56 ga Polyester, L = 10"

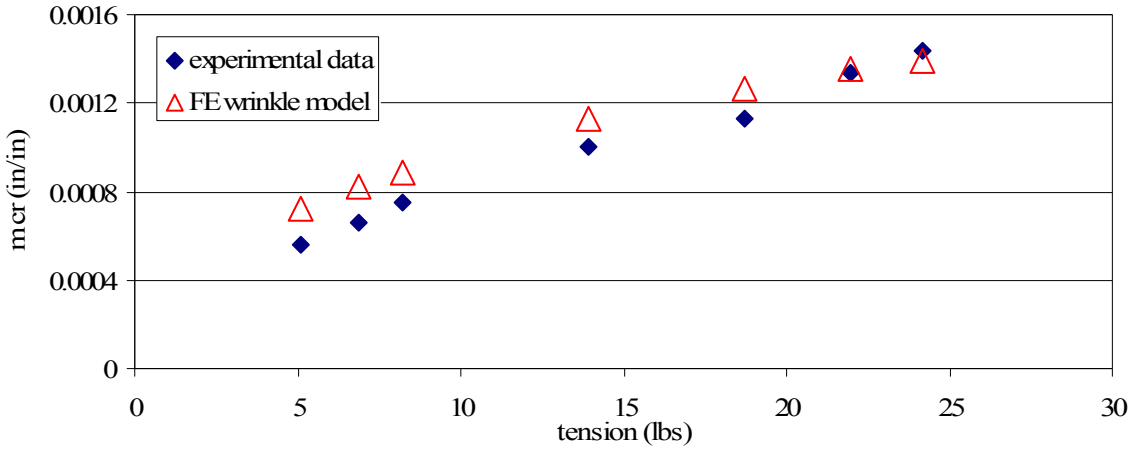

Figure 66 – Wrinkles Due to Taper, 56 ga Polyester, L = 20”

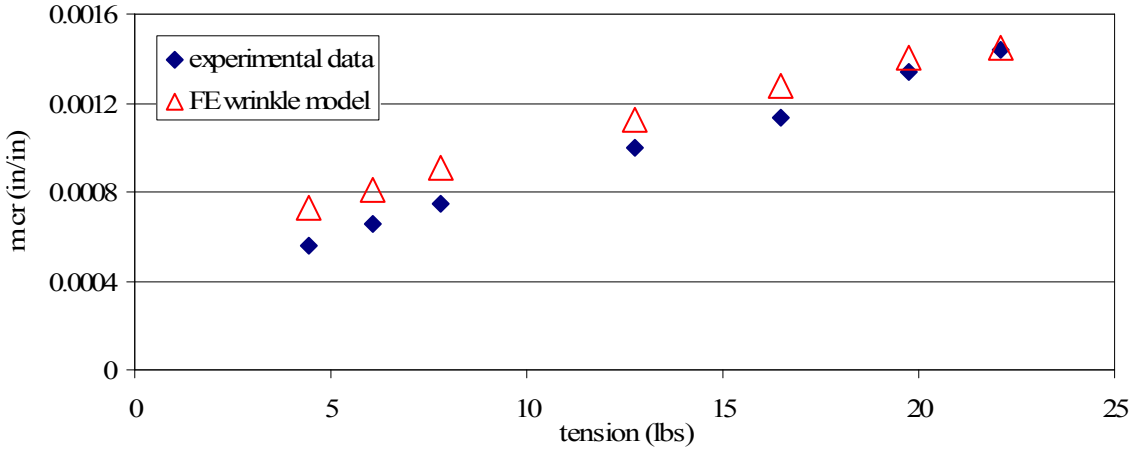

Figure 67 – Wrinkles Due to Taper, 56 ga Polyester, L = 30”

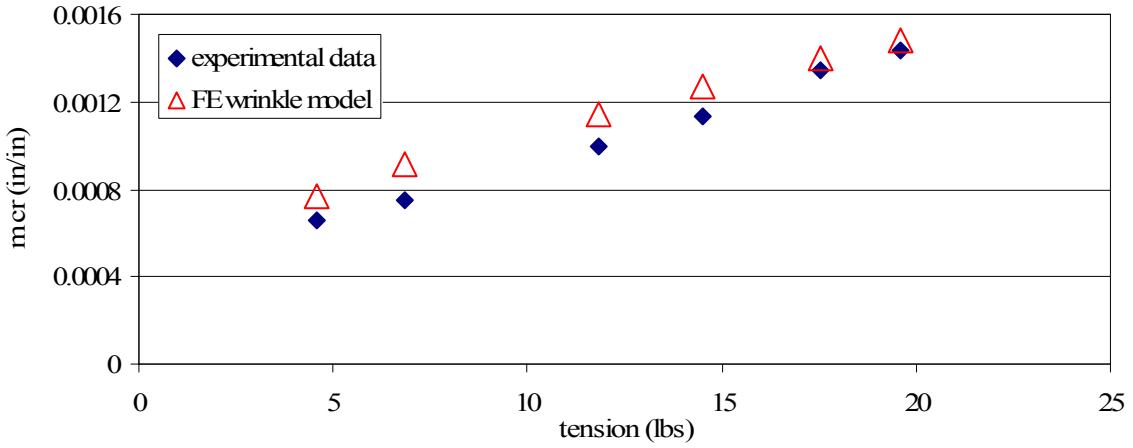

Figure 68 – Wrinkles Due to Taper, 56 ga Polyester, L = 40”

Analysis of Figure 65 may suggest the limitations of the model for use in short web spans with high web line tension. This may also be evident, to a lesser extent, in Figure 61. In the longer spans tested (20", 30", and 40"), the model follows experimental values. In all cases tested (both thicknesses), the high tension data seems to taper off compared to experiment suggesting another possible limitation of the model. This could in fact be due to high local stresses causing changes in modulus. Also of concern, the membrane elements in their wrinkled state do not account for shear stiffness that may be present in the shorter spans. Many of the higher tension data points (typically the two highest tension point in most cases) require localized MD stresses of greater than 7000 psi in the web. Figure 7 showed that linear elastic behavior of the 92 ga polyester only extended to around 700 psi. In conclusion, for the ranges tested, the proposed FE model provides acceptable results in all cases.

4.5 Conclusions of Wrinkles Due to Shear

A method for prediction of wrinkle formation due to shear in web spans has been developed. This method was employed specifically to the cases of wrinkling due to a downstream misaligned roller and to the case of a downstream tapered roller. Experiments were designed to test this model over various span lengths, web thicknesses, and web line tensions for both cases. When the models were compared to experimental values for the onset of wrinkle formation, both models gave acceptable performance. One limitation of the proposed models may be application to extremely "short" web spans.

The proposed model begins with a buckling criterion for the web on the roller in shell form, equation (79). Relevant boundary conditions were then prescribed to an FE model which used wrinkling membrane elements to simulate web with wrinkles formed in the span. When compressive CMD stresses, which are developed in the first row of elastic elements representing the tangent point of the web on the roller, reach the critical stresses predicted by equation (79), the point of wrinkle formation had been reached. This method was consistently applied to the cases of the misaligned and tapered roller in a consistent manner, achieving similar results, and similar limitations in each case. It appears that this method may be successfully applied to other cases involving shear wrinkling such as web steering due to uneven nip pressure between laminating rollers or other rubber covered rollers.

In applying this method, of importance was correct implementation of the boundary conditions. Specifically, achieving the correct MD stress profile was essential to a successful model. Also of importance was consideration of normal entry to the roller. This condition was harder to implement because coupling nodes in the elastic region interfered with the compressive stresses developed there. In both cases studied, normal entry was at least partially enforced through indirect means (the right hand side of the model helped achieve correct rotations at the end of the troughed span).

CHAPTER V

Prediction of Machine Direction Wrinkles

5.0 Introduction to Crowned Rollers

Crowned rollers are different in their interaction with webs than misaligned or tapered rollers. In the cases of roller misalignment and taper, the webs undergo a lateral steering. This lateral steering is caused by a shear force applied to the web which results from the web attempting to gain normal entry to the roller via frictional contact. It has been shown earlier how this shear force, along with web line tension, can generate compressive stresses across the web that result in wrinkles. In the case of a symmetrically crowned roller, no net steering occurs; therefore, the shear force across the end of the web must be absent. In fact, crowned rollers have traditionally been used as self centering pulleys for belts transmitting power between shafts. This application may work fine with stiff belts, but thin webs wrinkle easily on crowned rollers.

Experimental support for any modeling attempts would be needed. The multi-span test stand for the tapered roller was used in conjunction with crowned rollers. Initially, two crowned rollers were crudely machined on a lathe. The initial results suggested a range of crown that would be needed to conduct wrinkling experimentation. A series of rollers were ordered from Fife Co, Oklahoma City, OK. As indicated by our previous tests, the crown of these rollers needed to be slight. Machining such slight profiles with conventional equipment can be challenging. The roller manufacturers felt confident that rollers could be produced in 0.002" increments of diametric variation starting a 0.004in/8in width. There was some concern that 0.004" crown would not be slight enough to capture trough phenomenon, but no other options were currently available. Five rollers were delivered and qualified by the roller profiler previously described and shown in Figure 3. The profiles of these rollers are shown below.

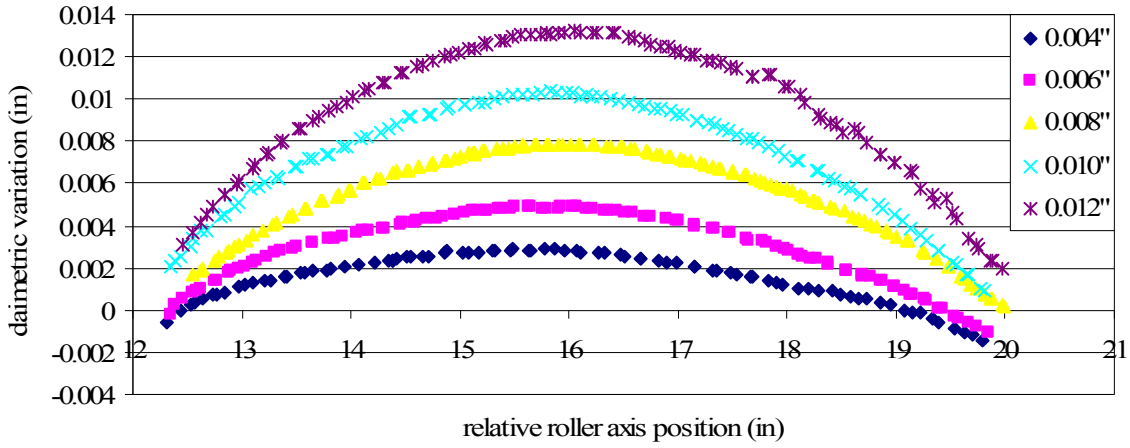

Figure 69 – Fife Crown Roller Profiles

Figure 69 shows the relative roller diameters (all rollers are nominally 3"). These rollers were covered in a high traction coating to ensure the web was not slipping on the rollers. Initial testing with these rollers revealed the presence of troughs in all cases.

Although these rollers may be useful in collection of wrinkle data, it was apparent that a crowned roller with less taper would be required.

5.1 Creation of an Adjustable Low Crown Roller

There are many difficulties associated with the manufacture of a low crown roller. From initial tests with crown rollers, it appeared that crown rollers with as little as 0.0005" radial difference per 8" of width may be needed to study trough formation on 92 gauge polyester films. These are not tolerances that typical machining practices can adhere to. Furthermore, the profiles need to be accurate in order to match experimental data to modeling attempts. Equipment capable of machining, based on measurement and feedback, were not available and would have been cost prohibitive.

The idea arose that a pressurized shell might be used to create a crowned roller. However, a pressurized thin cylinder with fixed ends would not give an exact crowned profile. In order for a shell to reach a near zero crown all machining should be done internally, so the outside of the shell would be cylindrical in the absence of internal pressure. After some consideration, it was discovered that to achieve the desired external roller profile, a shell would need internal variations of nearly 0.2", which are definitely within the capabilities of a common lathe. Ideally, the inside of the shell should be machined with a smooth curve that would require the use of a CNC lathe which was not readily available and cost prohibitive.

After some basic calculation and feasibility studies, a shell profile was proposed. The overall change in shell thickness was 0.182" with discrete steps every half inch. The smallest step would be 0.004" which could be achieved with some care. Due to symmetry, only ½ of the proposed step-wise profile was shown in Figure 70.

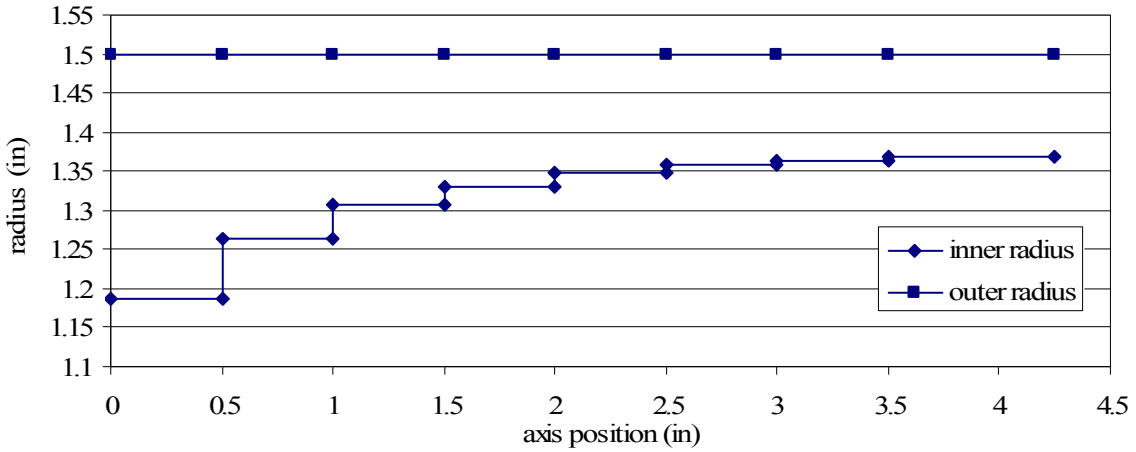

Figure 70 – Proposed Crown Roller Shell Profile

An FE analysis was performed to ensure the steps didn't interfere with expected deformations. Additionally, the stresses were analyzed to ensure safety, as pressurized cylinders can be hazardous, and re-use of the roller. A maximum operational pressure was established at 2000 psi which included a safety factor of 1.5 beyond the yield strength of the aluminum. The expected deformations obtained from the FE analysis are shown in below in Figure 71.

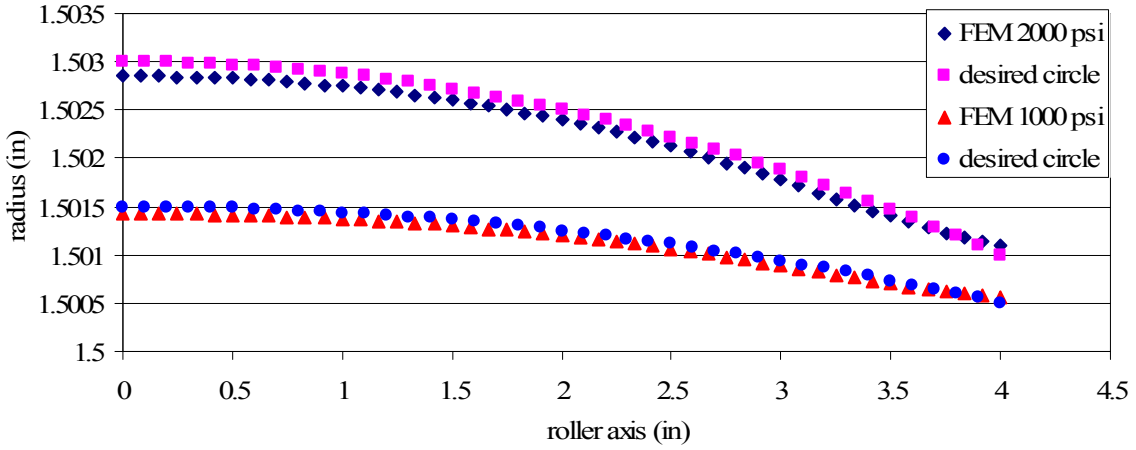

Figure 71 – FE Deformations Compared to Desired Profiles

The machined shell and the assembled pressurized crown roller are shown below in Figure 72 and Figure 73.

Figure 72 – Machined Shell for Pressurized Roller

Figure 73 – Pressurized Roller

Grease, due to its non-compressibility, was used to pressurize the roller shell. A quality hand grease gun is capable of supplying pressures up to 15,000 psi. Again, the roller profiler, shown previously in Figure 3, was used to qualify the crowned roller at various pressures which were determined by a pressure gauge. The resulting relative diameters (the roller is nominally 3") are shown below.

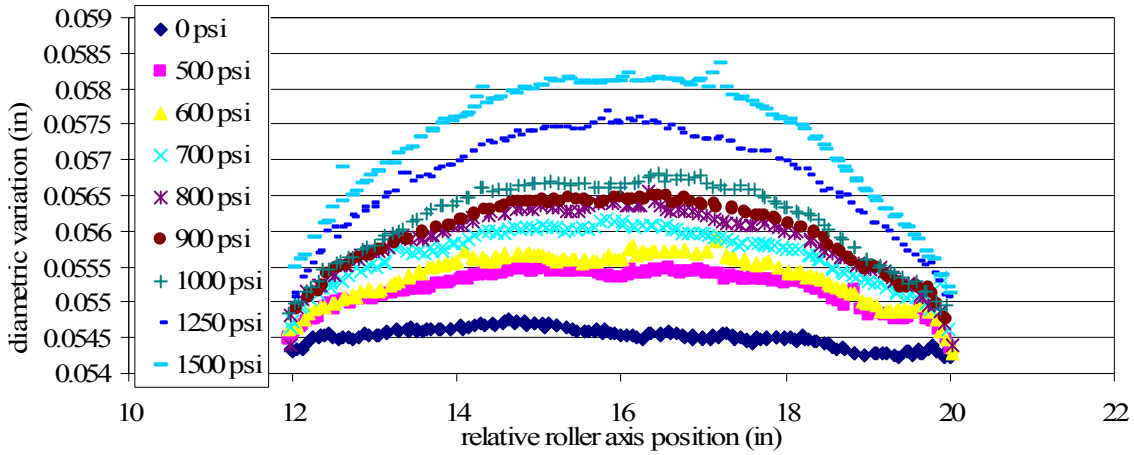

Figure 74 – Pressurized Crown Roller Profiles

Initial experiments with the pressurized crowned roller were unsuccessful. They showed the inadequacy of tension to easily induce trough phenomena. It became clear what was needed was a roller with a dynamically variable crown. This concept is difficult because the roller must remain free to turn with very little resistance. This limitation eliminated the possibility of rotary seals that would be required to operate under 2000 psi of pressure. After some consideration, it was decided that a piston could be fit into the turning roller itself. This piston could then be used to inflate the roller while the whole apparatus turned on bearings. The piston would be driven by a plunger and be isolated through the use of a thrust bearing. This would allow for large forces to

be applied and the unit could still rotate relatively freely. Photos of the apparatus are shown in Figure 75 - Figure 77.

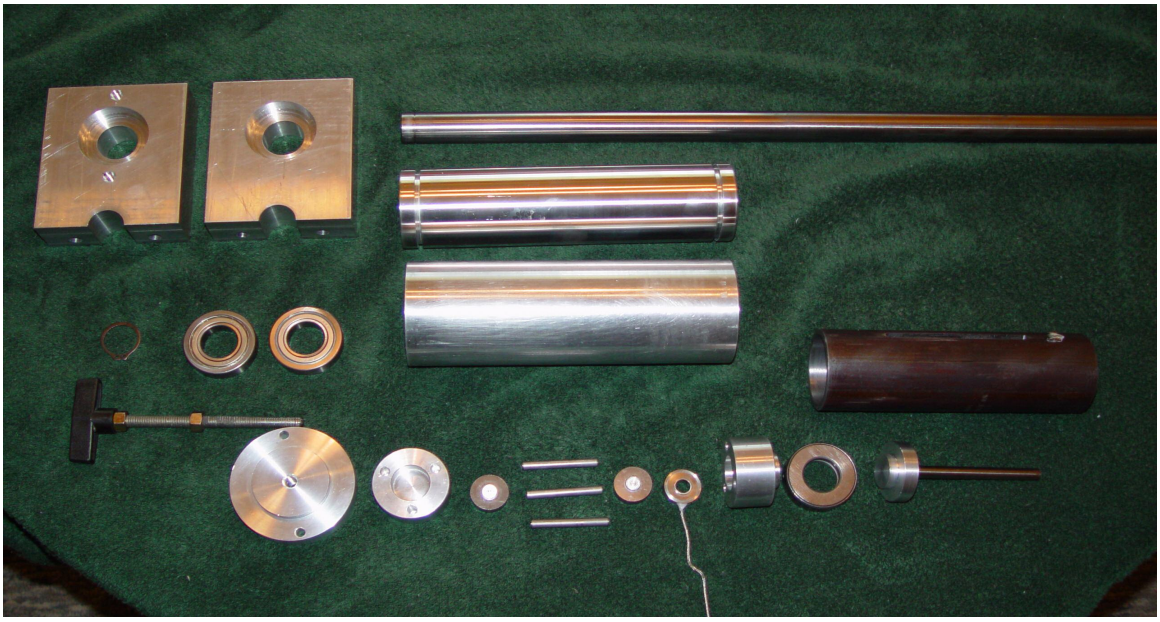

Figure 75 – Machined Parts for the Dynamically Variable Crown Roller

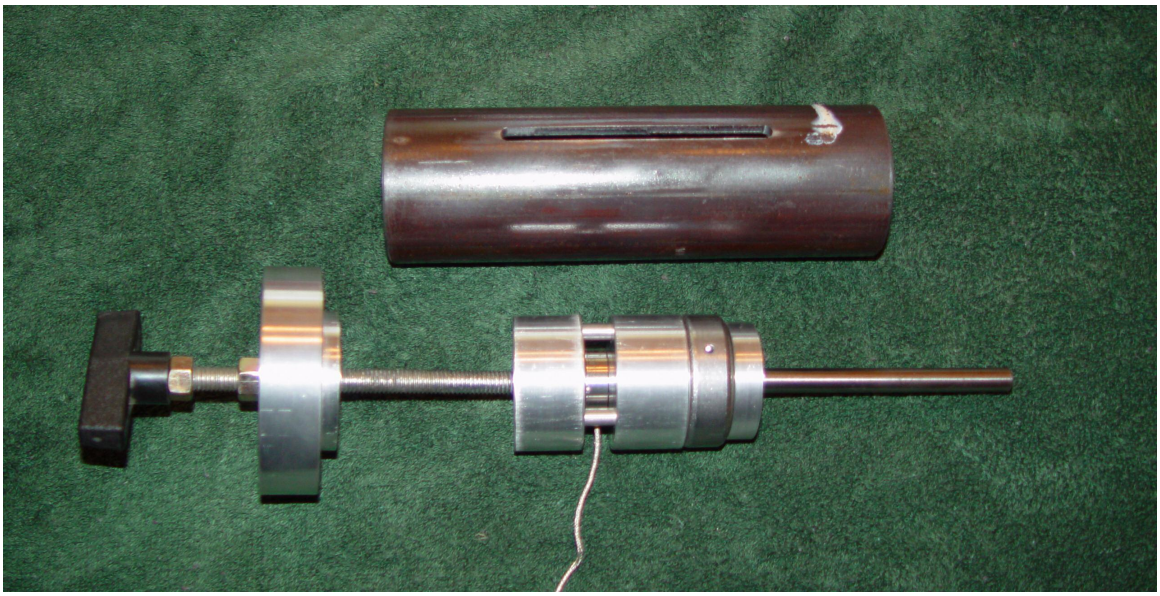

Figure 76 – Thrust Bearing Isolation of Piston

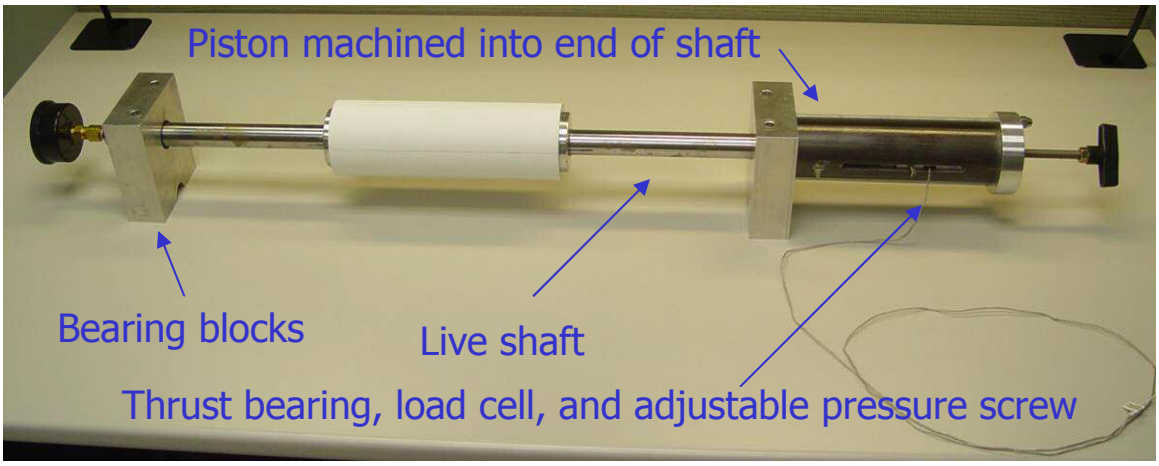

Figure 77 – Dynamically Variable Crown Roller

The dynamically variable crown roller shown in Figure 77 would be capable of generating data for trough formation in webs due to a downstream crowned roller. Additionally, this roller will allow the stress fields generated by the crowned roller to be studied in a near planar state (no developed troughs). This study of the stresses developed by a crown roller would be useful in setting boundary conditions for any modeling attempts. The next few sections will describe various attempts at mapping out the stress fields for a web approaching a crowned roller.

5.2 Strain Measurement with LDVs

Laser Doppler Velocimeters (LDVs) are a current commercial method of measuring the surface velocity of an object by measuring the Doppler shift of a laser reflected off of the surface of the object in question. If the velocity of a web can be accurately established in two points, then the relative difference in strain between those two points may be determined. Knowledge of the strain and corresponding stress distribution in a web as it approaches a contoured roller would be useful in setting boundary conditions for modeling. It would also serve as a check for stress distributions suggested by various models.

Initial testing with LDVs on webs approaching crowned rollers resulted in data where the noise associated with the measurement was larger than the signal intended to be measured. This was due to the small MD strain variations associated with crowned rollers acting on webs in the absence of troughs. If troughs have formed in the webs then the reflective techniques of the LDVs may be suspect. The LDVs were instead used to measure stresses in web approaching concave rollers. A concave roller does not cause troughs and wrinkles, but rather steers the two sides of the web apart, effectively being a web spreading device. This allows much greater variations in strain across the roller, especially when used with low modulus materials. The resulting MD strain proved large enough to measure.

Two concave rollers were on hand at the WHRC. These rollers were nominally 2.2” in diameter with concavities of 0.014” and 0.037” diametric variation from center to

outer edge of the 8" wide roller. The rollers were qualified with the in-house roller profiler and their profiles are shown below in Figure 78.

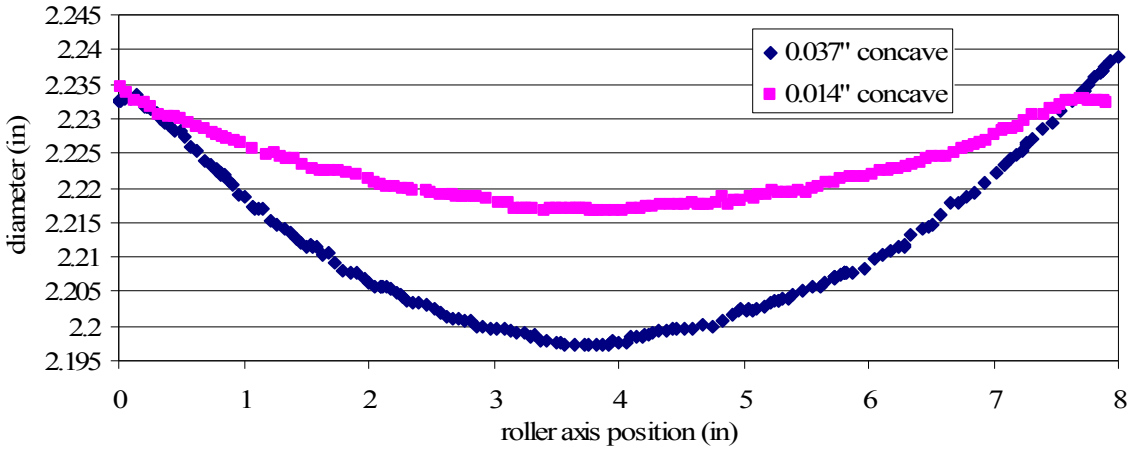

Figure 78 – Concave Roller Profiles

The web used in the concave roller experiments was an opaque 92 ga polyester (Melinex). The LDVs required use of a non-transparent web. The web had a Young's Modulus of E_x = 712000 psi, a Poisson's Ratio of ν = 0.3, and a width of W = 6". All tests associated with the concave rollers used a web span of L = 20".

In order to measure relative strain, two LDVs were required. One was positioned upstream at the center of the web, a presumed neutral position, to serve as a reference. The other LDV was positioned a set distance from the concave roller at a set location in the CMD. After the web was brought up to tension and stabilized, a counter board in a pc was used to simultaneously count the cycles of each LDV (which happen to be 1000 counts/ft). The counter stopped after a predetermined distance of web had passed through the test span. The output was then compared and the relative strain, free of strain due to web line tension, was then determined between the two points. By moving the second LDV to a new location in the CMD and repeating, the relative strain profile was

determined. After the relative strain across the web was measured, a new distance from the concave roll was selected and CMD strains were again measured.

The first test was conducted with the 0.037" concave roller. High traction tape was applied to the roller to ensure no slip conditions. The results are shown in Figure 79. The variable d in the legend refers to the distance that the measurement, LDV #2, was taken from the downstream contoured roller.

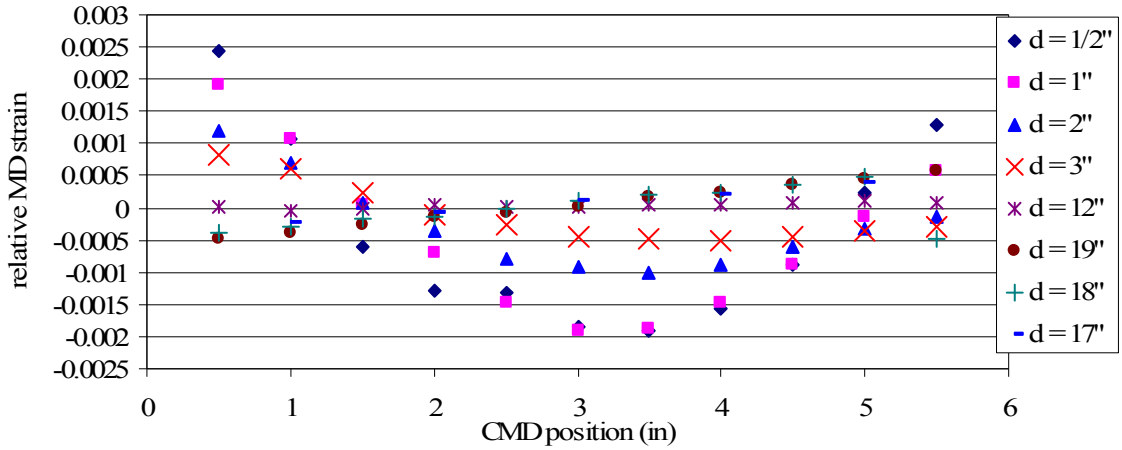

Figure 79 – First Test of MD strain Due to 0.037" Concave Roller

Figure 79 shows how the strain profile flattens out as measurements are taken farther away from the concave roller. At d = 12" the strain profile is almost level across the web. As measurements approached the upstream roller, a moment begins to develop. This result indicated the roller was steering the web. Also, if the strain profile is examined near the concave roller, it appears the web is not centered on the roller. This would cause higher steering forces in the web contacting more of one half of the concave roller, yielding an overall steering of the web. One other possibility would be camber in the web itself. To determine the cause, the roller was flipped over with care taken to

preserve its position in the web line. Additionally, the web was also flipped over. The results of these tests ate shown in Figure 80. All three tests were conducted at d = 2".

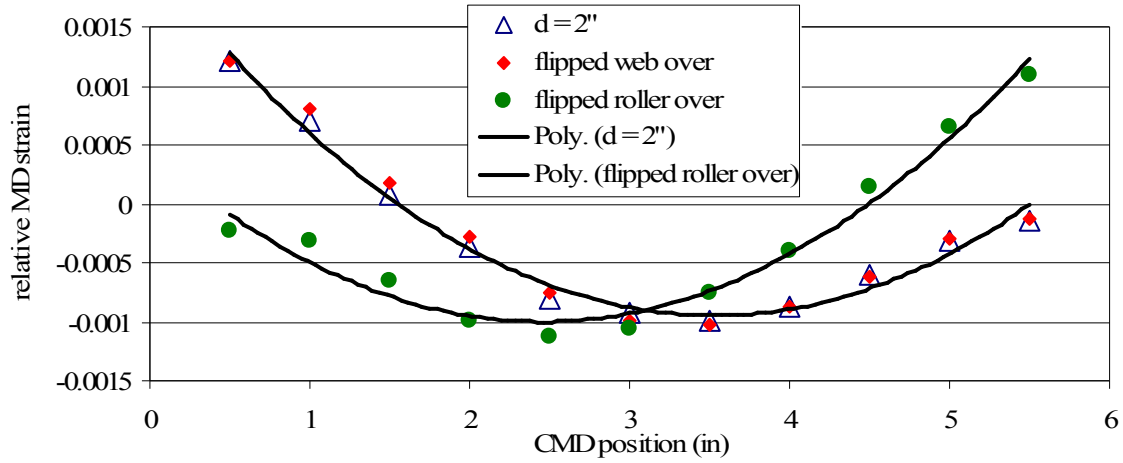

Figure 80 – Determining Cause of Steering Forces

The curve fit line was only added as a visual aid. Flipping the roller end for end had a large impact on the strain profile, while flipping the web resulted in no meaningful differences. This suggests that the steering previously observed was not due to web camber but rather being positioned non-symmetrically on the roller. Figure 80 shows the importance of centering the web in the middle of the roller curve in order to avoid steering effects. The web was repositioned on the roller and the following MD strain data was collected.

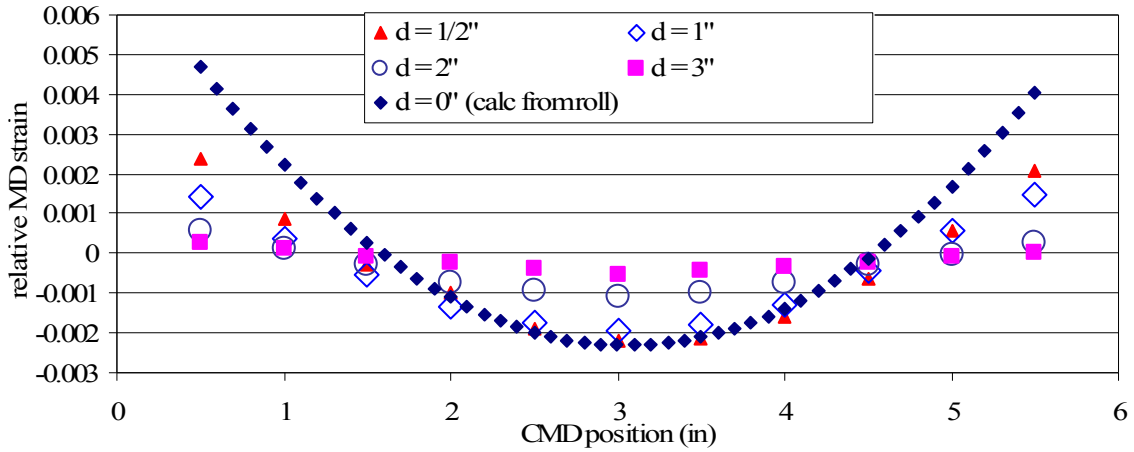

Figure 81 – MD Strain Profile, 0.037" Concave Roller

Additional test were performed with the less aggressive concave roller.

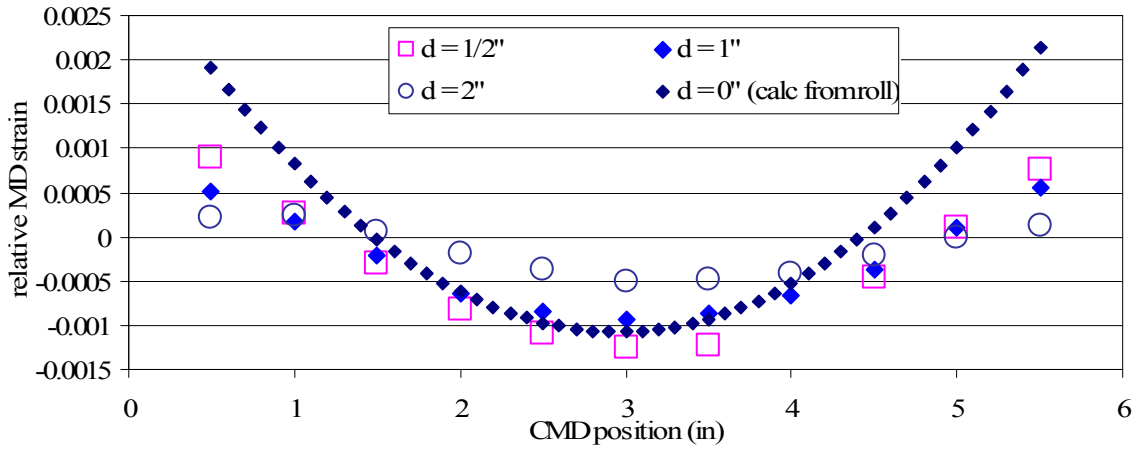

Figure 82 – MD Strain Profile, 0.014" Concave Roller

The data curve labels d = 0" (calc from roll) refers to a calculated strain based on roller diameter and the use of equation (4). The LDVs were not able to measure the strain profiles at the tangent point because the web was not totally opaque. The lasers would shoot through the web and detect roller movement, when close, causing interference. From this data, equation (4) seems to provide a reasonable prediction of MD strain, but without verification at the tangent point, uncertainty could remain. Figure 81 and Figure 82 display promising results for the use of LDV's for MD strain measurement in the case

of concaved rollers. However, they do not yet appear to have high enough sensitivity to measure the small strain variations due to typical crowned rollers (at least not the LDVs tested here). It is again stated that the experimentation with concave rollers was conducted largely due to their similarity to crowned rollers.

One additional test was performed to study the effect of tension on the relative strain across the web at d = 1" from the concave roller. The results shown below in Figure 83 suggest the effects of tension as being minimal. These results also suggest that a tension of 10 – 22 lbs was adequate to fully conform the web to the roller.

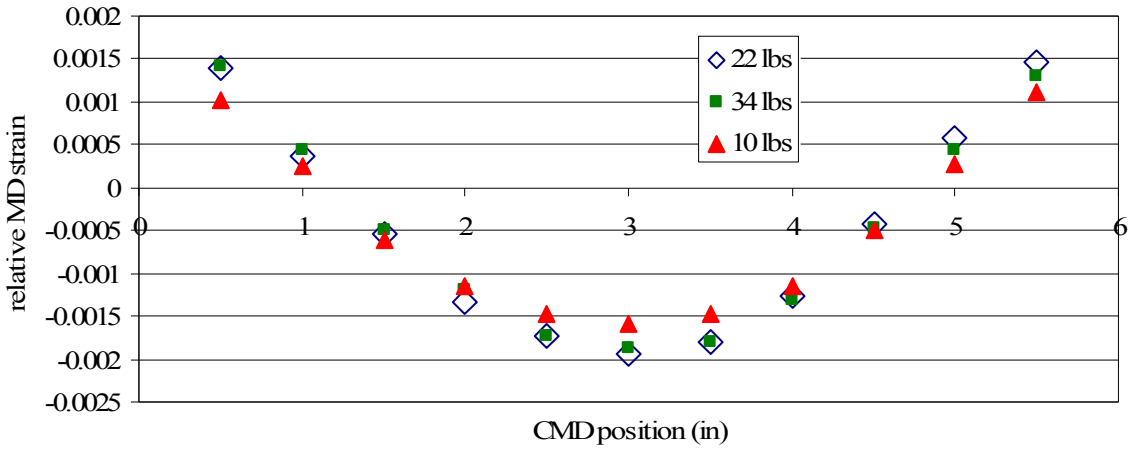

Figure 83 – Tension Effects on Strain Due to 0.037" Concave Roller, d = 1"

5.3 Strain Measurement with Speckle Interferometry

Speckle interferometry was also investigated as a potential non-contact method of strain measurement. While the LDVs were limited to measuring MD stain only, speckle interferometry offered the possibility of measuring MD and CMD strains. The method involves creating a random speckle pattern on the web. A photograph is taken from a fixed position. This first photo serves as a reference. After a load is applied to the web, another photo is taken. Software then correlates the speckle patterns of the two photos and reports the resulting strains.

Experiments were conducted to qualify the method of speckle interferometry for applications of webs approaching contoured rollers. The experimental setup consisted of an eight mega-pixel (3504x2336) digital camera mounted on a rail system above the web span in question. The web was marked in a certain location. The web would be brought to tension, stabilized, and then stopped under tension. The camera was positioned with the reference mark in the photo frame. This mark allowed the camera to create the same speckle pattern in each picture. Ideally, a reference photo would be taken near the upstream roller. Then, the camera and the web (under tension) could be moved toward a contoured roller incrementally, with photos being taken at each step. This series of photos could then be correlated through the use of software that would relate the photos to relative strains. This process could be repeated at different locations across the CMD to map out an entire web span.

This method was qualified using a somewhat simpler procedure. A web with a reference mark and speckle pattern was placed under tension across a span with two cylindrical rollers. A reference photo was taken. Tension was increased incrementally with a photo taken at each step. Weights were used to provide the tension levels so the strain in the web was precisely known. Proprietary software developed by Dr. H. Lu and Paul Carey, in house at the WHRC, was then used to relate the series of photos to relative strains. The experiment is depicted in Figure 84.

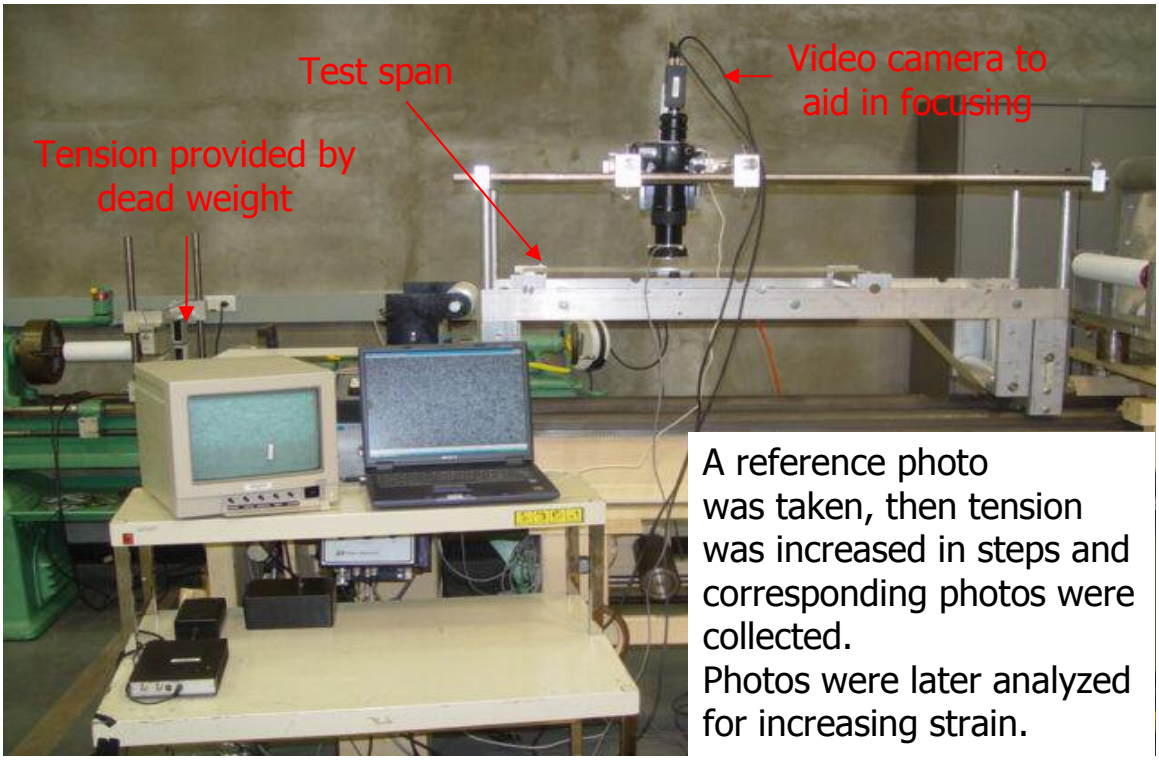

Figure 84 – Speckle Interferometry Experiment

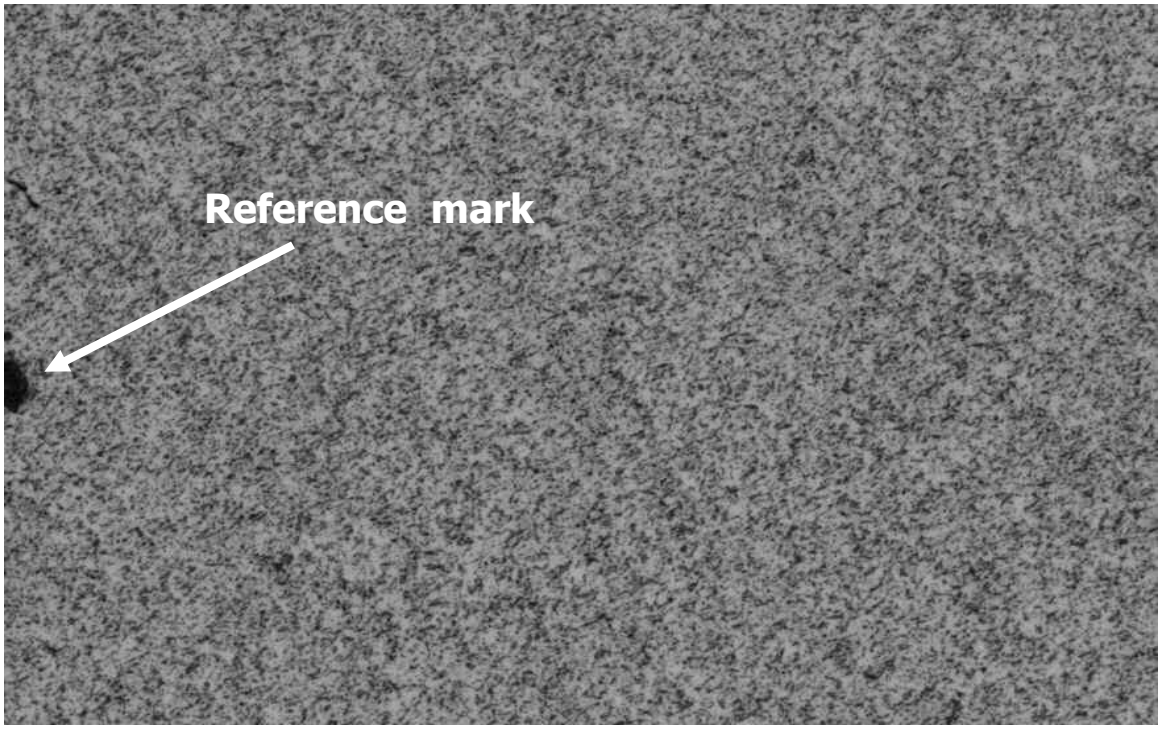

Figure 85 – Sample Speckle Pattern

Experiments were conducted in 10 lb increments, 5 lb increments, and 1 lb increments to determine the minimum strain resolution of the experimental setup. The results of these tests are shown below in Figure 86 - Figure 89. All webs were 6" wide.

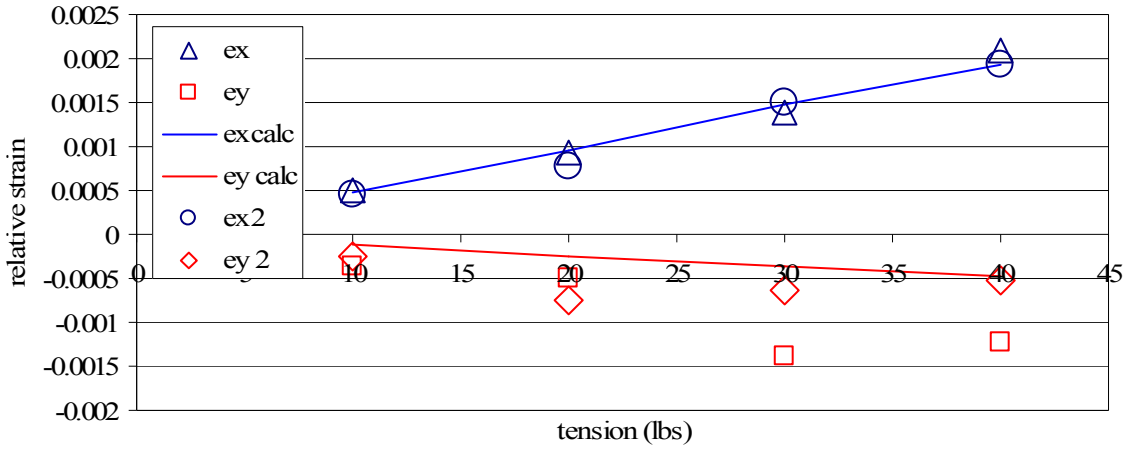

Figure 86 – 380 ga Coated Paper, 10 lb Increments

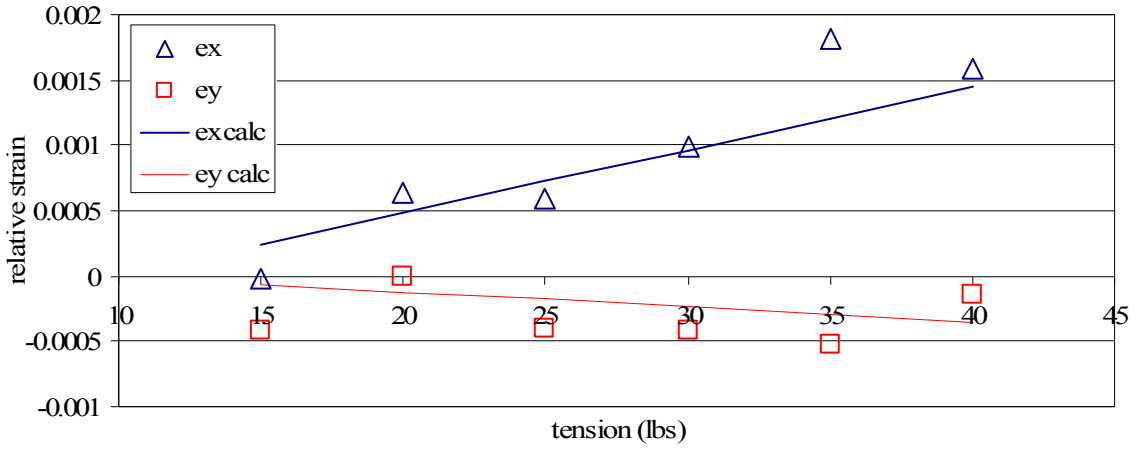

Figure 87 – 380 ga Coated Paper, 5 lb Increments

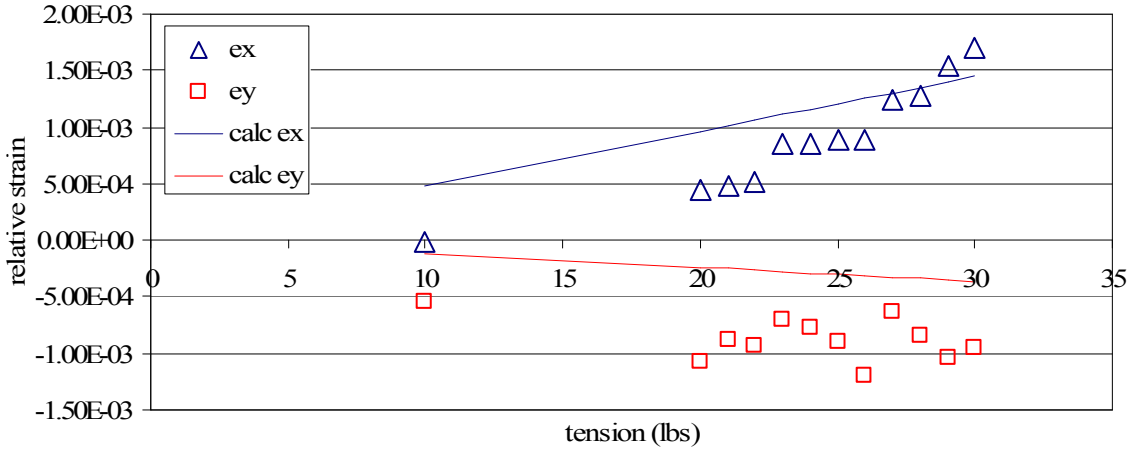

Figure 88 – 380 ga Coated Paper, 1 lb Increments

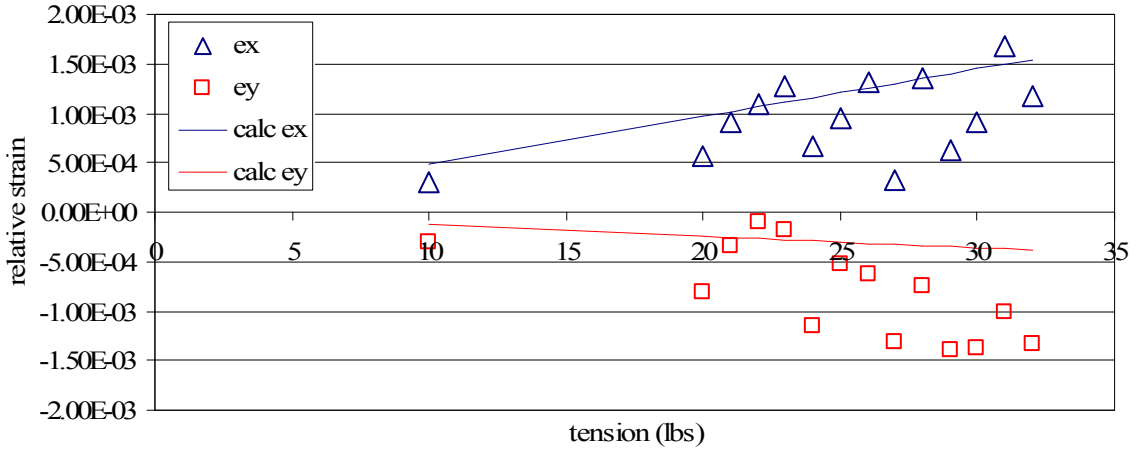

Figure 89 – 380 ga Coated Paper, 1 lb Increments

The results for the 5 and 10 lb increment cases follow expected values for strain. The traces labeled "calc" refer to calculated values for both the ε_x and ε_y stresses. The results for the 1 lb increment tests show the data moving in expected directions but individual datum points varied considerably and would not provide an adequate measurement for strain. In view of these results, the conclusion was made that the apparent minimum strain to be measured would be nearly 500 micro strains. This eliminated the use of speckle interferometry (with the current photo equipment) for most applications of strain measurement due to contoured rollers.

One additional effort was made to test the correlation software. The same series of photos was analyzed by the software developed by Dr. H. Lu and by a commercial package available from Correlated Solutions. The Correlated Solutions software was made accessible through 3-M Company. The comparison of these software packages is shown below.

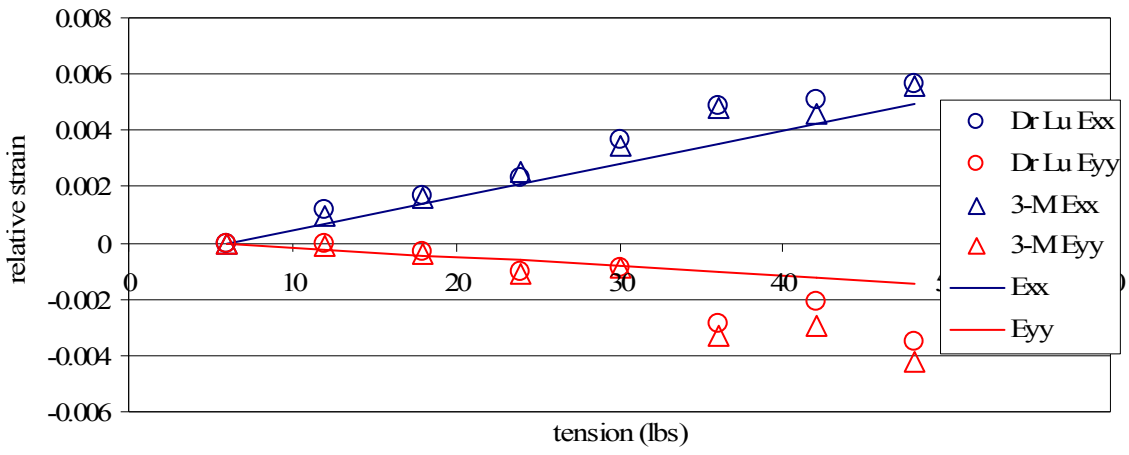

Figure 90 –Software Comparison, 200 ga Polyester, W = 6"

Figure 90 shows agreement between the two software packages. While the value of each data point may not be exactly the same (though close), the relative movement from one data point to another is consistent. In conclusion, the resolution of the speckle interferometry method is primarily dependent upon the digital images supplied to the software for correlation. A higher resolution image and possibly a better speckle pattern may yield accurate resolution of smaller strains. It appeared that further investment in increasingly high cost equipment for uncertain returns would not have been economically feasible for this research project.

5.4 Strain Measurement with Strain Gauges

The measurement of strain fields approaching crowned rollers was continued through the use of strain gauges. Strain gauges have an advantage of high resolution capabilities. They may be oriented in any direction, and they may be applied to a moving web for a limited distance. However, strain gauges are limited by their size as they are not point measurements and have a high potential for significant interference when applied to thin webs.

The strain gauges used were Vishay general purpose strain gauges. They have a polyimide backing that is approximately 4 times thicker than the web itself. In order to measure strains accurately, the gauges needed to be calibrated on the web to be used in experiments with known loads. Strain gauges were glued to strips of web oriented in both the MD and CMD directions. Weights were used to provide known tensions to the webs and the outputs from the strain gauges were recorded. The strain gauge data was compared to the known values of uniaxial strain caused by the weights. This process was repeated at different locations across the web to see if CMD location would affect the reinforcement factor. In all cases, the reinforcement factor was determined to be 1.9 with no apparent dependence on CMD position (care was taken to avoid the edges of the web), or gauge orientation.

The procedure of measuring strain in webs approaching contoured rollers required the use of two strain gauges. The first gauge was placed in the center of a long (relative to the test span) web span preceding the test span. This gauge served as a reference to

accurately monitor the strain due to web line tension (the web line load cells did not have high enough resolution). The second strain gauge was placed just prior to entering the test span in the CMD location to be measured. Both strain gauges were applied to the web after the web line was brought up to tension and speed, and then stabilized and stopped under tension. The gauges were attached to the web with a cyanoacrylate adhesive and given time to set (the web still under tension).

With the strain gauges in place and wires attached, the web line was started and the web slowly proceeded down the line at 5 ft/min. Simultaneously, the gauges were read and recorded by a computer equipped with a National data acquisition card. The second gauge entered the test span and proceeded toward the crowned roller. The test was stopped once the test gauge had traveled over the crowned roller. The setup experimental is shown below in Figure 91.

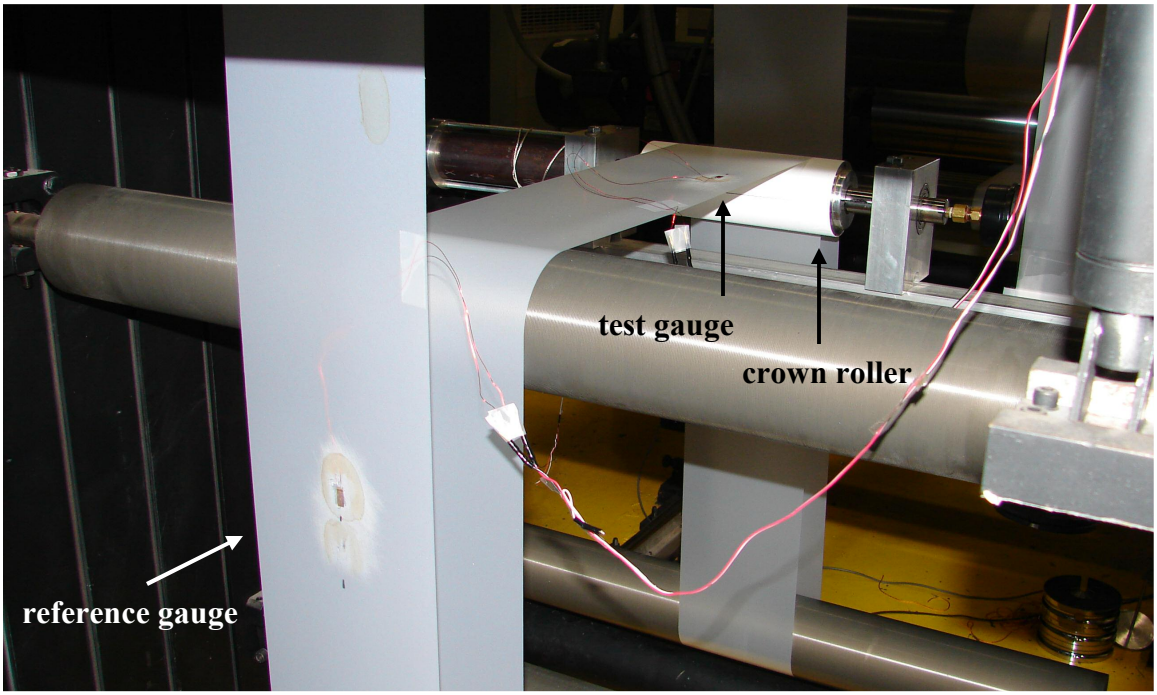

Figure 91 – Strain Mapping with Strain Gauges

A sample of initial output is shown in Figure 92, in this case the CMD position was 3".

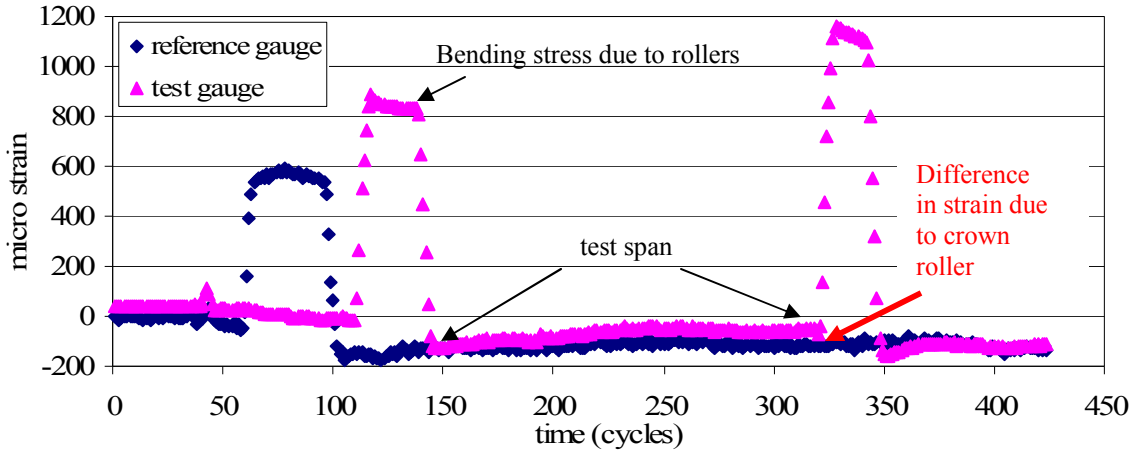

Figure 92 – Sample Strain Gauge Output

If the test span from the above graph is separated, and the difference between the reference and the test gauge data is plotted, the effects of the crowned roller may be seen. A sample of this is shown below in Figure 93, again the CMD position = 3" (center of web).

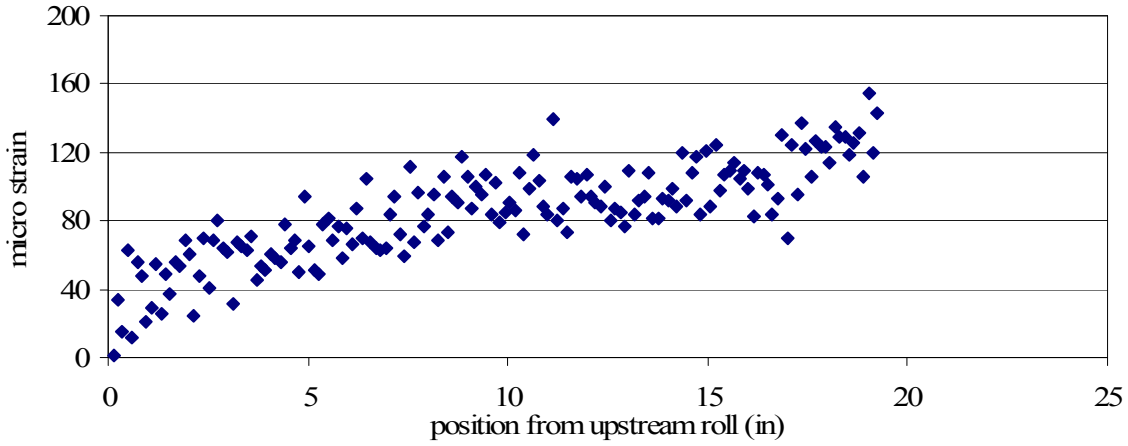

Figure 93 – Measured Strain due to a Crowned Roller, L = 19.5"

The first test was conducted with a 92 ga Polyester. It had a Young's Modulus of E_x = 712000 psi, a Poisson's Ratio of ν = 0.3, a width of W = 6", a span length of L =

19.5", and the crowned roller with 1000 psi internal pressure (which can be related to diameter through Figure 74). These are also the conditions under which Figure 92 and Figure 93 were generated. This first test was conducted at three positions across the CMD and repeated 5 times at each position. The results of which are shown below.

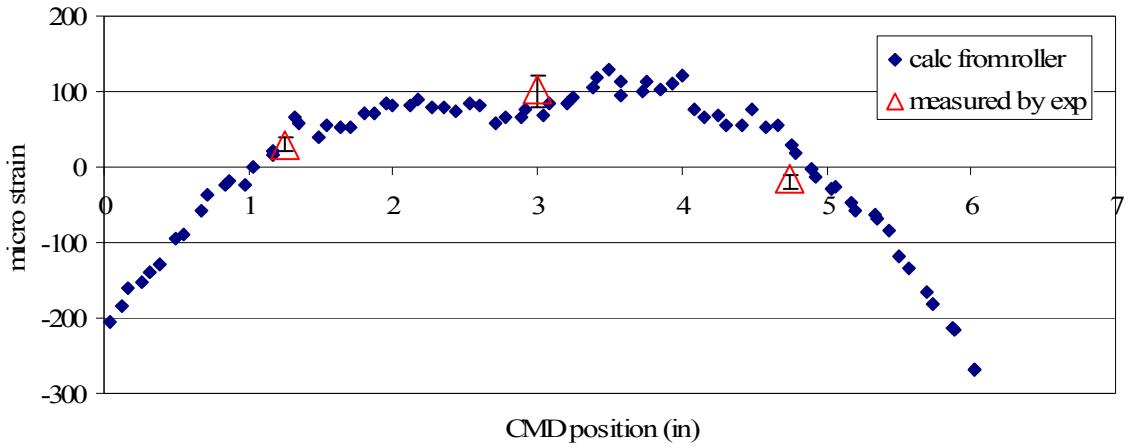

Figure 94 – Strain at Crowned Roller, P_{int} = 1000 psi

Figure 94 shows agreement between the strain profile suggested by using equation (4) and the value measured by strain gauges at the crowned roller. Strains could not be measured across the crown roller where measurements would be affected by bending strains. The internal pressure in this case was equal to 1000 psi. Other experiments would suggest that troughs have formed in this web span, making any CMD data collected unreliable. Additionally, Figure 93 suggests that strain is increasing linearly between rollers. This would suggest that, for the case of web spans with developed troughs, string method is applicable to webs (string method states the webs may be modeled as a series of independent uniaxial strings between rollers).

An additional case was measured, one with less internal pressure. This lower internal pressure, hence less crown, would allow a span without troughs to be measured.

No troughs had been observed below 600 psi of internal pressure for this web, so the next test was conducted with an internal pressure of 500 psi. The results of this test are shown below.

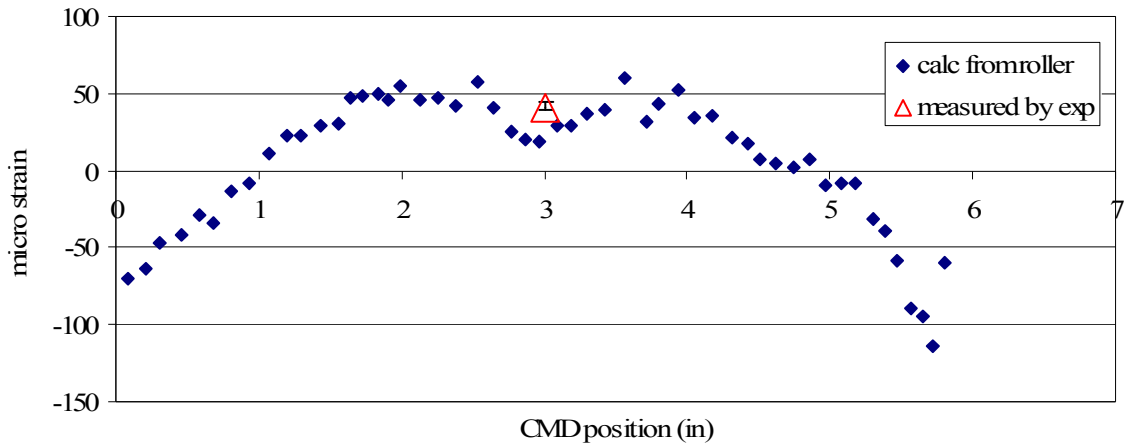

Figure 95 – Strain at Crowned Roller, P_{int} = 500 psi

Figure 95 exhibits agreement between expected values and those measured similar to the higher pressure case. Only the center point of the web was measured due to the ever decreasing strains. No reliable CMD data was collected for the same reason. The results again suggest that the MD strain profile at a contoured roller may be successfully predicted by use of equation (4) and knowledge of the roller geometry, whether troughs are present or not. However, if the raw data is analyzed, it is not clear from results obtained that the stress field can be assumed to follow string method for cases where the web remains planar.

5.5 Trough Formation Due to Crowned Rollers

Creation of the "low" crown roller allowed the possibility of obtaining experimental results for the onset of troughs in a free span, due to a downstream crowned roller. Experiments were conducted with the 92 ga polyester, W = 6", E_x = 712000 psi, ν = 0.3. High friction tape was used to ensure no slip conditions on the crowned roller.

Experiments consisted of bringing the web line up to tension and then slowly increasing the internal pressure of the crowned roller. The increase in internal pressure was directly correlated to roller diameter as was shown in Figure 74. When troughs were visually observed in the web span, web line conditions and internal roller pressure were then recorded. The initial troughs associated with crowned rollers were much smaller in magnitude than those associated with shear. This small amplitude of the troughs at their onset made measurement of this process difficult. In spite of the conditions, a set of data was collected and the results are shown below.

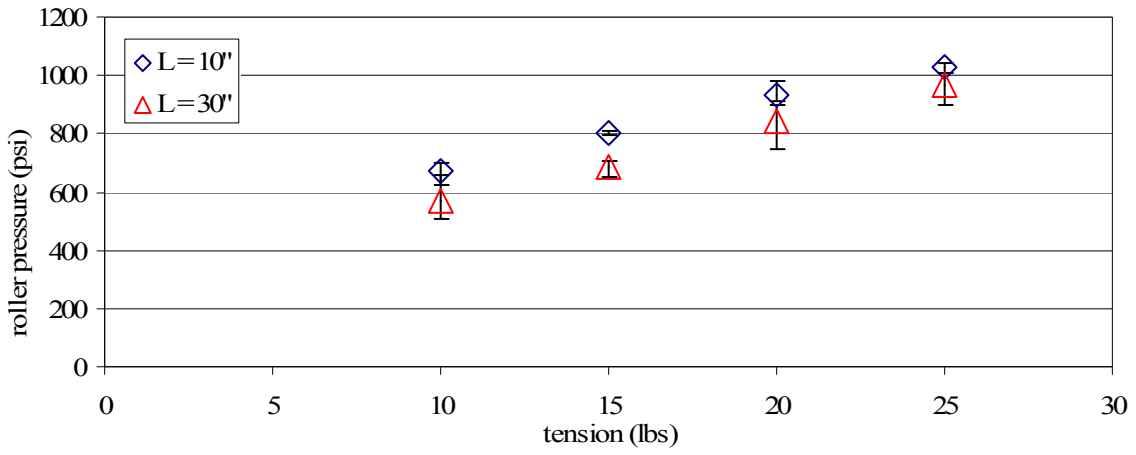

Figure 96 – Troughs Generated By Crowned Roller

Figure 96 shows a small dependence on span length and a greater dependence on web line tension. This behavior is expected due to buckling criteria of tensioned plates. A first attempt at modeling trough development used elastic elements in a FE model coupled with the plate buckling criteria used in the case of shear troughs. The boundary conditions for the FE model are shown below.

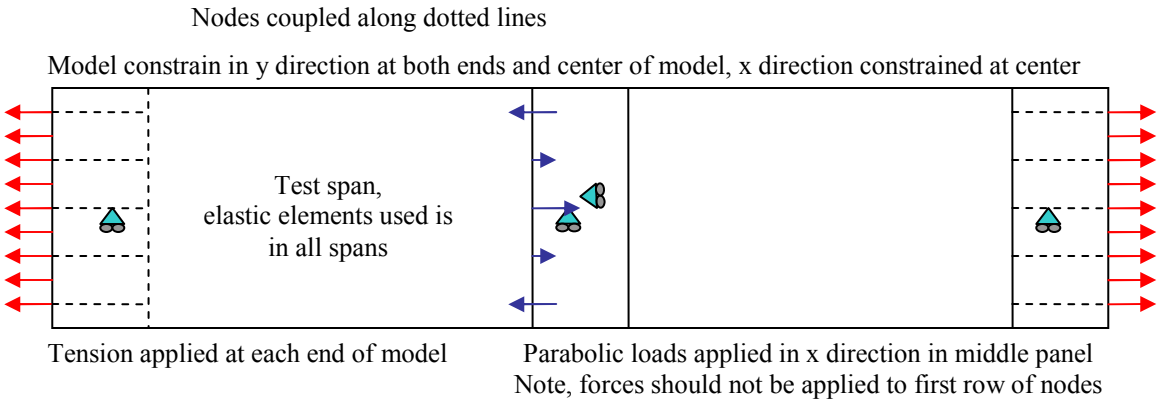

Figure 97 – Boundary Conditions for FE Trough Model

The MD load profile applied to the web should create the expected MD profile from the particular case of contoured roller being studied. The expected MD stress profile may be calculated by use of equation (4), Hook's Law, and the roller profile. In the case of crowned rollers a parabolic stress distribution is required. Initially, nodal loads were calculated to have parabolic magnitudes across the web; it was soon realized that some nodes needed different values to give a smooth MD profile at the first row of elastic elements where the compression would ultimately develop. The solution was to carefully change applied loads (mainly near the edges of the web) at individual nodes until the desired shape was achieved at the web to roller boundary. This load distribution could then be increased by a scaling factor in COSMOS. The location of these applied

loads was not critical, as long as they were not applied to the same row of nodes where the compressive stresses would develop. Also, some nodal forces were in the positive x direction and some where in the negative x direction with magnitudes that resulted in no net change in web line tension. The numerical solver in MS Excel aided with this aspect.

Initially, the critical stress for the web span was assumed to be that predicted by equation (39) for a tensioned panel being compressed uniformly along its length. Considering a typical web span of 30" under 20 lbs web line tension, Figure 96 suggests that an internal pressure of 933 psi in the crowned roller would be required to create a trough in the web. Equation (39) predicts a critical CMD stress of nearly 3 psi for these conditions. The MD stress profile was increased in the FE model until this critical value of compressive stress was observed in the web span. The resulting MD stress profile from this model is plotted below along with the MD profiles calculated form roller geometry for internal pressures in the variable crowned roller of 900 psi, and 1000 psi.

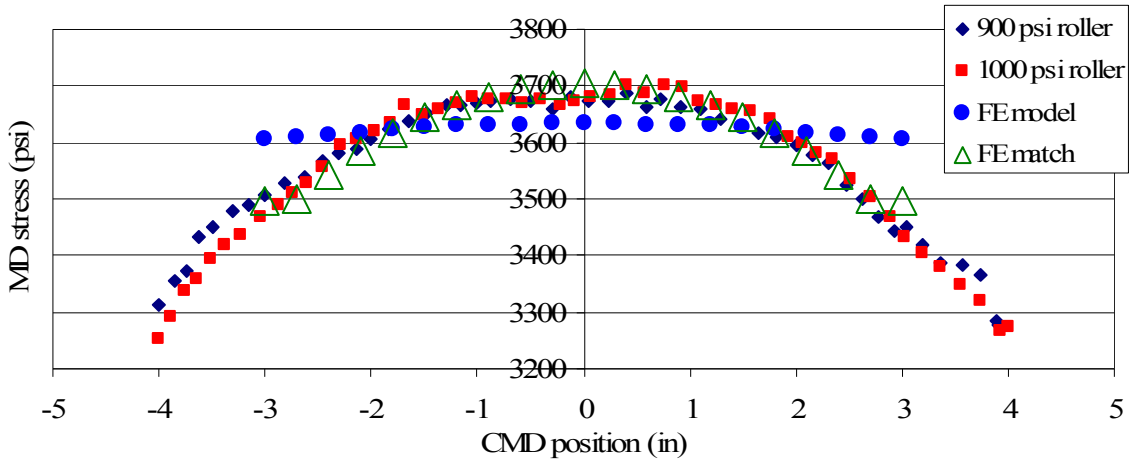

Figure 98 – MD Stress Profiles, L = 30", T = 20 lbs

The trace labeled "FE model" corresponds to a compressive stress of 3 psi developing in the web span, as suggested by equation (39). The above graph demonstrates the

inadequacy of this model to accurately predict the onset of trough formation due to a crowned roller. The applied MD stress was then increased in the model until a stress profile comparable to that observed in experiment was achieved. This is the trace labeled "FE match" in Figure 98. The compressive CMD stresses along the web centerline corresponding to the MD trace "FE match" is shown below in Figure 99.

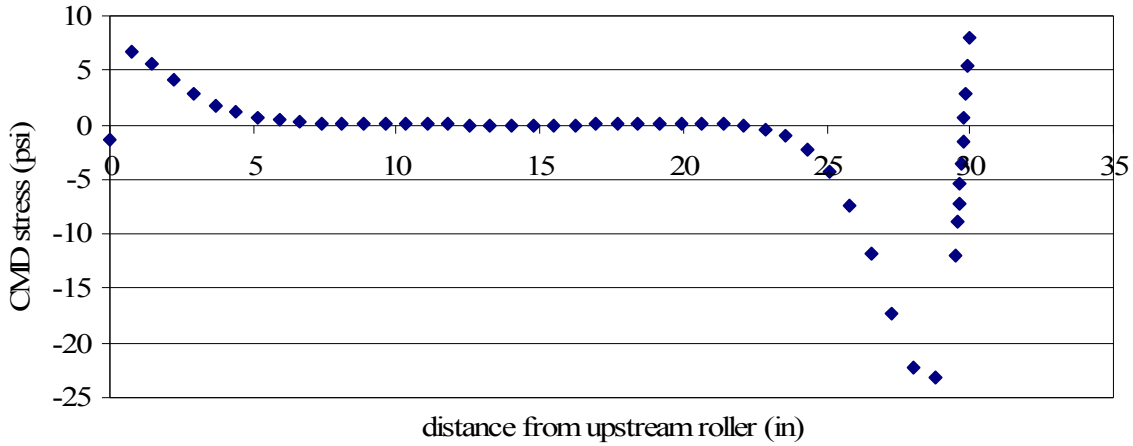

Figure 99 – CMD Stress Along Web Centerline, L = 30", T = 20 lbs

The previous graph shows the CMD stress profile from by a FE model that generates the MD stress profile suggested by experiment to cause trough formation in a web due to a crowned roller. The chart shows only a pocket of compressive stress just before the crowned roller. This helps to explain why equation (39) may not be applicable to this case of MD wrinkles.

In the case of shear wrinkling, the compressive stresses down the centerline of the web extend from near the upstream roller all the way to the downstream roller, simulating a tensioned plate experiencing a uniform compression per equation (39). A simple approximation was attempted to reconcile the FE analysis to the experimental data. From Figure 99 the region of the web experiencing substantial compressive stress may be used

to determine an “effective” plate length. This “effective” plate length was determined to be approximately 4”. If 4” is used as the length of the compressed-tensioned plate, equation (39) predicts the critical buckling stress to be $\sigma_{ycr} = 22$ psi. This was in fact the stress developed in the FE model based on critical experimental inputs.

A model based on an “effective” plate length was able to give agreement with experimental results. However, the model was based on inputs that resulted from measured critical values. It is suggested that an improved buckling criteria be developed for this case of MD troughs. An additional approach would be to conduct a full FE buckling analysis. This would limit assumptions, but may be computationally more intense. The topic of machine direction troughs due to a crowned roller will not be pursued farther here due to time constraints and limits of scope.

5.6 Wrinkles Due to Crowned Rollers; Finite Elements

Experimental data were needed for any comparison to modeling attempts. Initial efforts revealed that the 0.006" diametric crown/8" width would produce wrinkles in the 92 ga polyester that could be removed with an increase in tension. This roller was used in the same test stand that the tapered roller tests utilized. High friction tape was applied to the roller to ensure no-slip conditions. Care was taken to center the web on the crown. The tests began with a relatively high web line tension until the web stabilized in the machine. Tension was then decreased until wrinkles were observed traversing the crowned roller. The tension was recorded as the experimental variable. Data were from an average of 4 tests. Web properties were again; E_x = 712000 psi, ν = 0.3, W = 6". The experimental setup utilizing a 3" diameter crowned roller is depicted in Figure 100.

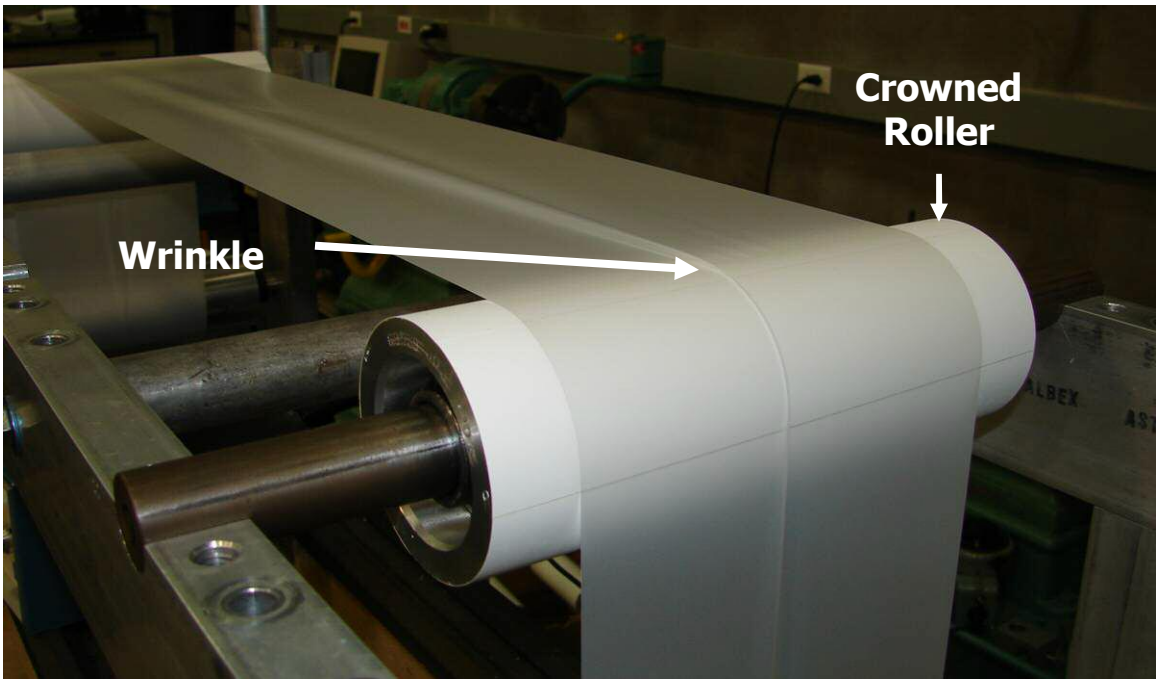

Figure 100 – Wrinkle Generated By Crowned Roller

Results from this experiment are shown below.

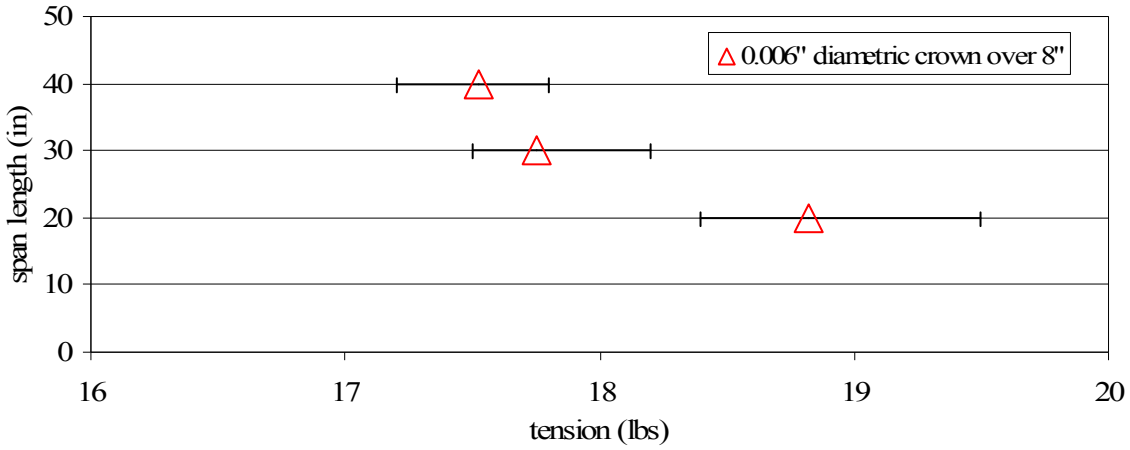

Figure 101 – Wrinkles Generated by a Crowned Roller, R_o = 1.5"

A Finite Element model is now constructed to generate a critical stress profile required for webs to wrinkle on rollers. The conditions obtained in the above graph will be used for comparison. The boundary conditions for a crowned roller require no net steering of the web, no rotation at the upstream end of the web, a downstream stress profile calculated from the use of equation (4) and knowledge of roller geometry, and the concept of normal entry. These conditions were incorporated into the FE wrinkling model through the following constraints. The parabolic loading is the same as that applied to the case of troughs described in the previous section

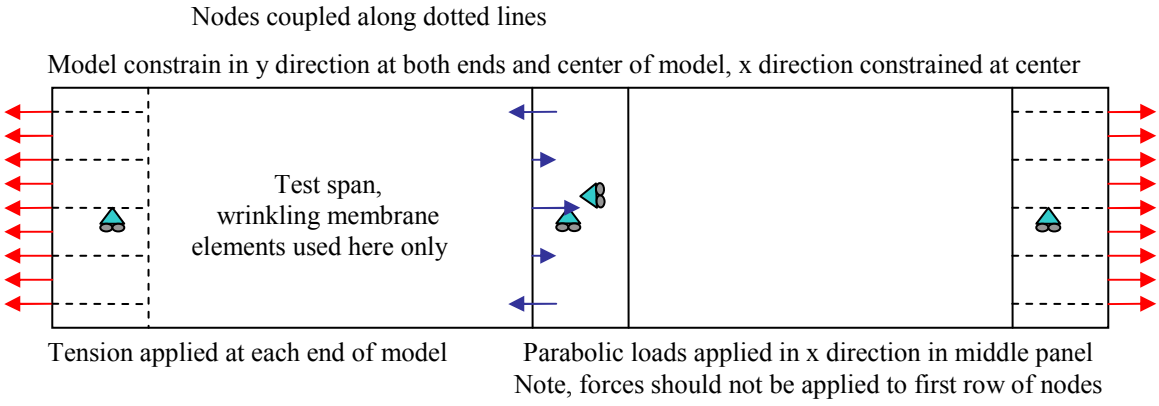

Figure 102 – Boundary Conditions for Wrinkling Due to Crown

Execution of the FE model proceeded as follows; Tension was applied to the web, then the parabolic MD stress profile was increased until the compressive stresses in the first row of elastic nodes reached the critical value determined by equation (79), σ_{ycr} = 265 psi, approximately. At this point, the MD stress distribution from the FE model was used to determine the critical crown by calculating the critical roller profile from equation (4), and uniaxial Hook's Law.

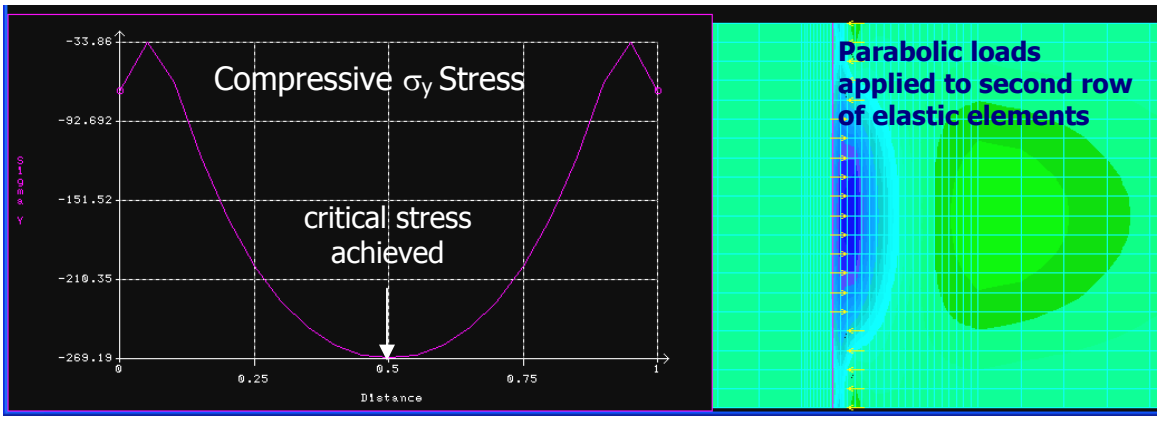

Figure 103 – Critical Compressive Stress, FE Crowned Roller Model

The data in Figure 101 suggests little dependence on span length, with the largest difference occurring between the 20 and 30 inch spans. Models were constructed for all three span lengths. Once the critical compressive stress was achieved, the models were evaluated by comparing the FE estimation of the MD stress across the web with that calculated from roller geometry and use of equation (4). The results are shown in the following graphs.

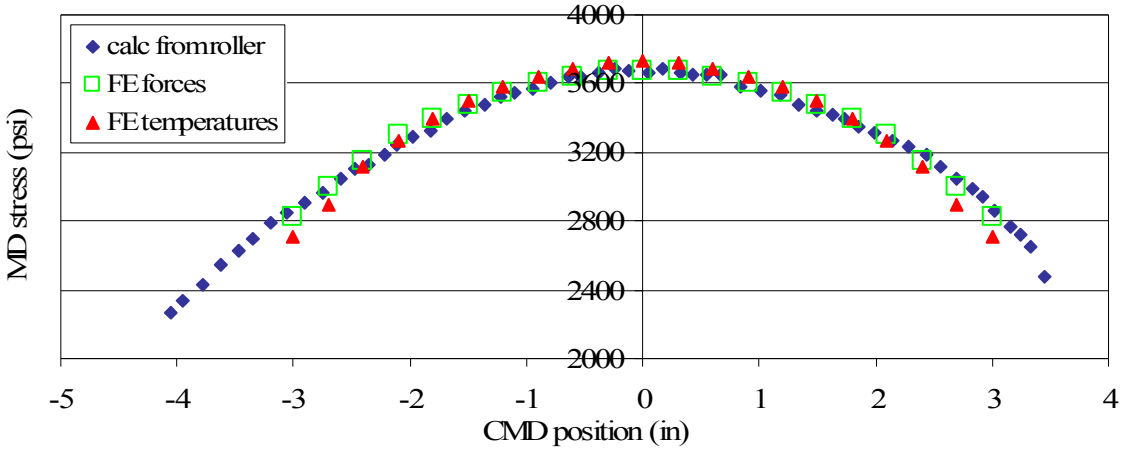

Figure 104 – FE Wrinkle Model; L = 20”, T = 18.6 lbs

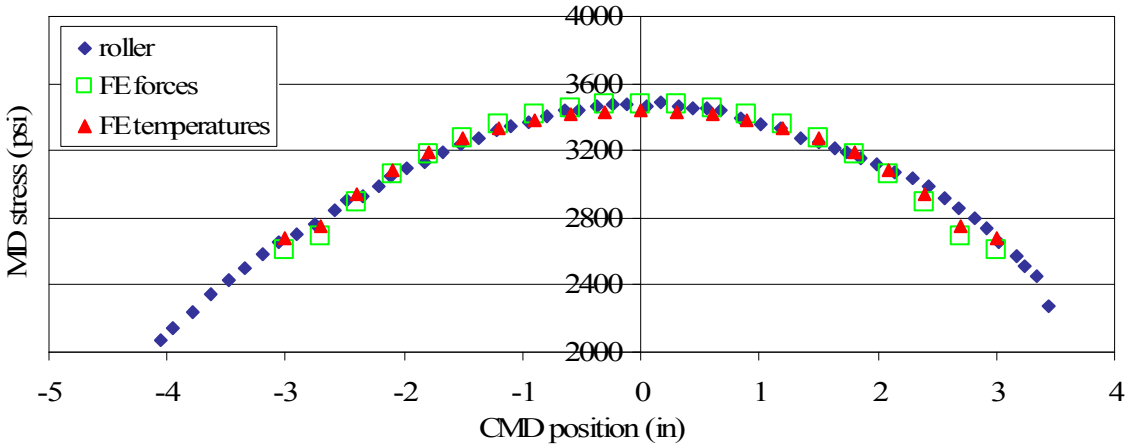

Figure 105 – FE Wrinkle Model; L = 30”, T = 17.6 lbs

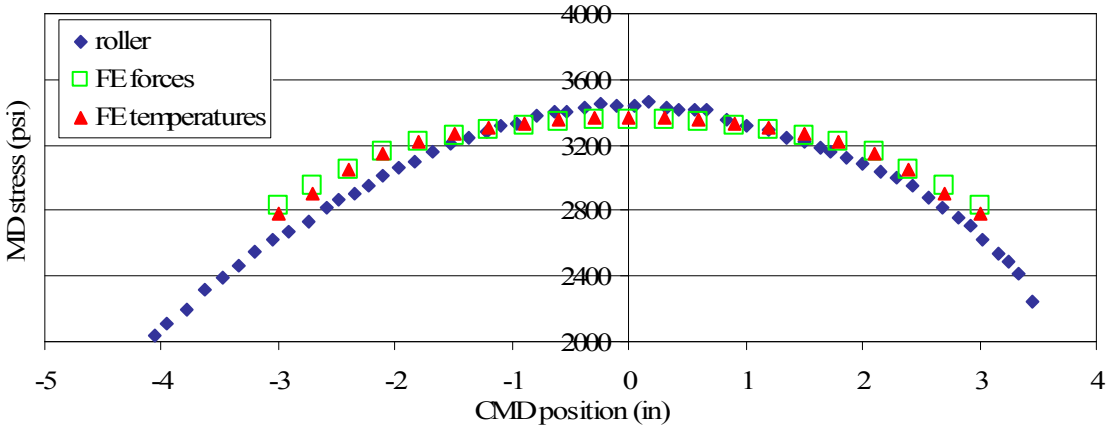

Figure 106 – FE Wrinkle Model; L = 40”, T = 17.4 lbs

Figure 104 - Figure 106 show two FE model results in addition to the expected value determined from experiment. One is due to the parabolic loading described above. The other case utilized a temperature distribution instead of applied forces to achieve the parabolic MD stress distribution. The two models yield similar results, and demonstrate the effectiveness of these modeling techniques applied to machine direction wrinkles. The force model may possibly be considered a more direct approach. In the case of MD wrinkles, it is worth note that neither forces nor temperatures should be applied to the first row of elastic elements where the compressive stresses are developed. Placement on the second row or farther is acceptable. Location of the forces after the second row is not critical. The only point of concern is that the MD stresses at the first row of elastic nodes (where compressive stresses are developed) are used to evaluate the model, not the applied forces. Additionally, with no net steering of the web, no efforts were made to explicitly enforce normal entry.

Acceptable agreement was achieved by the proposed model over the span lengths tested. The limited data available did not allow the model to be tested extensively for the effect of span length. However, the data for the 40” span may suggest a limitation of the current model for large ratios of L/W.

5.7 Wrinkle Due to an Enlarged Sector; Finite Elements

The method of wrinkle prediction developed for the case of the crowned roller will now be applied to the case of a roller with an enlarged sector. If the enlarged sector is located in the center of the web then, there is no net steering, resulting in machine direction wrinkles. This case is similar to that of the crowned roller with only differences in the MD stress profile.

Data for this case of MD wrinkles was collected by J.K. Good [14] and the 3-M web handling group in 3-M labs in St Paul in 2001. Details of their experiment are not given here. It is known that the roller profile was controlled with internal pressure. This internal pressure was related to roller diameter through measurements of the roller before and after pressurization. A diagram of this roller is shown below.

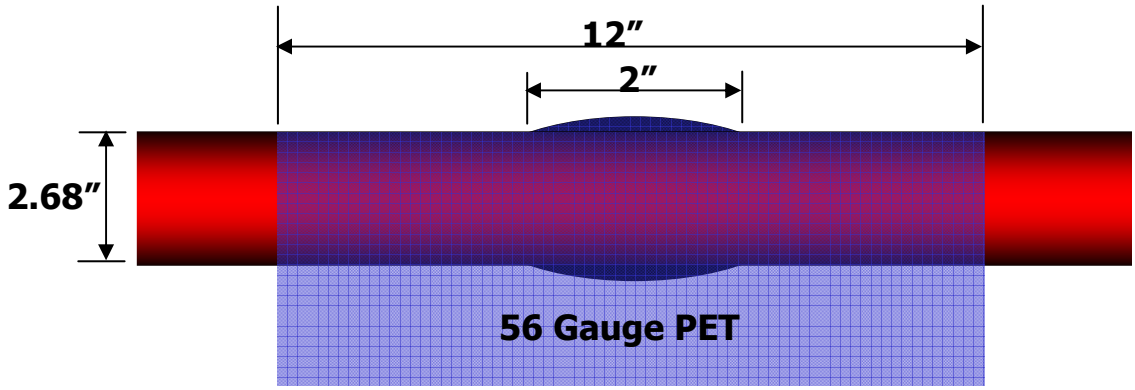

Figure 107 – Diagram of Roller with Enlarged Sector

Experiments were conducted to determine the onset of wrinkles due to a roller with an enlarged sector. A set of experimental data for a polyester web is shown below; wrap angle = 48 deg, W = 12”, t = 0.00056”, E_x = 712000 psi, ν = 0.3, R_o = 1.34”.

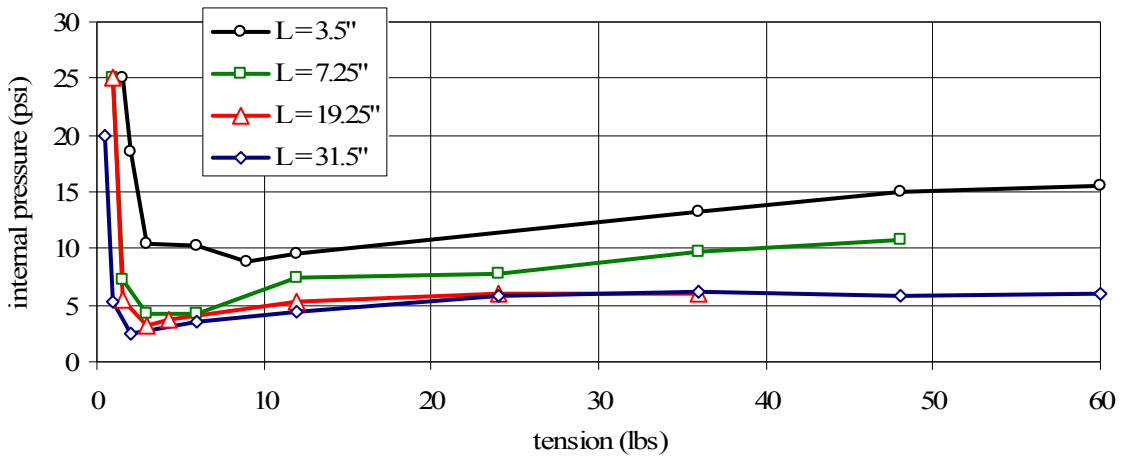

Figure 108 – Wrinkle Data Due to a Roller with an Enlarged Sector

Figure 108 relates critical internal pressure in the roller to web line tension at several span lengths. The pressurized roller was covered with a high traction coating to ensure no slip conditions. However, the upstream roller was bare aluminum. The effects of traction can be seen in the lowest tensions. Span length dependence can also be seen, but the effects of span seem to converge by the 19.25" span.

A FE model was developed for the case of wrinkles due to an enlarged sector on a roller. The implementation of the model was similar to the case of the crowned roller, with the major difference being the applied MD stress profile. The enforced boundary conditions are shown in Figure 109. The model is again executed by first applying web line tension, then the MD stress profile is increased until the critical compressive stress, equation (79), develops in the first row of elastic elements at the span – contoured roller boundary. The MD stress profile from the FE model is then compared to that calculated from the rollers used in experiment per equation (4).

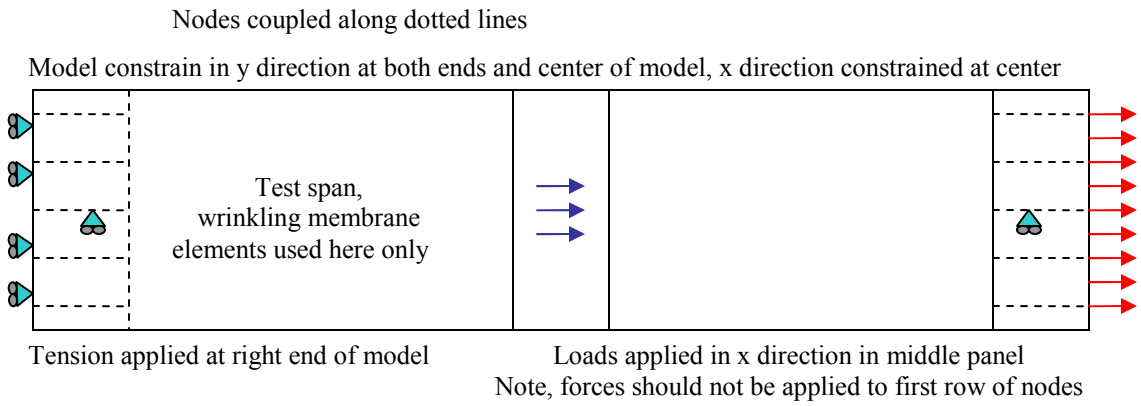

Figure 109 – Boundary Conditions for Wrinkling Due to an Enlarged Sector

An analysis of Figure 108 reveals that a 31.5" web span under 20 lbs web line tension will form a wrinkle at 5 psi of internal roller pressure. The profile of the roller is shown below in Figure 110.

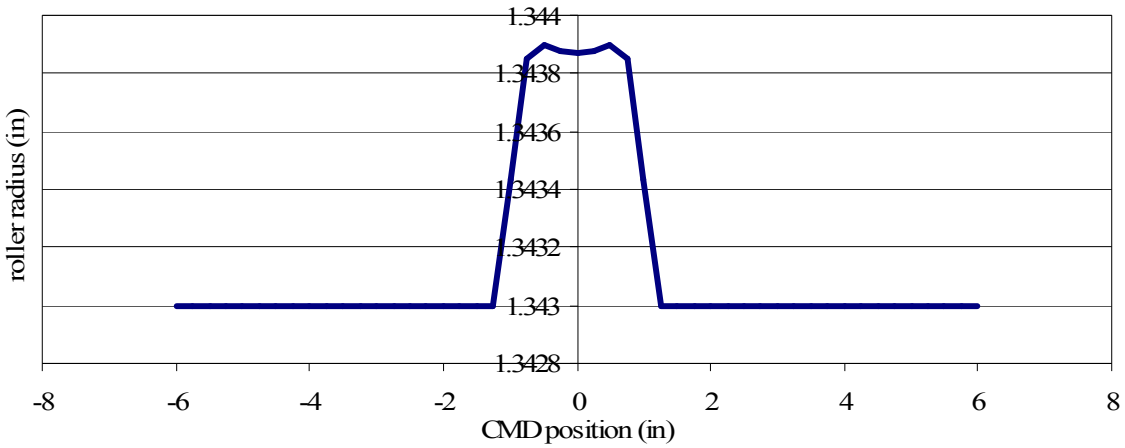

Figure 110 – Roller Profile, P_{int} = 5 psi

By using the above roller profile, equation (4) and Hook's Law, the stresses due to the roller may be calculated. The resulting MD stress profile that is to be considered the experimentally determined critical profile is shown below in Figure 112 and is represented by the trace "calc from roller". Equation (79) yields a critical buckling stress of σ_{ycr} = 180 psi. The CMD stresses resulting from the FE analysis are also shown below.

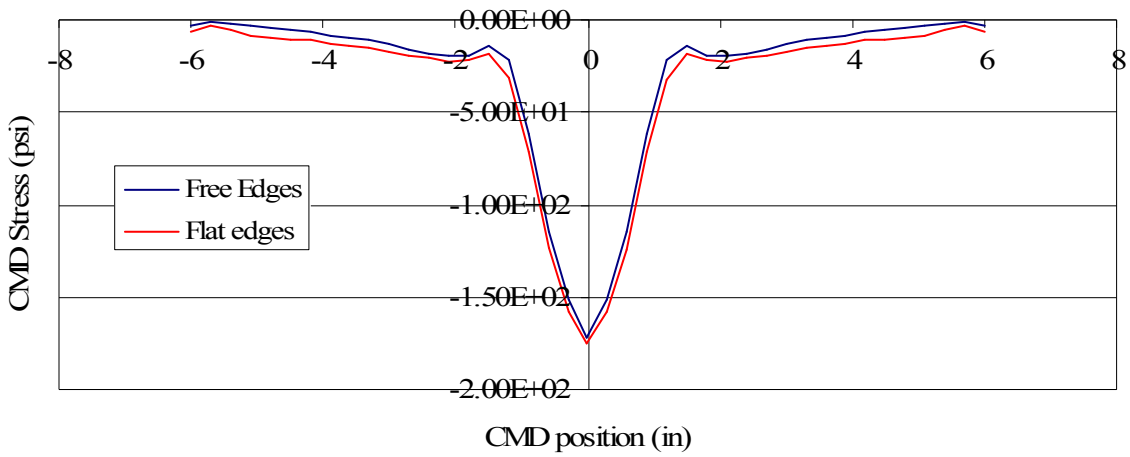

Figure 111 – FE Wrinkle Model; L – 31.5", T = 20 lbs

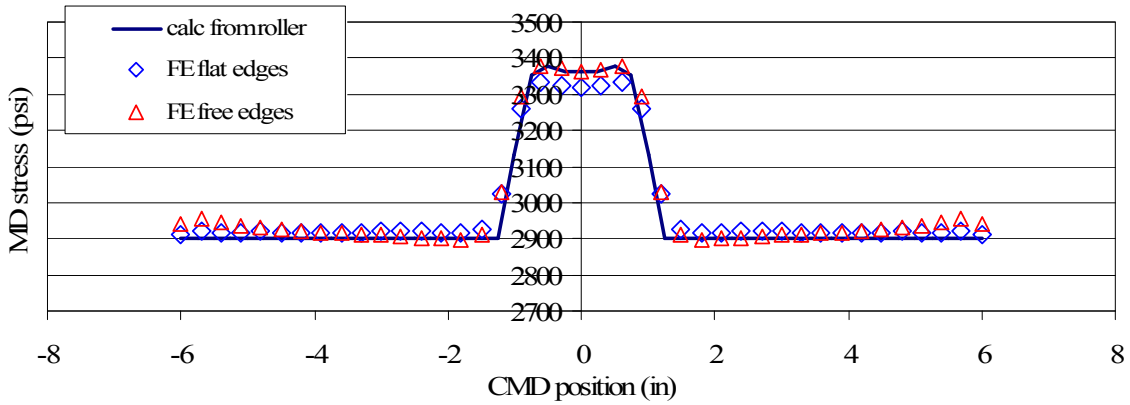

Figure 112 – FE Wrinkle Model; L = 31.5", T = 20 lbs

The above graph shows the expected results from the experiment, as compared to two FE models. One model forces the edges of the web to have a flat profile, achieved by pushing upstream on the web near the edges, while the other allows the edges to be free. No clear advantage is observed from forcing the edge of the web to be flat; also it is unclear if a roller could impose such negative MD forces on the web.

The agreement achieved in Figure 112 demonstrates the capability of the model to predict the onset of wrinkle formation due to a roller with an enlarged sector for a typical

span length, L/W = 2.6, and average web line tension. The model was next applied to a shorter span length, L = 19.25", shown below.

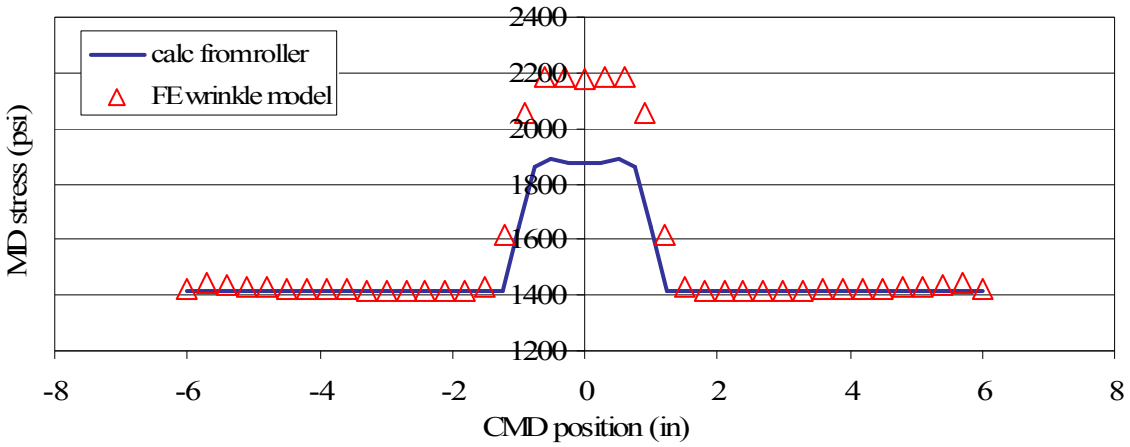

Figure 113 – FE Wrinkle Model; L = 19.25", T = 10 lbs

Figure 113 shows the proposed model requiring more variation in MD stress to achieve wrinkle than the experimental data suggests. There may be issues related to violation of boundary conditions in the experimental data. At a relatively low web line tension, the web could possibly be slipping on the upstream roller at a "short" span length. Since span length and tension were altered, combined effects could possibly be responsible for the variation. An additional model was constructed to check the effects of tension alone. Again, Figure 108 shows wrinkling at 6 psi internal roller pressure, with a span length of L = 31.5", and web line tension of t = 30 lbs.

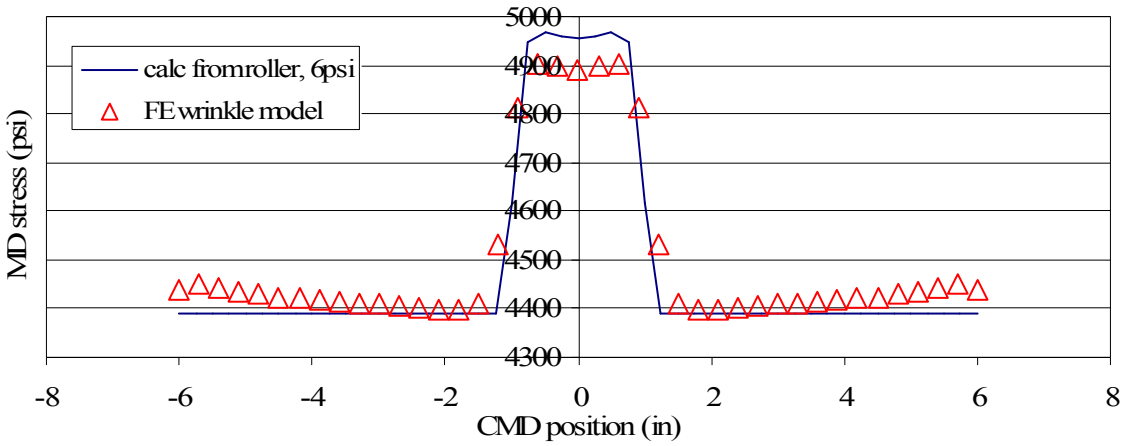

Figure 114 – FE Wrinkle Model; L = 31.5, T = 30 lbs

The model provides acceptable results when tension alone is varied, see Figure 114. Furthermore, the model is moving in the same direction as the experimental values. This suggests that the larger discrepancies observed in Figure 113 are the results of the relatively short span length. An additional point to be made, in this case, is the roller was made from a polypropylene shell. The roller was measured with various internal pressures but without the presence of a tensioned web partially wrapping it. It is not known how much effect the web had on the shape of the pressurized roller. Any effects would have been amplified by higher tensions.

5.8 Conclusions of Machine Direction Wrinkles

Machined direction wrinkles can be caused by a downstream crowned roller. Experiments were developed to study the behavior of webs encountering crowned rollers. This included the creation of a "low" crown roller. This roller has the potential of a variable crown that can be adjusted dynamically.

Attempts were made to explore the boundary conditions and strain fields associated with crowned rollers. Experiments with strain gauges support using simplified mass continuity, equation (4), as a method of predicting relative strain profiles across a web. This assumption is supported whether the web is planar or if troughs are present. These experiments also suggest that for a web with developed troughs that "string theory" is a reasonable approximation for stress in a web approaching a crowned roller.

Experiments were conducted to measure the onset of trough formation in a web span due to a downstream crowned roller. Modeling attempts were made using FE analysis. It was discovered that the compressive stress developed in elastic elements was localized, and did not extend down the length of the web span. Agreement was achieved with experimental values when an "effective" plate length was determined from the compressive stress generated by an FE model based on critical experimental inputs. Suggestions for future efforts include an improved buckling criterion, and possibly a full FE buckling analysis.

Experiments were conducted to measure the onset of wrinkle formation due to a downstream crowned roller. A FE model was proposed that modeled a web span with developed troughs using wrinkling membrane elements. The compressive stresses generated were then compared to critical stresses required for shell buckling, equation (79). The proposed models were successful in predicting wrinkle formation over the ranges of parameters tested. A similar FE model was developed to test wrinkles formed due to a downstream roller with an enlarged section. This model also achieved acceptable agreement with experiment, for typical span/width ratios. If both cases of machine direction wrinkles are used for support, the proposed models appear to be applicable for span/width ratios from over 2 to nearly 6.

When the results of trough formation due to crown, wrinkling due to crown, and wrinkling due to an enlarged section are compared simultaneously, further conclusions may be drawn. The trough due to crown analysis revealed that before troughs form the web span does not experience compression down the whole length of the span. This may imply similar behavior after troughs have developed. Also, the trough experiments show the ability of the web to resist local compressions up to nearly 22 psi for the test case (compared to 3 psi if the whole span is in compression). This may imply that regions of the web where troughs are not formed may have more ability to resist compression than originally assumed. Furthermore, if the developed pocket of compressive stress is dependent on a fixed distance from the crown roll and not overall span length, then the convergence of the data in the longer spans would be explained, and a model for a mid-length span could be used for all span lengths, as long as the span is long enough to allow

the compressive pocket to fully develop. One possible area of future work may include a full FE buckling analysis to determine troughs with the same model used to develop post buckling behavior up to the point of wrinkle formation based on critical stresses developing at the tangent of the roller.

CHAPTER VI

Summary and Conclusions

The objective of this research was the study of trough and wrinkle phenomena caused by downstream roller positioning or geometry. Both shear and machine direction wrinkling cases were studied, modeled, and verified experimentally. Specific accomplishments are:

1.0 The prediction of trough formation due to a tapered downstream roller was developed in the form of a closed form algorithm, with consideration of shear effects, tension effects, and orthotropic web properties. This method is consistent with other cases of shear wrinkling and is presented along with the case of a misaligned roller in Chapter 3.

2.0 The modeling of wrinkle phenomenon on rollers by use of wrinkling membrane elements in a FE analysis linked to classic shell buckling criterion for the cases of both the misaligned and the tapered roller with one consistent method, Chapter 4.

3.0 The study of boundary conditions of a web approaching a crowned roller, the study of trough formation due to crowned rollers. The modeling of wrinkle formation due to a downstream crowned roller again using membrane elements in a FE analysis linked to a shell buckling criterion, application of this model to other cases of machine direction wrinkles. Specifically, to the case of a roller with an enlarged section was accomplished in Chapter 5.

4.0 An additional conclusion was also reached. Troughs form in webs when a few psi of compressive stress are needed in the web. In order for wrinkles to form, typically hundreds of psi of compression are needed. When the wrinkling membrane elements were not used to simulate troughs in a web the compressive stresses required for wrinkling were not reached, and in fact there was no boundary for these stresses to develop along. Hence, in every case studied herein, trough formation in the web was necessary to produce web wrinkling on rollers.

Additional accomplishments and a summary of conclusions are presented in following sections of this chapter.

6.0 Summary of Troughs Due to Shear

Webs approaching tapered rollers have been modeled as tensioned beams with consideration of shear effects and orthotropic material properties. This model accurately predicts steering of the web due to a tapered roller. When combined with plate instability theory, equation (39), the model provides a closed form algorithm to predict the onset of trough formation due to a downstream tapered roller. This model has been verified by experiment for a typical range of web line parameters. During the web deflection experiment it was observed that the model accurately predicted deflections even after troughs had formed in the web. An observation made during the trough formation experiments revealed that "thin" webs are unusually unstable. The 56 ga polyester web (if extrapolated) did not appear to be headed to the origin. This would suggest that the web in question would still form troughs on a perfect, aligned roller under certain conditions, particularly low tensions. Web geometry and non-uniformities were suspect.

The method developed for prediction of troughs due to tapered rollers was consistent in methodology with an analysis of trough formation due to misaligned rollers, previously developed. This consistency supports the generality for the proposed model for use on additional cases of trough formation due to shear. Additionally, the case combined of a misaligned and tapered roller was studied. A model was developed by adding the shear forces developed by both misalignment and taper. This model was also verified experimentally.

6.1 Summary of Wrinkling Due to Shear

The wrinkling of web on rollers is a topic long discussed in web handling. The concept of modeling web on rollers as a thin shell with a related shell buckling limit has been previously proposed. Such a model for shell buckling suited to webs on rollers has been presented, equation (79). The model is for a free, unsupported shell. In reality the web is under tension and rigidly supported by the roller. Experiments were conducted to measure the buckling load of aluminum cylinders. These tests measured the effects of internal pressure and a rigid mandrel support. In both cases, the experimental buckling loads measured supported the use of equation (79) for determining wrinkling of tensioned webs on rollers. Of note, equation (79) is applicable to all types of wrinkling and not exclusive to wrinkles due to shear.

A model was developed to predict the wrinkling of webs due to shear by use of wrinkling membrane elements. These elements were used to model web with developed troughs. The assumption is that once troughs develop in webs the amount of compressive stress they can support is negligible. A FE model using these elements was used to develop the stresses in the web. These stresses were then compared to the critical stress predicted by equation (79). This model was applied to the cases of misaligned rollers and tapered rollers. Experiments were conducted which successfully verified the models. The consistency which the model was applied to both cases suggests the possibility of application to other cases of shear wrinkles, such as wrinkling due to uneven nip pressure in sets of rubber covered rollers.

In application of this method, of importance was correct implementation of boundary conditions. Specifically, developing the correct MD stress profile at the boundary between wrinkling and elastic elements was essential. Also, normal entry must be considered.

6.2 Summary of Machine Direction Wrinkles

Crowned rollers, where crowns are unintentional, are a common source of machine direction wrinkles. Experiments were conducted to measure the MD strains associated with crowned rollers. These tests required creation of crowned rollers that would not cause troughs in the web. A low crown roller was created capable of small crowns and was dynamically variable. Experiments with strain gauges approaching crowned rollers and the use of LDV's on the similar case of concaved rollers supported the use of equation (4) in the determination of strains developed at contoured rollers, whether troughs are present in the web or not. The strain gauge experiments also suggest "string method" as appropriate in describing MD strain in webs with developed troughs.

Experiments were conducted to determine the onset of troughs approaching crowned rollers, which made use of the variable "low" crown roller. A FE model using elastic elements and plate buckling theory, equation (39), initially failed at predicting trough formation. However, when inputs determined from the trough experiments were used to determine an effective "plate length" agreement was achieved. This agreement shows the potential of the method if a more suitable buckling criterion were developed. Also, a full FE buckling analysis might also prove effective in this case.

Models were developed to predict wrinkle formation due to crowned rollers. Wrinkling membrane elements were again coupled with shell buckling criterion, equation (79). Experiments were conducted to verify the model. Acceptable agreement was achieved for conditions tested. A similar model was constructed for the case of a roller

with an enlarged section. Experimental data was previously collected by Good [14]. Good's data only covered relatively short span lengths with low span/width ratios. Comparison of model output and experiment showed excellent agreement with the longest span length which would be considered a typical span/width ratio. Larger discrepancies were observed in the shorter span lengths.

If the results of trough formation and both cases of wrinkling are analyzed simultaneously, further conclusions may be drawn. The modeling of trough formation revealed the compressive stress developed did not extent the length of the web span. It is possible that if this is true after troughs have formed then using wrinkling membrane element for the entire span length may not be appropriate for the longer span lengths. The data shows convergence of the data in the longer spans suggesting independence of span length once this compressive region is fully developed.

6.3 Recommendations for Future Study

The work presented here made a basic assumption of no-slip conditions between web and their transport rollers. Issues related to available web traction have long been discussed in web handling. Future efforts may be made to incorporate these traction effects into the proposed models.

Trough and wrinkling phenomenon due to shear have been thoroughly studied. However, exceptionally short span lengths have not been tested in the case of wrinkling. Studies of the rolling boundary condition at the ends of web spans may become important where short spans are concerned. Also, enforcement of normal entry without interference to developing stresses may be improved.

The prediction of machine direction toughs would be improved by a buckling criterion suited to the "pocket" of compressive stress developed in front of a crowned roller. An additional approach, one involving less assumptions, would be a full FE buckling analysis. If successful such a buckling analysis may have the additional advantage of describing post buckling behavior without the use of wrinkling membrane elements. This may help to resolve span related issues with the current wrinkling models.

Bibliography

1. "ASTM D882-05: Test Method for Tensile Properties of Thin Plastic Sheeting (strip tensile)", *Annual book of ASTM Standards*, vol. 08.01.

2. "Summary of Major Areas of Web Handling Research", Oklahoma State University, Stillwater, OK, October 25, 1985.

3. Allen, H.G. and P.S. Bulson, Background to Buckling, McGraw-Hill, Maidenhead, 1980.

4. Beisel, J.A., "Prediction of Single Span Web Buckling and Experimental Verification", M.S. Thesis, Oklahoma State University, July 2000.

5. Bensen, R.C., et al., "Simulation of Wrinkling Patterns in Webs Due to Non-Uniform Transport Conditions", Proceedings of the Second International Conference on Web Handling, Stillwater, OK, WHRC, Oklahoma State University, June 1993.

6. Brown, J.L., "Effects of Concave Rollers, Curved Axis Rollers and Web Camber on the Deformation and Translation of a Moving Web", Proceedings of the Eighth International Conference on Web Handling, Stillwater, OK, WHRC, Oklahoma State University, June 2005.

7. Brown, J.L., "A New Method for Analyzing the Deformation and Lateral Translation of a Moving Web", Proceedings of the Eighth International Conference on Web Handling, Stillwater, OK, WHRC, Oklahoma State University, June 2005.

8. Cheng, S. and C.C. Cheng, "Relation Between E, ν, and G and the Invariants of the Elastic Coefficients for an Orthotropic Body ", Mechanics of Wood and Paper Materials, ASME, Vol. AMD-112, MD-23, p. 63-65.

9. Delahoussaye, R.D. and J.K. Good, "Analysis of Web Spreading Induced by the Concave Roller", Proceedings of the Second International Conference on Web Handling, Stillwater, OK, WHRC, Oklahoma State University, June 1993.

10. Delahoussaye, R.D. and J.K. Good, "Analysis of Web Spreading Induced by the Curved Axis Roller", Proceedings of the Second International Conference on Web Handling, Stillwater, OK, WHRC, Oklahoma State University, June 1993.

11. Dobbs, J.N. and D.M. Dedl, "Wrinkle Dependency on Web Roller Slip", Proceedings of the Second International Conference on Web Handling, Stillwater, OK, WHRC, Oklahoma State University, June 1993.

12. Gehlbach, L.S., J.K. Good, and D.M. Kedl, "Prediction of Shear Wrinkles in WEB Spans", TAPPI Journal, Vol. 72, No. 8, p. 129-134, Aug. 1989.

13. Good, J.K., "Shear in Multispan Web Systems", Proceedings of the Fourth International Conference on Web Handling, Stillwater, OK, WHRC, Oklahoma State University, June 1997.

14. Good, J.K., "Wrinkling of Webs", IAB Review Stillwater, OK, WHRC Oklahoma State University.

15. Good, J.K. and J.A. Beisel, "Buckling of Orthotropic Webs in Process Machinery", Proceedings of the Seventh International Conference on Web Handling, Stillwater, OK, WHRC, Oklahoma State University, June 2003.

16. Good, J.K., D.M. Kedl, and J.J. Shelton, "Shear Wrinkling in Isolated Spans", Proceedings of the Fourth International Conference on Web Handling, Stillwater, OK, WHRC, Oklahoma State University, June 1997.

17. Good, J.K. and P. Straughan, "Wrinkling of Webs Due to Twist", Proceedings of the Fifth International Conference on Web Handling, Stillwater, OK, WHRC, Oklahoma State University, June 1999.

18. Gopal, H. and D.M. Kedl, "Using Finite Element Method to Define How Wrinkles Form in a Single Web Span Without Moment Transfer", Proceedings of the First International Conference on Web Handling, Stillwater, OK, WHRC, Oklahoma State University, 1991.

19. Hashimoto, H., "Prediction Model of Paper-Web Wrinkling and Some Nemerical Calculation Examples with Experimental Verifications", Proceedings of the Eighth International Conference on Web Handling, Stillwater, OK, WHRC, Oklahoma State University, June 2005.

20. Hosford, W.F. and J.L. Duncan, "The Aluminum Beverage Can", The Scientific American, p. 48-53, Sept. 1994.

21. Iwasa, T., M.C. Natori, and K. Higuchi, "Evaluation of Tension Field Theory for Wrinkling Analysis With Respect to the Post Buckling Study", Journal of Applied Mechanics, Vol. 71, p. 532-540, July 2004.

22. Jones, D.P. and M.J. McCann, "Wrinkling of Webs on Rollers and Drums", Proceedings of the Eighth International Conference on Web Handling, Stillwater, OK, WHRC, Oklahoma State University, June 2005.

23. Lekhnitskii, S.G., Anisotropic Plates, Gordon and Breech, New York, 1968.

24. Lorig, E.T., "Automatic Self-Centering Rolls and Pulleys", AISE Convention, Cleveland, Ohio, 1950.

25. Markum, R.E. and J.K. Good, "Design of Contoured Rollers for Web Spreading", Proceedings of the Sixth International Conference on Web Handling, Stillwater, OK, WHRC, Oklahoma State University, June 2001.

26. Miller, R.K. and J.M. Hedgepeth, "An Algorithm for Finite Element Analysis of Partly Wrinkled Membranes", AIAA Journal, p. 1761-1763, Dec. 1982.

27. Olsen, J.E., "Lateral Mechanics of an Imperfect Web", Proceedings of the Sixth International Conference on Web Handling, Stillwater, OK, WHRC, Oklahoma State University, June 2001.

28. Olsen, J.E., "Lateral Mechanics of Baggy Webs at Low Tensions", Proceedings of the Eighth International Conference on Web Handling, Stillwater, OK, WHRC, Oklahoma State University, June 2005.

29. Olsen, J.E., "Shear Effects and Lateral Mechanics of Imperfect Webs", Proceedings of the Seventh International Conference on Web Handling, Stillwater, OK, WHRC, Oklahoma State University, June 2003.

30. Papandreadis, A., "The Development of Finite Element Modeling Techniques of Webs and the Analysis of Web Wrinkle Formation", M.S. Thesis, Oklahoma State University, July 1984.

31. Przemieniecki, J.S., Theory of Matrix Structural Analysis, McGraw-Hill, New York, 1968.

32. Reddy, J.N., An Introduction to the Finite Element Method, 3rd ed, McGraw-Hill, 2006.

33. Shelton, J.J., "Buckling of Webs from Lateral Compressive Forces", Proceedings of the Second International Conference on Web Handling, Stillwater, OK, WHRC, Oklahoma State University, June 1993.

34. Shelton, J.J., "Derivation of Equations of Lateral Behavior", IAB Review, Stillwater, OK, WHRC, Oklahoma State University, June 1998.

35. Shelton, J.J., "Effects of Camber on Handling", Proceedings of the Fourth International Conference on Web Handling, Stillwater, OK, WHRC, Oklahoma State University, June 1997.

36. Shelton, J.J., "Interaction Between Two Web Spans Because of a Misaligned Downstream Roller", Procedings of the Eighth International Conference on Web Handling, Stillwater, OK, WHRC, Oklahoma State University, June 2005.

37. Shelton, J.J., "Lateral Dynamics of a Moving Web", PhD. Thesis, Oklahoma State University, 1968.

38. Swanson, R.P., "Mechanics of Non-Uniform Webs", Proceedings of the Fifth International Conference on Web Handling, Stillwater, OK, WHRC, Oklahoma State University, June 1999.

39. Swift, H.W., "Camber for Belt Pulleys", Proceedings - Institute of Mechanical Engineers, June 1932.

40. Szilard, R., Theory and Analysis of Plates, Prentice Hall, Englewood Cliffs, New Jersey, 1974.

41. Timoshenko, S.P. and J.M. Gere, Theory of Elastic Stability, 1st ed, McGraw-Hill, New York, 1936.

42. Timoshenko, S.P. and J.N. Goodier, Theory of Elasticity, 3rd ed, McGraw-Hill, New York, 1987.

43. Ugural, A.C. and S.K. Fenster, Advanced Strength and Applied Elasticity, 3rd ed, Prentice-Hall PTR, New Jersey, 1995.

44. Wang, C.Y., "Tension Distribution Across a Moving Web", M.S. Thesis, Oklahoma State University, July 1989.

45. Webb, D.K., "Prediction of Web Wrinkles Due to Misalignment of a Downstream Roll in a Web Span", M.S. Thesis, Oklahoma State University, Dec. 2004.

46. Weingarten, V.I., E.J. Morgan, and P. Seide, "Elastic Stability of Thin-Walled Cylindrical and Conical Shells Under Combined Internal Pressure and Axial Compression", AIAA Journal, Vol. 3, No. 6, p. 1118-1125, June 1965.

Appendix A

The FE package used in modeling was COSMOS 2.8. A typical model was started by first creating the geometry on a blank screen. Then, the material properties E_x and ν were entered. Next, the thickness was entered under Real Constants. After that, the element group for the elastic portions of the model was selected. This element group utilized the Shell4 element in COSMOS. This element is a 4 node quadrilateral meant to model thin shells. This element can support in-plane as well as bending stresses. All default settings (such as regular elastic behavior) for these elements were used except that large displacement formulations were selected. Once the elastic elements were defined in the geometry the second element group was defined. This element group was used to model web with developed troughs. The elements were again Shell4 elements but the membrane option was selected. Furthermore, the next input selected was the wrinkling membrane option. This option created the elements that could not withstand compression in the σ_2 direction. It should be noted that once the wrinkling membrane option is selected, the analysis is required to be non-linear due to the state dependent material properties. Also, COSMOS substitutes in a 4 node element made up of 4 triangles instead of a true quadrilateral element. These elements were then applied to the appropriate geometries and merged with adjacent nodes.

Grid size was initially set to 80 elements across the 6" width of the web, with elements being approximately square. This number was then reduced to 40 elements across the width, and then finally to 20. 20 elements across the width adequately modeled the relatively slowly changing stresses across the web and still resulted in reasonable computational times. No difference in results was observed between 80 elements and 20 elements. Additionally, the aspect ratio of the elements was altered. In the web span where stresses changed slowly, the elements were set to be approximately 3 times longer than they were wide. In the area of the rollers, in particular the boundary between element types where compressive stresses were expected to develop, the length of the elements was set to 1/3 their width. In the case of tapered rollers, node coupling just prior to the boundary between element types, required a similar decrease in element length, not for convergence but to limit the distances the couplings were applied to.

An importance issue relating to the convergence of this model was the time step. The non-linear analysis was required to converge at each step but if too large a time step of load increment was applied then convergence was not achieved. The total time was set to 1 with a time step of 0.05. This led to the loads being applied in 20 steps. In some cases fewer time steps were needed for convergence, but computational time was not a large issue, typically 5-10 minutes, thus, 20 steps were used in all the final models. The convergence and constraint tolerances were left at their default values of 0.001. The load curves are shown below in Figure 115.

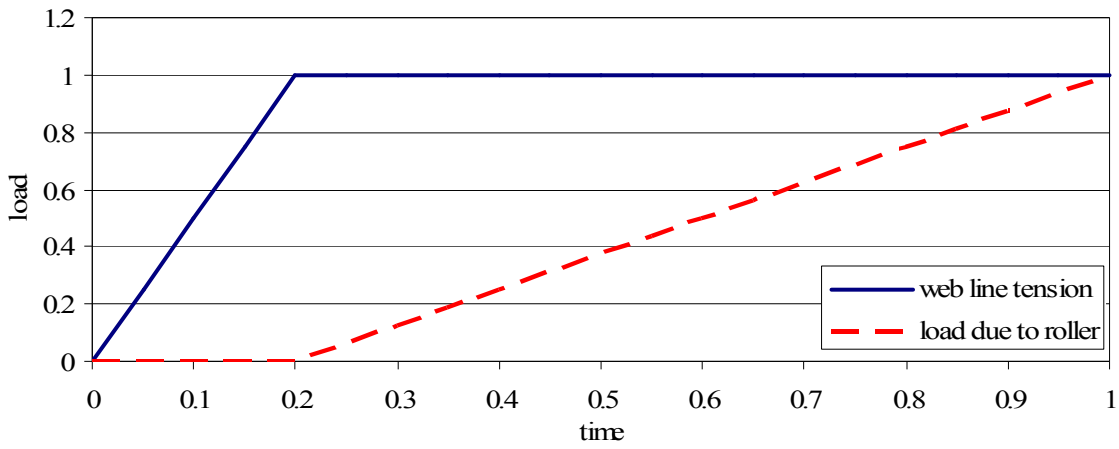

Figure 115 – Load Curves for FE models

Additional settings other than defaults in COSMOS were, not to update nodal coordinates after each run, usually several iterations were necessary to find the critical stress, and to set the displacement dependent load flag. Also of importance to use with the wrinkling membrane elements was the Newton Raphson solution method instead of the default Modified Newton Raphson method. Additional discussion of application of the COSMOS wrinkling elements may be found in Webb's thesis [45].

A sample sec. file is given below; this is for wrinkle formation due to a tapered roller. E = 712000 psi, $\nu = 0.3$, t = 0.00092", W = 6", L = 20", R = 1.49". Equation (79) yields a critical compressive stress of 265 psi for this case. A web line tension was set at T = 18.57 lbs. The scaling factor for the lateral load was set at 1.05, a value known to cause the critical CMD stress. Normally iterations are required to find this value. For ease of use files were created and then loaded for node coupling and applied loads. The file for web line tension applies 10 lbs evenly across the web which may then be scaled

by use of time curve 1. The lateral loads equal 1 lb which may then be scaled by time curve 2.

sec. file which may be loaded into COSMOS, by selecting FILE, LOAD, then selecting a text file which may be created from copying and pasting the following into notepad or another text editor.

```
C*
C* COSMOSM GeoStar 2.8 (256K Version)
C* Problem : Example              Date : 10-10-2006  Time : 22:18:46
C*
PT,3,2.25,0,0
PT,4,2.25,6,0
PT,5,21.75,0,0
PT,6,21.75,6,0
PT,7,22.25,0,0
PT,8,22.25,6,0
PT,9,24.5,0,0
PT,10,24.5,6,0
PT,11,44.5,0,0
PT,12,44.5,6,0
PT,13,46.75,0,0
PT,14,46.75,6,0
CRLINE,1,1,2
CRLINE,2,3,4
CRLINE,3,5,6
CRLINE,4,7,8
CRLINE,5,9,10
CRLINE,6,11,12
CRLINE,7,13,14
SF2CR,1,1,2,0
SF2CR,2,2,3,0
SF2CR,3,3,4,0
SF2CR,4,4,5,0
SF2CR,5,5,6,0
SF2CR,6,6,7,0
EGROUP,1,SHELL4,2,0,0,0,0,1,0,0
MPROP,1,EX,712000
MPROP,1,NUXY,0.3
RCONST,1,1,1,7,0.00092,0,0,0,0,0,1E-008
M_SF,1,1,1,4,20,20,1,1
```

M_SF,4,4,1,4,20,20,1,1
M_SF,6,6,1,4,20,20,1,1
EGROUP,2,SHELL4,2,1,0,0,10,1,0,0
M_SF,3,3,1,4,20,10,1,1
M_SF,2,2,1,4,20,30,1,1
ACTSET,EG,1
M_SF,5,5,1,4,20,30,1,1
NMERGE,1,2856,1,0.0001,0,1,0
NDUPDATE,0
DND,1,UZ,0,2835,1,RX,RY,
DND,662,UX,0,662,1,
DND,662,UY,0,662,1,
CPDOF,1,UY,9,421,400,379,358,337,316,295,274,253
CPDOF,2,UY,9,421,232,211,190,169,148,127,106,85
CPDOF,3,UY,5,421,64,43,22,1
CPDOF,4,UY,9,422,401,380,359,338,317,296,275,254
CPDOF,5,UY,9,422,233,212,191,170,149,128,107,86
CPDOF,6,UY,5,422,65,44,23,2
CPDOF,7,UY,9,423,402,381,360,339,318,297,276,255
CPDOF,8,UY,9,423,234,213,192,171,150,129,108,87
CPDOF,9,UY,5,423,66,45,24,3
CPDOF,10,UY,9,424,403,382,361,340,319,298,277,256
CPDOF,11,UY,9,424,235,214,193,172,151,130,109,88
CPDOF,12,UY,5,424,67,46,25,4
CPDOF,13,UY,9,425,404,383,362,341,320,299,278,257
CPDOF,14,UY,9,425,236,215,194,173,152,131,110,89
CPDOF,15,UY,5,425,68,47,26,5
CPDOF,16,UY,9,426,405,384,363,342,321,300,279,258
CPDOF,17,UY,9,426,237,216,195,174,153,132,111,90
CPDOF,18,UY,5,426,69,48,27,6
CPDOF,19,UY,9,427,406,385,364,343,322,301,280,259
CPDOF,20,UY,9,427,238,217,196,175,154,133,112,91
CPDOF,21,UY,5,427,70,49,28,7
CPDOF,22,UY,9,428,407,386,365,344,323,302,281,260
CPDOF,23,UY,9,428,239,218,197,176,155,134,113,92
CPDOF,24,UY,5,428,71,50,29,8
CPDOF,25,UY,9,429,408,387,366,345,324,303,282,261
CPDOF,26,UY,9,429,240,219,198,177,156,135,114,93
CPDOF,27,UY,5,429,72,51,30,9
CPDOF,28,UY,9,430,409,388,367,346,325,304,283,262
CPDOF,29,UY,9,430,241,220,199,178,157,136,115,94
CPDOF,30,UY,5,430,73,52,31,10
CPDOF,31,UY,9,431,410,389,368,347,326,305,284,263
CPDOF,32,UY,9,431,242,221,200,179,158,137,116,95
CPDOF,33,UY,5,431,74,53,32,11
CPDOF,34,UY,9,432,411,390,369,348,327,306,285,264

CPDOF,35,UY,9,432,243,222,201,180,159,138,117,96
CPDOF,36,UY,5,432,75,54,33,12
CPDOF,37,UY,9,433,412,391,370,349,328,307,286,265
CPDOF,38,UY,9,433,244,223,202,181,160,139,118,97
CPDOF,39,UY,5,433,76,55,34,13
CPDOF,40,UY,9,434,413,392,371,350,329,308,287,266
CPDOF,41,UY,9,434,245,224,203,182,161,140,119,98
CPDOF,42,UY,5,434,77,56,35,14
CPDOF,43,UY,9,435,414,393,372,351,330,309,288,267
CPDOF,44,UY,9,435,246,225,204,183,162,141,120,99
CPDOF,45,UY,5,435,78,57,36,15
CPDOF,46,UY,9,436,415,394,373,352,331,310,289,268
CPDOF,47,UY,9,436,247,226,205,184,163,142,121,100
CPDOF,48,UY,5,436,79,58,37,16
CPDOF,49,UY,9,437,416,395,374,353,332,311,290,269
CPDOF,50,UY,9,437,248,227,206,185,164,143,122,101
CPDOF,51,UY,5,437,80,59,38,17
CPDOF,52,UY,9,438,417,396,375,354,333,312,291,270
CPDOF,53,UY,9,438,249,228,207,186,165,144,123,102
CPDOF,54,UY,5,438,81,60,39,18
CPDOF,55,UY,9,439,418,397,376,355,334,313,292,271
CPDOF,56,UY,9,439,250,229,208,187,166,145,124,103
CPDOF,57,UY,5,439,82,61,40,19
CPDOF,58,UY,9,440,419,398,377,356,335,314,293,272
CPDOF,59,UY,9,440,251,230,209,188,167,146,125,104
CPDOF,60,UY,5,440,83,62,41,20
CPDOF,61,UY,9,441,420,399,378,357,336,315,294,273
CPDOF,62,UY,9,441,252,231,210,189,168,147,126,105
CPDOF,63,UY,5,441,84,63,42,21
CPDOF,64,UY,9,883,904,925,946,967,988,1009,1030,1051
CPDOF,65,UY,9,883,1072,1093,1114,1135,1156,1177,1198,1219
CPDOF,66,UY,5,883,1240,1261,1282,1303
CPDOF,67,UY,9,884,905,926,947,968,989,1010,1031,1052
CPDOF,68,UY,9,884,1073,1094,1115,1136,1157,1178,1199,1220
CPDOF,69,UY,5,884,1241,1262,1283,1304
CPDOF,70,UY,9,885,906,927,948,969,990,1011,1032,1053
CPDOF,71,UY,9,885,1074,1095,1116,1137,1158,1179,1200,1221
CPDOF,72,UY,5,885,1242,1263,1284,1305
CPDOF,73,UY,9,886,907,928,949,970,991,1012,1033,1054
CPDOF,74,UY,9,886,1075,1096,1117,1138,1159,1180,1201,1222
CPDOF,75,UY,5,886,1243,1264,1285,1306
CPDOF,76,UY,9,887,908,929,950,971,992,1013,1034,1055
CPDOF,77,UY,9,887,1076,1097,1118,1139,1160,1181,1202,1223
CPDOF,78,UY,5,887,1244,1265,1286,1307
CPDOF,79,UY,9,888,909,930,951,972,993,1014,1035,1056
CPDOF,80,UY,9,888,1077,1098,1119,1140,1161,1182,1203,1224

CPDOF,81,UY,5,888,1245,1266,1287,1308
CPDOF,82,UY,9,889,910,931,952,973,994,1015,1036,1057
CPDOF,83,UY,9,889,1078,1099,1120,1141,1162,1183,1204,1225
CPDOF,84,UY,5,889,1246,1267,1288,1309
CPDOF,85,UY,9,890,911,932,953,974,995,1016,1037,1058
CPDOF,86,UY,9,890,1079,1100,1121,1142,1163,1184,1205,1226
CPDOF,87,UY,5,890,1247,1268,1289,1310
CPDOF,88,UY,9,891,912,933,954,975,996,1017,1038,1059
CPDOF,89,UY,9,891,1080,1101,1122,1143,1164,1185,1206,1227
CPDOF,90,UY,5,891,1248,1269,1290,1311
CPDOF,91,UY,9,892,913,934,955,976,997,1018,1039,1060
CPDOF,92,UY,9,892,1081,1102,1123,1144,1165,1186,1207,1228
CPDOF,93,UY,5,892,1249,1270,1291,1312
CPDOF,94,UY,9,893,914,935,956,977,998,1019,1040,1061
CPDOF,95,UY,9,893,1082,1103,1124,1145,1166,1187,1208,1229
CPDOF,96,UY,5,893,1250,1271,1292,1313
CPDOF,97,UY,9,894,915,936,957,978,999,1020,1041,1062
CPDOF,98,UY,9,894,1083,1104,1125,1146,1167,1188,1209,1230
CPDOF,99,UY,5,894,1251,1272,1293,1314
CPDOF,100,UY,9,895,916,937,958,979,1000,1021,1042,1063
CPDOF,101,UY,9,895,1084,1105,1126,1147,1168,1189,1210,1231
CPDOF,102,UY,5,895,1252,1273,1294,1315
CPDOF,103,UY,9,896,917,938,959,980,1001,1022,1043,1064
CPDOF,104,UY,9,896,1085,1106,1127,1148,1169,1190,1211,1232
CPDOF,105,UY,5,896,1253,1274,1295,1316
CPDOF,106,UY,9,897,918,939,960,981,1002,1023,1044,1065
CPDOF,107,UY,9,897,1086,1107,1128,1149,1170,1191,1212,1233
CPDOF,108,UY,5,897,1254,1275,1296,1317
CPDOF,109,UY,9,898,919,940,961,982,1003,1024,1045,1066
CPDOF,110,UY,9,898,1087,1108,1129,1150,1171,1192,1213,1234
CPDOF,111,UY,5,898,1255,1276,1297,1318
CPDOF,112,UY,9,899,920,941,962,983,1004,1025,1046,1067
CPDOF,113,UY,9,899,1088,1109,1130,1151,1172,1193,1214,1235
CPDOF,114,UY,5,899,1256,1277,1298,1319
CPDOF,115,UY,9,900,921,942,963,984,1005,1026,1047,1068
CPDOF,116,UY,9,900,1089,1110,1131,1152,1173,1194,1215,1236
CPDOF,117,UY,5,900,1257,1278,1299,1320
CPDOF,118,UY,9,901,922,943,964,985,1006,1027,1048,1069
CPDOF,119,UY,9,901,1090,1111,1132,1153,1174,1195,1216,1237
CPDOF,120,UY,5,901,1258,1279,1300,1321
CPDOF,121,UY,9,902,923,944,965,986,1007,1028,1049,1070
CPDOF,122,UY,9,902,1091,1112,1133,1154,1175,1196,1217,1238
CPDOF,123,UY,5,902,1259,1280,1301,1322
CPDOF,124,UY,9,903,924,945,966,987,1008,1029,1050,1071
CPDOF,125,UY,9,903,1092,1113,1134,1155,1176,1197,1218,1239
CPDOF,126,UY,5,903,1260,1281,1302,1323

```
CPDOF,127,UX,9,421,422,423,424,425,426,427,428,429
CPDOF,128,UX,9,421,430,431,432,433,434,435,436,437
CPDOF,129,UX,5,421,438,439,440,441
CPDOF,133,UY,2,442,1513
CPDOF,134,UY,2,443,1514
CPDOF,135,UY,2,444,1515
CPDOF,136,UY,2,445,1516
CPDOF,137,UY,2,446,1517
CPDOF,138,UY,2,447,1518
CPDOF,139,UY,2,448,1519
CPDOF,140,UY,2,449,1520
CPDOF,141,UY,2,450,1521
CPDOF,142,UY,2,451,1522
CPDOF,143,UY,2,452,1523
CPDOF,144,UY,2,453,1524
CPDOF,145,UY,2,454,1525
CPDOF,146,UY,2,455,1526
CPDOF,147,UY,2,456,1527
CPDOF,148,UY,2,457,1528
CPDOF,149,UY,2,458,1529
CPDOF,150,UY,2,459,1530
CPDOF,151,UY,2,460,1531
CPDOF,152,UY,2,461,1532
CPDOF,153,UY,2,462,1533
TIMES,0,1,0.05
CURDEF,TIME,1,1,0,0,0.2,1.857,1,1.857
FND,1,FX,-0.25,21,20
FND,2,FX,-0.5,20,1
FND,1303,FX,0.25,1323,20
FND,1304,FX,0.5,1322,1
CURDEF,TIME,2,1,0,0,0.2,0,1,1.05
FND,443,FY,0.028,461,18
FND,444,FY,0.056,460,1
FND,863,FY,0.028,881,18
FND,864,FY,0.056,880,1
FND,422,FY,-0.028,440,18
FND,423,FY,-0.056,439,1
FND,884,FY,-0.028,902,18
FND,885,FY,-0.056,901,1
NL_CONTROL,0,1
A_NONLINEAR,S,1,1,20,0.001,0,N,1,0,1E+010,0.001,0.01,0,1,0,0
C*
C* COSMOSM GeoStar 2.8 (256K Version)
C* Problem : Example              Date : 10-10-2006  Time : 22:23:43
C*
```

VITA

JOSEPH A.BEISEL

Candidate for the Degree of

Doctor of Philosophy

Thesis: SINGLE SPAN WEB BUCKLING DUE TO ROLLER IMPERFECTIONS IN WEB PROCESS MACHINERY

Major Field: Mechanical Engineering

Biographical:

Personal Data: Born in Shattuck, OK, On July 23, 1975, the son of Aaron and Dianna Beisel.

Education: Graduated from FHS High School, Fargo, OK in May 1993; received Bachelor of Science in Engineering Physics, from Southwestern Oklahoma State Univ. in Weatherford, OK, in May 1997; received Master of Science in Mechanical Engineering from Oklahoma State University, Stillwater, Oklahoma in August 2000. Completed the requirements for the Doctor of Philosophy degree with a major in Mechanical Engineering at Oklahoma State University, Stillwater, Oklahoma in December 2006.

Experience: Employed by Department of Mechanical Engineering at Oklahoma State University, Stillwater as a graduate teaching and research assistant, 1999 to present.

Professional Memberships: Society of Physics Students (SPS), National Physics Honor Society (ΣΠΣ).

Name: JOSEPH A. BEISEL Date of Degree: December, 2006

Institution: Oklahoma State University Location: Stillwater, Oklahoma

Title of Study: SINGLE SPAN WEB BUCKLING DUE TO ROLLER IMPERFECTIONS IN WEB PROCESS MACHINERY

Pages in Study: 171 Candidate for the Degree of Doctor of Philosophy

Major Field: Mechanical Engineering

Scope and Method of Study: To study instabilities in webs resulting from contact with imperfect rollers, whether in their geometry or their orientation in a web span. The instabilities covered include trough formation in web spans and wrinkling of webs on rollers. Webs are modeled as beams successfully, until trough form in the web spans. A buckling criterion for web in a free span is linked to various models to predict the formation of troughs in the web. In the case of web wrinkling, finite elements models using wrinkling membrane elements are used to simulate webs with developed troughs. These are linked to shell buckling criterion in order to predict webs wrinkling on rollers. Cases these techniques are applied to in a consistent manner are: misaligned rollers, tapered rollers, misaligned *and* tapered rollers, crowned rollers, and rollers with an enlarged section.

Findings and Conclusions: Experimental verification is provided for comparison to all proposed models. It was found that the presence of troughs in a web does not affect the deflection in the case of tapered rollers. Simplified mass continuity is applicable to predict strains due to contoured rollers. In all cases studied troughs are required to allow wrinkles to form in webs.

ADVISER'S APPROVAL: Dr. J.K. Good